Università degli Studi di Padova

School of Engineering

Department of Industrial Engineering

Master of Science in Aerospace Engineering

Design of structural components for a hybrid sounding rocket

Advisor

Prof. Daniele Pavarin

Co – Advisor

Ing. Francesco Barato

Candidate:

Davide Squarcina

Student n° **1183817**

Academic Year 2018/2019

"Everyone knows that something

is impossible to achieve,

until a fool arrives who does not know

and invents it."

– Albert Einstein –

Abstract

The University of Padua in collaboration with T4i (Technology For Propulsion and Innovation) its spin-off, has designed and developed a Hybrid Sounding Rocket.
Hybrid rockets are an attractive alternative to solid and liquid rockets for their unique features, in a world becoming more careful about safety, costs and environmental impact. Hybrid motors show several advantages, like safety, operational reliability, throttling capabilities, environmental friendliness and low costs. The safety in the management of this engine has allowed proposing the project to university students.
The present research studies the behaviour of some structural components of the rocket, focusing on the junctions of the different subsystems. The theoretical bases on composite materials, their behaviour under structural loads are described. Furthermore, the structural parameters to design bolted joints are shown. To size these components, the loads acting in the flight of the rocket are used.
In the junction, there are three main parts: the connection screws, the metal joints and the glueing that interfaces the junction with the external structure. Each component has been tested after being dimensioned. The tests carried out are intended to represent the operating conditions in the rocket and to observe the behaviour to validate the design of the components.
After describing the tests to be performed, the results obtained and the graphs showing how the tested samples behaved are reported. The results obtained confirm what has been studied from the theory.

Sommario

L'Università di Padova in collaborazione con l'azienda T4i (Technology For Propulsion and Innovation), una sua spin-off, ha progettato e sviluppato un sounding rocket ibrido.

I razzi ibridi sono un'alternativa interessante ai razzi solidi e liquidi per le loro caratteristiche uniche, dal momento che l'attenzione si sta spostando verso la sicurezza, i costi e l'impatto ambientale. I motori ibridi presentano diversi vantaggi, come ad esempio la sicurezza, l'affidabilità operativa, la modulabilità, il rispetto ambientale e i costi ridotti. La possibilità di utilizzare in sicurezza questo tipo di motori ha permesso di orientare il progetto anche agli studenti universitari.

La ricerca presente studia il comportamento di alcuni componenti strutturali del razzo, focalizzandosi sulle giunzioni che uniscono i diversi sottosistemi. Vengono descritte le basi teoriche dei materiali compositi, il loro comportamento strutturale e vengono mostrati i parametri dimensionali per la progettazione di giunzioni bullonate. Nel documento sono descritti i passaggi per ottenere il dimensionamento di tutti i componenti delle giunzioni e sono riportati i carichi utilizzati per rappresentare il razzo nella fase di volo. Queste componenti sono costituite da tre parti principali; vi sono presenti delle viti di collegamento, due piastre metalliche e due incollaggi che permettono di interfacciare la giunzione con la struttura esterna. Ciascuno di questi elementi è stato testato per verificare che il dimensionamento analitico fosse corretto e che il componente rispettasse le specifiche richieste. Alcuni dei risultati ottenuti dai test svolti sono riportati e discussi, ottenendo così delle ottime conclusioni e dei confronti con la teoria studiata.

Table of Contents

Chapter 1

Sounding Rocket

Sounding rockets are launchers used since the late 1950s as launch systems for missions in the upper atmosphere [1]. The rockets originally take their name from the nautical term “to sound”, which means “to take measurements”. It was the first propulsive systems to bring scientific instruments into the upper atmosphere that could study it and provide data on its vertical profile. Their use is efficient in high-density atmospheric areas where the satellites cannot orbit; although for a few minutes of measurements, the sounding rockets allow reaching these areas with low mission costs. The sounding rocket allows to launch payloads with masses between a few kilos up to one hundred kilograms, the range of launch is about a few kilometers to a few thousand kilometers. They are composed generally about two subsystems, the first is the propulsion system and the second is a payload for measurements, this made the sounding rockets simples and efficiently. Their simplicity makes them easily achievable with low costs and production times. Some disadvantages of the sounding rocket are they allow to launch payloads limited in weight and dimensions, they allow little measurement time to scientific instruments and moreover, they don't allow to reach high quotas, and it is difficult to obtain a complete mapping of the Earth.
Sounding rockets initially used solid propulsion, while they have recently evolved using hybrid propulsion systems. The solid propulsion allows to have simpler and more compact systems but also less safe and manageable. Even small companies can use these launchers with relatively low costs and be able to launch small satellites in the desired orbit. In this way, it is no longer necessary to exploit the launch of large space companies to gain access to space, with the limits imposed by them.

1.1 Hybrid Rocket Propulsion System

The rocket engines are divided according to the type of technology used to realize the propulsive thrust [2,3]. There are engines with chemical propulsion, electric

propulsion and nuclear propulsion. The most engines used for launchers are chemical engines, which extract energy from the chemical reaction between a fuel and oxidizer. This type of engine differentiates their structure according to the phase with which the propellant is stored; for this reason, they are divided into solid, liquid and hybrid rockets.

1.1.1 Solid Engine

In solid-propellant engines the fuel and the oxidizer are mixed composing a single solid phase, this allows the solid engines a high compactness, but the thrust profile is predetermined. For the ignition of the propellant it is necessary to use an ignition system, once turned on the solid engine can self-sustain the combustion.

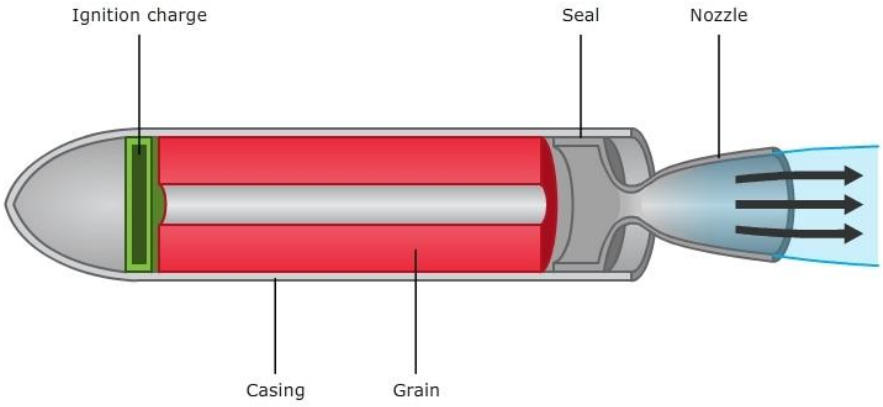

Figure 1. Solid Engine

In this design, the engine does not need the valve system or ducts to ensure engine operation making the whole system more reliable. The disadvantage of solid motors is their safety because once they are turned on, they cannot be turned off. In addition, the grain must be carefully made without having cracks or fissures that could lead to engine failure due to increased internal pressures.

To date, these propulsion systems are used for small amateur rockets or for large launchers.

1.1.2 Liquid Engine

In liquid engines, both oxidant and fuel are in the liquid phase and are mixed at the inlet of the combustion chamber generating a chemical reaction that allows propulsion; for example, they use liquid liquid hydrogen or kerosene as fuel, while as oxidant they use liquid oxygen. They are sprayed into the combustion chamber through injection nozzles, they rapidly mix and react before being ejected. Some combinations of propellants are called hypergolic, due to their instantaneous combustion when they are mixed. Other combinations of propellants require the same as in the solid engines of an initial ignition system. To make combustion take place, a combustion chamber is used before the nozzle.

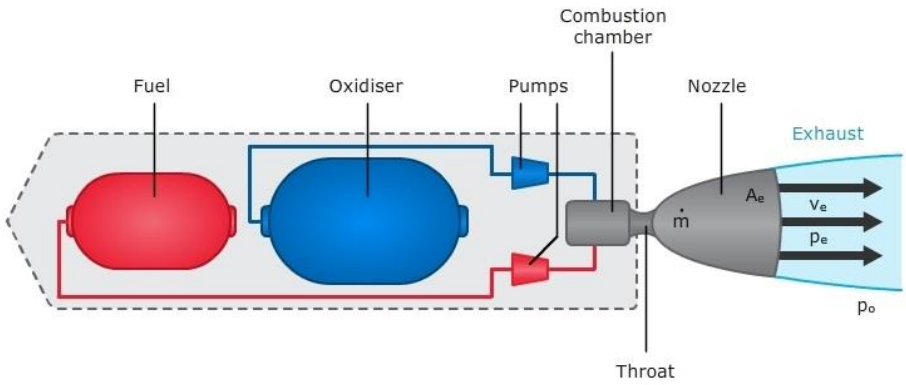

Figure 2. Liquid Engine

1.1.3 Hybrid Engine

Hybrid engines are very safe and not expensive systems to implement, for this reason, they are used in space propulsion. The hybrid rockets are much more nonexplosive than solids and are therefore used for amateur academic groups. They use solid and liquid propellants together. However, they have many similar aspects to solid and liquid engines as they derive from the union of both. The hybrid, however, burns as a macroscopic turbulent diffusion flame where the oxidizer-to-fuel ratio (O/F) varies down the length of the chamber, ending at a composition that determines engine performance. Their architecture is generally formed by the solid propellant in the combustion chamber and an oxidant in the liquid or gaseous phase. The pressurized

oxidant is discharged into the combustion chamber and reacting with the solid propellant to start combustion generating the propulsive thrust. The system must be pressurized to realize the pressure jump between the start and the exit of the

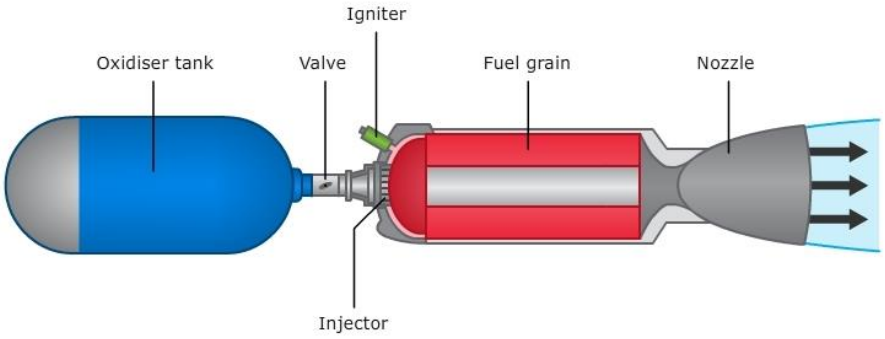

Figure 3. Hybrid Engine

combustion chamber. Their use includes primary propulsion for launch vehicles, upper stage propulsion and the emerging field of commercial space transportation. They are much more controllable systems during the flight phase compared to solid engines, guaranteeing good levels of specific impulse.

Hybrid engines differ from solids and liquids due to various advantages and disadvantages. Comparing them for the different mechanical characteristics such as:

- *Safety propellant storage.* The system keeps the oxidizer and fuel separate to be able to manage the rocket safely. Both phases are inert and not explosive, they can be transported to the launch site and stored in the rocket at launch. Furthermore, the system can be aborted on command using safety valves.
- *Single fluid line.* The oxidant is made to flow into the combustion chamber through a single fluidic line. No more fluid lines must be synchronized to ensure the correct mixing of two fluids as in liquid motors. The flow of fuel depends on the oxidant flow as it derives from vaporization due to the oxidizer flow rate.

- *Grain Robustness.* Unlike solid motors where a propellant grain break is catastrophic as it increases the burning area and therefore the pressure in the combustion chamber. In hybrid engines the burning area depends on the area that comes into thermal contact with the flame. If there are cracks in the solid fuel the flame cannot propagate inside them due to the boundary layer. for which there is a progressive and superficial consumption of fuel.
- *Temperature Sensitivity.* The effects of the burn rate are small, the launch environment has little effect on the operating pressure in the combustion chamber.
- *Low Cost.* The costs for the construction of a hybrid engine are relatively reduced since the propellant can be done in a commercial facility and must not comply with all the safety standards that are used in solid engines. The system can have wider design margins and therefore be able to reduce manufacturing costs.
- *Controlled propulsion.* The fluidics line can be easily controlled via valves. This allows to determine the ignition of the rocket and its possible extinction, but also allows to regulate the flow of oxidizer and determine the thrust profile.

The hybrid propulsion rockets have not only advantages but have some disadvantages such as:

- *Low Regression Rate.* The combustion characteristics are complex, hybrid engines suffer a lot from a low regression rate. If the combustion chamber has a diameter greater than one foot, the propellant grain must provide multiple doors in order to guarantee an adequate burning area to obtain the desired thrust. This is because if the shape of the grain was simple the chamber would be much longer to guarantee the necessary mass of fuel, this would involve a much greater inert mass and dimensions.
- *Large Diffusive Flame.* The nature of a large diffusive flame in a lower degree of mixing and, hence, a lower impulse efficiency.
- *Shift O/F.* During combustion the burning area increases increasing the surface that releases fuel and the regression rate decreases. These two unbalanced phenomena cause a decrease in fuel production rate. Therefore, this causes a mixture ratio variation with burning time, and thus generally a decrease in the

average specific impulse. In the figure {NUMBER} it is possible to observe how combining a solid fuel HTPB with different oxidants varies the vacuum I_{sp} (specific impulse in vacuum) with the variation of the O/F ratio.

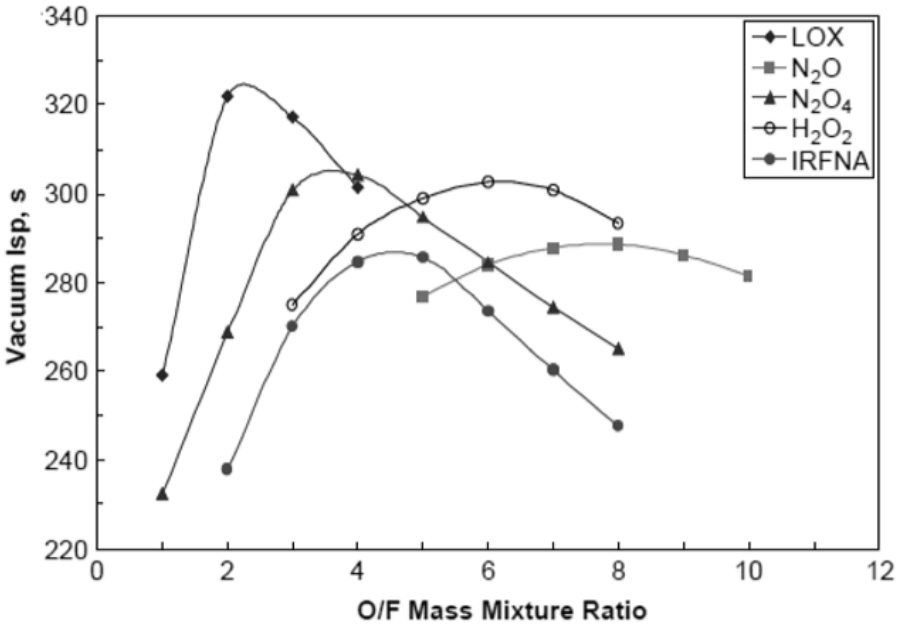

Figure 4. Engine Parameters

The hybrid rocket developed in the present university project, uses for propulsion the combination of paraffin as fuel, and hydrogen peroxide as an oxidant. The oxidant is in the liquid phase, so an external tank containing N_2 (nitrogen gas) is used with the function of pressurizing the oxidant and allowing pressure in the combustion chamber. This type of configuration takes the name of hybrid engine with gas pressurization. Through a pressure regulator the hydrogen peroxide tank is kept at a constant pressure ensuring the correct operation of the motor. The hydrogen peroxide is stored at 90% and before mixing with the paraffin it passes through a catalytic in order to decompose the hydrogen peroxide into O_2 and water, the decomposition produces an exothermic reaction with oxygen around 1100 K which reacts with the paraffin burning in the combustion chamber. The reaction is:

$$2H_2O_2 \xrightarrow{catalitic} O_2 + 2H_2O$$

The oxidant, after decomposing, enters the combustion chamber and begins to react with fuel, generating the combustion. The generated flame has a temperature profile and a characteristic speed profile. The heat of the flame is such as to allow the vaporization of the paraffin which enters in the burning flame. The peculiarity of using paraffin is that in the passage from solid to liquid a layer of liquid paraffin is generated on the grain surface. The liquid layer allows limiting the thermal gradient on the grain, avoiding that even the lower layer melts before the flame arrives.

The use of hydrogen peroxide as the oxidizer and a catalytic bed, offer greater added simplicity because they exclude the need for a complicated and costly igniter system. The advantage of using hydrogen peroxide allows an increase of regression rate,

$$\dot{r} = \frac{aG^n}{x^m};$$

where G is local mass flux, x the axial location from aft to the end of grain, a is the regression rate coefficient, n the regression rate exponent and m the length exponent. In this equation a and n depends of fuel characteristics.

1.2 Sounding Rocket Structures

The choice to use sounding rockets for small missions is given by their simplicity and their excellent availability. The same for their architecture, in fact in addition to using simple and reliable propulsion systems, even the structural design is relatively simple. Depending on the expected altitude and the maximum speed reached, the structure created allows the system to be assembled in all its parts.

This project targets the launch of a sounding rocket to an altitude higher than 20 km, and the purpose of this launch is to test the engine that was under research for the past years. Thus, reliable structural design and analysis is a must to ensure the success of the launch.

To have a successful launch it is necessary to be able to test the individual subsystems independently. For this reason, it has been chosen to realize a structure that can be assembled and not composed in a single piece. All subsystems are structurally supported by an external shell. This structural element is divided into parts, able to be assembled to make up the entire rocket. The outer shell does not have only the function

of keeping the rocket assembled during launch, but it is also a functional element for the subsystem.

1.2.1 Materials of the Sounding Rocket Structures Designed

To satisfy the structural lightness and the excellent stiffness and resistance to loads, the main structure is made of carbon fiber composite material.

Fiber-reinforced polymer composite materials (FRP) are finding widespread use in structural applications where high mechanical performance and low weight are required, becoming a valid alternative to metallic materials [4]. In general, the basic idea of composites is precisely to optimize, in terms of mechanical characteristics and lightness, the performance of so-called conventional materials. In fact, by combining a material with certain properties, with another witch properties are different, it is possible to obtain a material with better characteristics. The composite material consists of the union of two or more materials in different phases and quantities, resulting in a structurally highly performing material. For the realization of the rocket, composite materials are used, consisting of carbon fibers and a polymer-based matrix (epoxy resin). Due to the presence of a continuous phase (matrix) and a discontinuous phase (fiber), the composites exhibit marked characteristics of anisotropy both from an elastic and mechanical strength point of view. The degree of anisotropy depends on how the reinforcements are placed inside the layer and this can lead to an increase or decrease of this value. The anisotropic characteristics of these materials lead to a careful and accurate study for their use, in fact the composite material is often used by overlapping several layers one with the other constituting a laminate. The reason to join multiple layers is to obtain an optimal final configuration for the individual case. The response of the single lamina will be different depending on whether it is stressed in the direction of the fibers or in the direction orthogonal to them, and will be linked, all other conditions being equal, to the quantity of fibers used. The union of the different layers is given by a layer of resin which when solidified glues them.

In the *figure 5* the stress-deformation trends of the single components of a composite material are shown.

The presence of the fibers in the polymeric matrix allows to obtain a material with mechanical resistances (tensile strengths) much higher than a material consisting of

the single matrix polymer. The properties of the fibers are decreased, but in order to use them, the presence of a matrix is fundamental. Furthermore, fibers have excellent properties along their direction, and without a support (given by the matrix) they do not have flexural stiffness. The reasons for using the matrix as reinforcement on carbon fibers are:

- To give structural rigidity even outside the fiber shaft.
- Keep the fibers together without contacting them.
- Protect the fibers from the external environment such as high temperatures, presence of oxygen, contact abrasion or chemical.
- Allow the transfer of the load between the different fibers and discharge the same over the entire structure.
- slow down the propagation of cracks and defects, especially near the interfaces between the edges.

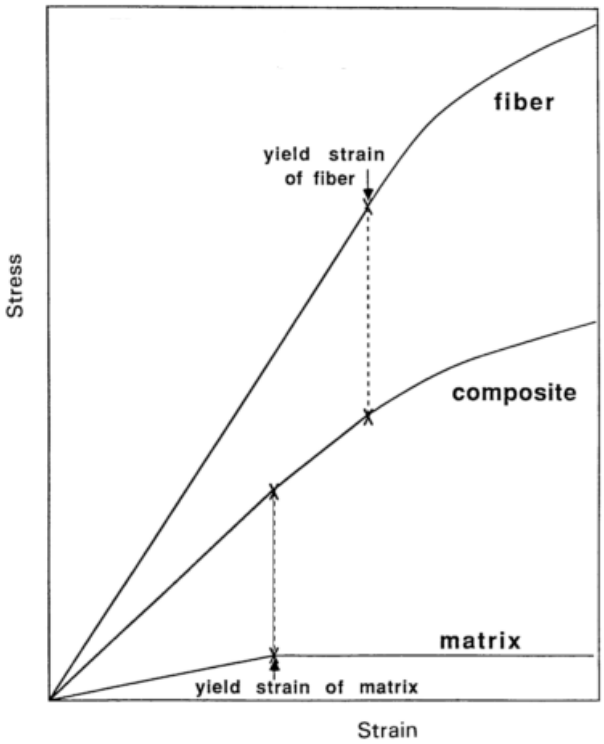

Figure 5. Composite propriety

To give shape and stiffness to epoxy matrix composite materials, a cure in autoclave is expected after lamination. This process is necessary for the correct solidification of

the resin and the correct distribution inside the laminate. The composite is prepared with a vacuum bag so that the resin and the air in excess can escape, when pressure decrease and temperature increase. Therefore, each type of lamination and process has its main characteristics, but the desired result always is that the piece does not deform, and the cure can remove the air inside the different layers.

The durability of composite structures reinforced with glass or carbon fibers is influenced by the durability of the individual constituents, the fibers, the matrix and the fiber-matrix interface. The external environment greatly influences this aspect, in fact external agents such as temperature, presence of charged particles, contact with reagent substances, etc... can greatly limit the durability of composites. In the industrial and engineering field, the choice of materials is fundamental and in the last period composites are finding wide use in substitution of metals. The difference between these two types of material are many.

Metals are homogeneous and isotropic; they have the same mechanical properties in all directions; their behaviour following the application of a load is determined once only two elastic constants that are known in the literature. However, a unidirectional lamina or symmetrical and balanced laminate is like an orthotropic material, it has three mutually orthogonal planes of elastic symmetry. In addition to the difficulties of determining the mechanical properties, the composites do not behave well when drilled or if openings are made on continuous areas. For example, without the use of inserts, the composite cannot be threaded to insert the screws, and in the perforated area there is a strong structural weakening. However, if used correctly they provide numerous advantages over the use of high-performance metals such as aluminium alloys. They give the possibility to place the layer in the most suitable direction to the applied loads, thus avoiding that part of the material goes to reinforce an unstressed direction. This aspect is very important in the space sector because it allows to considerably reduce the excess weight and obtain considerably lighter structures with the same performance. To make the rocket it is chosen to use carbon composite materials where possible, while in the more detailed structural parts high-performance aluminium alloys are used. To join together composite and aluminium are used bonded joint in order to avoid using bolted joints. Two different aluminium alloys were used for the entire rocket. The 2024-T6 series has been used in areas with greater thermal sources,

while the 7075-T6 series, commonly defined as Ergal, has been used in areas structurally lacking in important thermal sources.

1.2.2 Aluminium Alloy 2024-T6

The 2024-Aluminium alloy is used mainly in the aeronautical and space sector thanks to its excellent mechanical properties. In fact, it is the aluminium alloy with greats mechanical properties and the lowest density. The choice to use this alloy derives from the external operating temperatures during flight, which can reach 120 °C especially in some parts of the rocket that are exposed to aerodynamic frictions. In addition to the resistance of the material, and its trend as a function of temperature, it is also necessary to study the trend of the modulus of elastic resistance. As the temperature increases, the properties generally decrease due to the cohesion between the atoms and the approach of the melting point.

These properties are summarized in a *table 1* that shows the datasheet for an aluminium alloy 2000 series [5].

Aluminium 2024-T6	
Density	2780 kg/m^3
Elastic Modulus (23 °C)	72400 MPa
Poisson's ratio	0.33
Ultimate Stress (23 °C)	440 N/mm^2
Ultimate Stress (150 °C)	310 N/mm^2
Yield Stress (23 °C)	393 N/mm^2
Yield Stress (150 °C)	248 N/mm^2
Fusion temperature	635.0 °C

Table 1

Exposure of the material to a thermal source changes its physical properties. In the *table 1* and in the *figure 6* the values and trends of alloy 2024-T6 are shown [6]. Through the stress-strain curve it can be observed how the yield strength ($\sigma_y(T)$) of the material decreases together with the elastic deformation ($\gamma_{max\ elastic}(T)$) with the increase

in temperature. Through the study of the deformation it is possible to obtain the elastic modulus at a given temperature:

$$E(T) = \frac{\sigma_y(T)}{\gamma_{\max elastic}(T)};$$

The elastic modulus at 150 °C decrease of 95% to the modulus at room temperature (23 °C) while at 200 °C its decrease grows up to 85% resulting in:

- $E_{150°C}$ = 68.8 GPa;
- $E_{200°C}$ = 61.5 GPa;

These values have been taken into consideration for the analysis models implemented. It is also important to highlight how the value provided by the references refers to a simple in a thermal environment for a time of 360 seconds in the case of the elastic module, while a continuous thermal environment for the stresses. Since the sounding

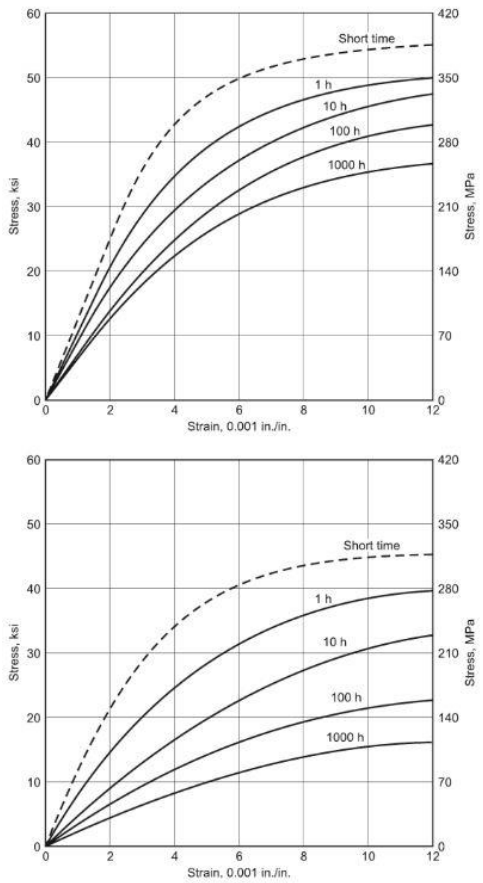

WA.047 2024-T6 aluminum alloy, isochronous stress-strain curves in tension

Tested at 150 °C (300 °F) (top) and 205 °C (400 °F) (bottom). Composition: Al-4.5Cu-1.5Mg-1Mn. UNS A92024

Source: "Isochronous Stress-Strain Curves for Several Heat-Treated Wrought Aluminum Alloys at 300 and 400 F," Alcoa Research Laboratories, 29 April 1958. As published in *Aerospace Structural Metals Handbook*, Vol 3, Code 3203, CINDAS/Purdue University, 1995, p 24

Figure 6. Aluminium 2024-T6 proprieties trend in function of temperature of the sample

rocket is exposed to an external temperature around 120 °C for a time of about 30 seconds, using these values for the analysis allows to dimension the components in safety advantage.

In the *figure 6*, the stress-strain graphs for alloy 2024-T6 are shown in the two high temperature conditions (150 and 200 ° C). Furthermore, the trends for different sample exposure times at the selected temperature are shown before the test is performed. It can be observed that for short exposure times there are increasingly closer trends to the behaviour at room temperature. The mechanical properties of the material diminish a little due to very short exposure times, allowing the properties to be used at room temperature.

1.2.3 Aluminium Alloy 7075-T6

The 7075-T6 aluminium alloy is commonly called Ergal, it is an aluminium alloy with superior properties of the series 2000 under ambient temperature conditions. It is a series widely used in the aeronautical and space field due to its excellent mechanical characteristics. In design, it is used in areas of the structure where excessive operating temperatures are not reached and where it is necessary to use metal components rather than composite ones. In the *table 2* are descripts the principal mechanical proprieties of Ergal.

Aluminium 7075-T6	
Density	2880 kg/m^3
Elastic Modulus (23 °C)	71700 MPa
Poisson's ratio	0.33
Ultimate Stress (23 °C)	572 N/mm^2
Yield Stress (23 °C)	503 N/mm^2
Fusion temperature	635.0 °C

Table 2

The properties of the Ergal compared to the 2000 series are superior for operating conditions around 23 ° C, while they decrease noticeably as the operating temperature increases. For this reason, only some components have been made in Ergal.

1.2.4 Carbon Fiber Composites

In the applications with the composite material there are three types of usable ply, the woven, the unidirectional and the biaxial. These types can be different due to the different type of material that composes them but above all for the way in which the fibers are arranged. The different layers are superimposed according to the chosen design, allowing to obtain the ideal configuration. It is important to know the properties of each individual layer to derive the mechanical properties of the final laminate. Depending on the orientation and number of layers, the optimized configuration can be obtained. The properties for the three types of layers used are shown below.

1.2.4.1 Woven

The woven fibers are woven with a specific weft and warp. These layers are mainly used as an external finishing layer to contain the lamination of the entire sheet. The fiber orientation is 0 ° and 90 ° overlapping and intertwining repeatedly [7]. The mechanical proprieties about woven layers are descript in the follow table.

Woven	
Tensile Modulus$_{11\ \&\ 22}$	60.8 GPa
Tensile Strength$_{11}$	719 MPa
Compressive Strength	719 MPa
ILSS	74.8 MPa
Density	1650 Kg/m^3
Poisson's ratio	0.28
Thickness	0.23 mm

Table 3

1.2.4.2 Unidirectional Layer

In unidirectional composites all fibers are arranged in the same direction, at 0 °, allowing us to have excellent mechanical properties along this direction. Their

application has a structural function with the possibility of orienting the layer in the desired direction [8].

T700S with Epoxy Resin	
Tensile Modulus$_{11}$	135 GPa
Tensile Modulus$_{22}$	10 GPa
Tensile Strength$_{11}$	2550 MPa
Compressive Strength	1470 MPa
In Plane Shear Strength	90 MPa
ILSS	90 MPa
90'Tensile Strength	70 MPa
Density	1650 Kg/m^3
Poisson's ratio	0.28
Thickness	0.3 mm

Table 4

1.2.4.3 Biaxial Layer

Finally, there are the biaxial composites where the fibers are oriented in two directions. In these composites the fibers are not intertwined but are two overlapping unidirectional layers with given orientation. These layers are used with structural and interlaminar containment functions [7].

Biaxial carbon fibre composite	
Tensile Modulus	63.8 GPa
Tensile Strength	1124 MPa
Compressive Strength	595 MPa
ILSS	49.7 MPa

Table 5

The lamination process of the composite structures is done by the company Sita Compositi S.r.l. expert in the composite field. To maintain a uniform thickness and a continuous structure a single composite pipe is produced with the same lamination. Subsequently the necessary components are made by cutting the pipe into several parts, in this way all the main structures follow the lamination of the most critical element made, the oxidizing tank. Since this element is subject to high internal pressure, and even to launch loads, the component is structurally the most stressed component. The chosen lamination is given through a structural study [9].
The lamination is done by overlapping more overlap obtaining a final thickness around 3 mm. And result that the total mechanical propriety of laminate composite is:

E_{11}	63.3 GPa	E_{22}	72.8 GPa	G_{12}	9.84 GPa

Table 6

To make the composite tube, the layers of prepreg composite were laminated. The lamination is made around a spindle having a cylindrical shape which gives the desired shape and tolerance to the entire structure. Externally the whole is covered with a vacuum bag for autoclaving. The pre-impregnated composites are composites with the fibers already impregnated with resin, which is already partially solidified and frozen, at moment it is used in lamination, the resin finishes solidifying and hardens, giving the properties to the composite.

Chapter 2

Sounding Rocket Design

Through the University of Padua and its spin-off the T4i (Technology for Propulsion and Innovation), the project to launch a sounding rocket is being carried out and the flight is planned by the beginning of the year 2020. The mission has the main objective to study the flight behaviour of the engine designed and tested in these years. A reduced model for rocket sounding with a power of 5 kN was made from the 7 kN test engine. The fuel used is paraffin which is combusted with O_2 gaseous oxygen at high temperature produced by the decomposition of hydrogen peroxide (oxidant). The system used upstream pressurization made by N_2 gas; the nitrogen is stored in a tank separate from that of the oxidant to maintain the latter under constant pressure.
In the *figures 7* is shown the rocket designed by the students and researchers of the University of Padua.

Figure 7. Sounding Rocket

The rocket can be divided by subsystems, which take their name from their main function. Five subsystems can be obtained, from the tip to the end of the rocket, respectively: the avionics subsystem, the recovery, the gaseous fluidics, the liquid fluidics and the engine with the nozzle. By dividing the rocket into separate subsystems it is possible to test individually allowing greater safety in the test phase, this also allows that in the pre-launch phase in case of malfunctions it is possible to operate with the replacement.

The rocket has a size of about 5 m in length and 0.2 m in diameter, the altitude that can be reached as a theoretical estimate is more than 20 km with a maximum speed M=2 (M is the Mach number). The structure and also some internal components are made of composite carbon fiber, making the development very modern and an excellent basis for future developments.

The individual subsystems are briefly described below.

2.1 Avionics Subsystem

Avionics is contained in the nosecone which is the tip of the rocket.

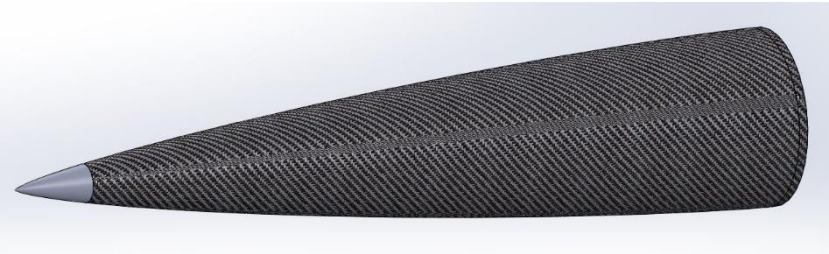

Figure 8. Nosecone

The nosecone must be independently assembled. The design of the nosecone includes a laminate central body following a Von Karman profile, a metal tip insert and a bottom laminate cylindrical ring to allow the fastening to the recovery bay.

To reduce drag the nosecone has a Von Karman profile. This profile has been chosen due to the maximum Mach number of sounding rocket and the duration of flight. Von Karman's profiles are built using the following mathematical equations:

$$\theta = \cos^{-1}\left(1 - \frac{2x}{L}\right)$$

$$y = \frac{r}{\sqrt{\pi}} * \sqrt{\theta - \frac{\sin(2\theta)}{2}}$$

Where:

- r: final radius, in this case 97.9 mm;
- L: total length of the nosecone;
- y: instantaneous diameter of the nosecone along the distance from the nosecone tip.

For the length of the nosecone the parameter L/D has been fixed, which corresponds to the length of the nosecone in relation to the diameter. This value derives from the analytical study of how different ratios influence lift and drag during the flight phase. As the length of the nose increases, the drag increases in subsonic but decreases in supersonic. In this scheme the increase of L/D decreases the *wave drag* because the shock waves are weaker having a smaller angle of deviation. Increasing this ratio too (fineness ratio) can however be counterproductive in that the surface is also being increased in contact with the fluid. Increasing the *skin drag*. The length of the nose must therefore be chosen in order to balance these two components to find the minimum drag. The value chosen for the ratio L/D is equal to 4.7.

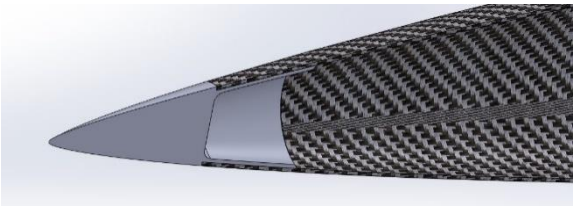

Figure 9. Nosecone Tip View

The nosecone is one of the elements exposed to greater thermal stress having the stagnation zone at its tip. For this reason, it is important that it is thermally shielded and appropriately designed to prevent the creation of structural damage. Considering a maximum temperature of 300°C, an aluminium insert has been chosen. The connection with the composite structure happens through adhesive bonding.

Since it will be realized on female moulds, the external surface will have a good surface finishing ensuring a good aerodynamics. On the inside the geometric definition

is not guaranteed. The internal diameter could be different from the designed one at the section could be ovalized. Thus, the connection metal part of the recovery bay should have a diameter slightly bigger than the internal diameter of the nosecone, allowing machining processes once the nosecone has been realized and its actual measurement are known.

The purpose of the avionics is to receive the operating data of the entire rocket in real-time and to be able to memorize and send it to the ground. Moreover, it allows managing the activation of some electronic valves present in the fluidic line to determine the rocket operation or the possible abortion of the mission. It is equipped with a power system for its operation and is sealed to avoid damaging the memory during the ditching phase. Inside there are accelerometer sensors, and a GPS to track the rocket when it returns to the ground.

2.2 Recovery Subsystem

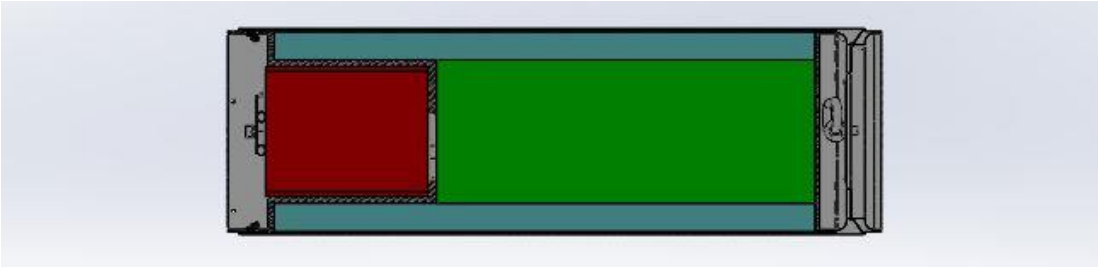

Figure 10. Recovery Subsystem

The recovery subsystem placed between the nosecone and the gaseous fluidic line aims to allow the rocket to slow down and float at sea. Most of the European launch bases are in coastal areas with the launch window on the sea. This is for security reasons. For this reason, the spaces have been prepared to contain the floating systems; while to slow down the rocket descent, it was decided to use a parachute system which is deployed through a lateral opening during descent. To avoid damage during deployment, shock cords are used, which are linked to the entire rocket structure. A door has been set up for the opening system, with the possibility of being opened about an opening mechanism controlled by avionics. When the panel is opened, a parachute is first extracted in order to slow down the descent of the rocket, to then open a second

parachute with the function of further slowing down the descent and letting the floats escape by inertia. At the moment of arrival at sea to avoid losing the system, some floats swell in contact with water through a CO_2 cylinder. For this reason, the spaces have been prepared to contain the floating systems. The sizing has been done to obtain the desired impact speed with the ground without causing the whole rocket to break.
The system was placed in the final part of the rocket to separate the components used for the ascent phase from those for the descent phase. In this subsystem, it is very important the correct functioning of the parachute opening and exit mechanism. Since the opening speed is high and the system is made of ropes, it must be carefully designed to prevent it from tangling. Also, the floats have been sized to ensure the flotation of the rocket.

2.3 Gas Line and Fluid Line Subsystem

Figure 11. Fluidic Subsystem

The fluidics system is described by combining the gas and liquid fluid subsystem. There are two tanks, the first smaller contains the pressurizer (N_2) at a pressure higher than 200 Bar. Its presence is essential to guarantee the functioning of the engine and the entire mission. The second is the oxidizer tank which contains hydrogen peroxide kept in pressure by the pressurizing gas that flows controlled. The connection between the two tanks is made by the gas fluidic line to control the flow of pressurizing in the oxidizer tank. Inside, safety valves have been set up to prevent overpressure of the various components and also structural supports have been prepared to avoid vibrations or excessive loads on the connections between the various components of the fluidics. Through a pressure regulator, it was possible to guarantee an almost constant operating pressure on the oxidant, allowing the hydrogen peroxide to flow into the motor at a set pressure. By pressurizing the oxidizer tank while maintaining

an unchanged operating pressure as it is emptied, it is possible to guarantee a constant engine speed operation. The liquid flow is introduced to the motor through a line of the fluidics that allows the operation. In this part of the system, there are safety valves with the possibility of stopping the flow in the event of a malfunction.

2.4 Engine Subsystem

The engine subsystem consists of a combustion chamber where the fuel is stowed, a catalytic to decompose the oxidizer, and the nozzle. The motor is assembled separately to the rocket and then interfaced with the fluidics connections and through a junction with the structure. Its components are designed to withstand operating pressures in order to guarantee their operation. The flow of hydrogen peroxide comes into contact in a catalytic which has the function of decomposing it producing the gaseous oxygen at high temperature. The gases leaving the catalytic react in the combustion chamber with the fuel-producing the combustion that propagates throughout the chamber. Finally, all the products are propelled through the nozzle. Structurally the loads are kept through an external carbon composite case. Inside the engine, the thermal loads are contained by the same paraffin which liquefies and evaporates, thus avoiding the propagation of the thermal gradient by shielding the external area. In this system the positioning of the nozzle with respect to the rocket is very important to obtain the alignment of the thrust. Its geometry also makes it possible to obtain the performance of the I_{sp} according to the height to obtain the maximum thrust performance.

2.5 Structure Subsystem

The structural subsystem is designed to guarantee the assembly of the other subsystems ensuring structural strength. Another important aspect is to allow the rocket to be aligned within the set requirements. It also allows the interior of the rocket to interface with the outside through special openings. The structural part also includes the configuration of the joints that allow the assembly and the fin elements.

The main structure is made by laminating composite carbon fiber material, in a spindle which allows to guarantee the tolerances and the alignment of the tube made. To the access of fluidics four openings have been made. This allows access to the valves even when the rocket is on the ramp. To avoid structural weakening, it was decided to reinforce the composite through a metal frame. This frame also acts as a support to screw the panel externally to close the access and guarantee the maintenance of the aerodynamics. The presence of these openings makes it possible to assembly the fluidics and subsequently close the system. The size of these openings has been realized allowing to have enough space to access with the wrenches and to be able to operate on the whole line of the fluidics. The metal reinforcement was inserted both on the panel and on the rocket structure and was glued, allowing the two parts to be joined by screws. The function of this reinforcement is twofold, it allows the two parts to be joined together with simple assembly and disassembly, and in the same way it allows to reinforce the external structure where the opening was made.

Another important element for maintain the trajectory during the launch are the fins. The function is to guarantee lift during the flight to reach higher maximum levels. As the geometry of the fins, a rectangular trapezoid shape was chosen, this for simplicity in the realization and alignment phase, furthermore this geometry allows to obtain minor movements when stressed. At Mach greater than one the geometry has no influence on lift, but this depends only on the total area of the fin. Four have been inserted to obtain smaller dimensions and greater aerodynamic symmetry. They are fixed on the rocket near the nozzle with a special insert. The material with which the fins are made is such as to withstand the high temperatures reached, allowing the fins to be kept in position and aligned. In the part of the tip is used a metal for high temperatures which interfaces with the central carbon area which is made of composite material. The resin used for the composite layers in this area of the rocket is an epoxy resin for high temperatures. By symmetry and to obtain smaller fins dimensions, four fins of equal size were used. This allowed the area of each individual fin to be reduced and therefore to reduce the problems due to bending under the lift loads. Finally, the last elements that make up the structures are the joints. These were used to assemble and allow the subdivision of the various subsystems. They interface with the two adjacent structural components and are fixed allowing structural continuity.

Chapter 3

Junction in the Sounding Rocket

The various subsystems are connected to each other through metal junctions that allow the structural strength and assembly of all system. In the overall system, four junctions were necessary to connect the five subsystems created. Each individual joint is divided into two parts, one upper and one lower, which are join together by screws. The joints chosen are with symmetrical axial geometry and have been sized to withstand the launch loads. Being an element of structural discontinuity, it is important that it guarantees the overall alignment of the system and transfers loads homogeneously. The material chosen to make them is aluminium alloy 7075-T6 for its high mechanical properties; to connect the two parts are used screws that are stressed only to shear. This choice was made both to limit the overall height of the joint, and to prevent any combination of forces acting on the screws. Based on the theory for bolted elements the junctions were dimensioned, both the study on the single screw and on the forces acting on the junction element were considered.

3.1 Theory of Bolted Joint

The bolted elements are widely used in the structural field as they allow two elements to be connected and disconnected several times, allowing assembly without difficulty. The bolted joint is composed of two or more plates that are fixed together by a bolt. The bolt is make by a threaded screw and a nut, sometimes the nut is replaced by a thread hole on the plate to be fixed. The screw element is made from two different parts, the stem which can be totally or partially threaded and the head of the screw which differs according to the applications. The functions of the screw head are multiple, the main function is to allow the screw to be tightened using tools, but it also has the function of distributing the working stress on the flange avoiding localized stress. Its shape can be chosen to allow it to adapt to the material of the plates and to

the spaces available for fixing. Another important element of the screws is the type of thread. In fact, there are more thread geometries depending on the application of the screw, the most common in the structural field are the triangular threads; while conical threads are used in the context of connections for fluidics elements.
In the design phase it is useful to study separately the behaviour and the loads acting on the screw and on the fixed elements (flanges or plates).

3.1.1 The Screws

The screws are elements that can be represented as bars that have the function of connecting and joining two elements. They were the first connecting elements and are still used in the engineering field.
By law the screws are divided into classes of resistance. Each class, identified by two numbers, satisfies the certified and tabulated structural properties [10]. The material with which the different classes are made is steel and its resistance is often directly proportional to its fragility. Through the resistance class it is possible to ascend through tables how much the yield and ultimate strength limits. Through these values, by imposing the safety coefficient the tensile and shear resistance is obtained. The class of resistance are composed by two numbers. The first number represents the breaking load divided by 100, the second represents the yield strength as a percentage of the breaking load.

Class of Resistance	Ultimate strength [MPa]	Yield Strength [MPa]
3.6	300	180
4.6	400	240
4.8	400	320
5.6	500	300
5.8	500	400
6.8	600	480
8.8	800	640
10.9	1000	900
12.9	1200	1080

Table 7

Classes 8.8, 10.9 and 12.9 are used for aerospace and structural applications as they are those with the greatest resistance.

As the strength of the material increases, so does fragility, this limits the application where the screw must withstand impulsive load.

In the project of sounding rocket using the safety coefficient sf = 2 the admissible values of stress and shear strength are obtained:

$$\sigma_{adm\ screw} = \frac{yeild\ strength}{sf},\ \tau_{adm\ screw} = \frac{yeild\ strength}{sf\sqrt{3}};$$

These values obtained must be compared with those that act on the screw when the system is loaded.

Two types of forces can act on the screw, axial and transverse. The axial forces act in the direction along the axis of the screw and determine the axial stresses of both compression and traction depending on the direction of the load (defined as sigma σ) whose value must be compared with the $\sigma_{adm\ screw}$. The forces transverse to the screw axis generate shear stresses (taw τ) whose value must be compared with the $\tau_{adm\ screw}$. The shape of the section has no influence on the calculation of deformations and tensions. In mechanical applications it is possible that the forces act in a combined manner and therefore there are simultaneously sigma and taw [11]. Depending on whether only a combination of tensile or shear forces are involved, tensile and shear connections are called respectively.

3.1.1.1 Connections in Shear

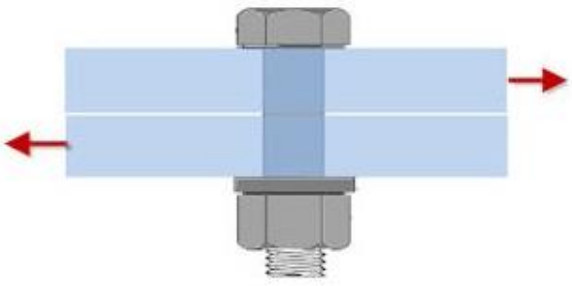

Figure 12. Connection in Shear

When designing bolted joints, you can choose to design the friction or shear connection [11]. The joints designed to resist friction are used when there is no need for relative displacements between the two plates. In this case, all the force that must support the joint is supported by the friction developed by the head of the screw and the nut with the respective plates. All bolted joints have an initial resistance due to the friction of the screw with the plates, when the friction resistance force is exceeded relative displacements take place between the plates (due to the coupling tolerances) and the junction only supports the shear force. In the shear joint it is important to define how many sliding planes there are, this because it allows to define in how many sections of the screw the load is divided. and consequently, also how much is the maximum load that can sustain the joint. As mentioned above, transversal stresses generate shear stresses on the screw, to determine its value one must proceed by studying case by case in order to observe where and with what intensity the forces act. In the case of elements that resist shear, the forces act on the section of the screw that coincides with the sliding planes.

To define the number of sliding planes, just do:

$$n = N - 1;$$

with *n* the number of sliding planes and *N* the number of plates that are joint.

If the total force *F* acting on the joint and the area of the screw section is known, it is possible to define a shear stress given by:

$$\tau_{screw} = \frac{F\gamma}{nA_{screw}};$$

The area of the screw section depends on the diameter of the screw used but also if the screw is completely threaded or partially. If the section under load is the threaded section, the area with the smallest diameter is taken as the area of the screw, if the section that resists cutting is that on the part of the unthreaded, the nominal diameter is taken for calculating the area of the screw.

$$A_{screw} = A_{res} = \frac{\pi d_{pitch}^2}{4};$$

while when the section is on the nominal diameter the area is:

$$A_{screw} = A_{nom} = \frac{\pi d_{nom}^2}{4};$$

The value of the parameter γ is usually equal to $\gamma = 1.25$, and is a value used to consider that in the real case bending moments can develop that cause an increase in stress on the screw. This value can be changed by the designer depending on the type of system and how reliable the representation of forces is. The τ_{screw} value obtained must be compared and lower than the admissible one obtained on the screw. If the value obtained is lower than the admissible one, the screw does not yield and the junction operates correctly. If the value of the taw obtained is higher than the admissible one, then the bolted union fails and it is necessary to increase the design diameter of the screws, increase the sliding planes or increase the number of screws.

3.1.1.2 Connections in Traction

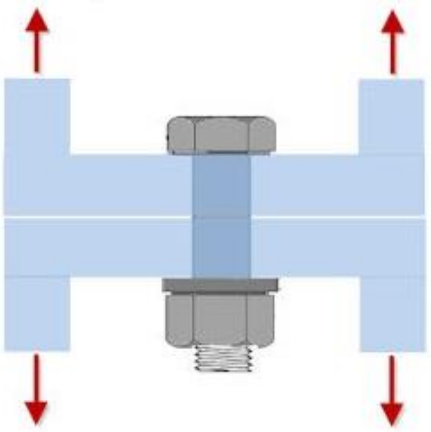

Figure 13. Connection in Tension

When forces act in the axial direction respect to the screw it is called load in traction. In this case the number of sliding surfaces no affects the stress on the screw. All the load *N* is supported by the head and the thread of the screw, in this case axial stresses are developed, defined as sigma (σ).

$$\sigma_{screw} = \frac{N\gamma}{A_{screw}};$$

Gamma represents, as in the case of pure cutting, the presence of a bending moment due to a real case that can deviate from the ideal one. The value of sigma obtained from this formula must be compared and less than that allowed for the screw. In the case of tensile load, the screws are produced with geometries such as to always yield the shank before the threads. In any case, checking the size of the loaded threads is

important. Depending on the geometry of the thread, the load distribution is distributed differently between the threads [12]. In general, you always choose to use five fillets, but it is shown in the *table 8* in the case of screw in traction as the load% is divided between the threads.

SCREW WITH THREAD	N° THREAD	% of N_1	% of N_2	% of N_3	% of N_4	% of N_5	% of N_6
TRIANGULAR COMPRESSED	6	33.9	23.0	15.8	11.3	8.6	7.4
TRIANGULAR TENSILE	6	25.9	18.6	14.4	12.2	13.0	15.5

Table 8

For simplicity of accounts and to increase the safety factor in the calculations it can be considered that the first thread resists 33% of the overall force thus obtaining:

$$F_{yield\ thread} = \frac{\tau_{adm\ screw}(\pi d_{pitch} * p_{screw})}{0.33};$$

where, p_{screw} is the pitch of the screw and represent the distance from two peack of threads.

3.1.2 Sizing of Bolted Plates

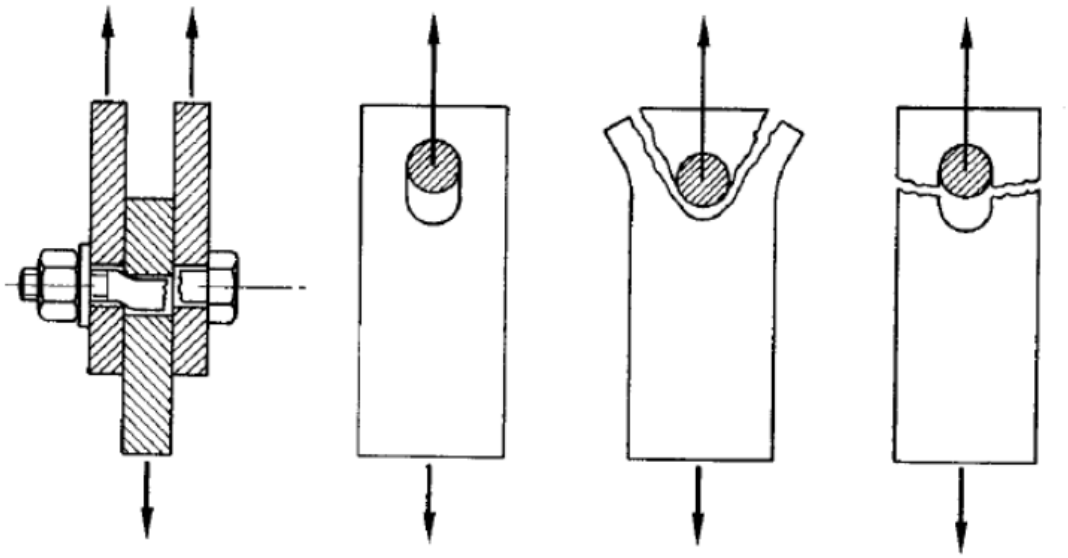

Figure 14. Bolted Plate Rupture

In addition to the stress on the bolt, the other elements subject to the load are the plates to be tightened. Subjected to loading may occur in addition to the bolt breaking, three types of junction failure. This because the load is transferred from one sheet to another through the holes and consequently through the bolt. The bolt generates surface pressures in the area of the holes that must be supported by the sheet material. The failure criteria of the sheet are represented in the *figure 14*, the first has already been described in the paragraph dedicated to the screws, the other three will be described. From left to the right of the *figure 14* the failure represented are respectively, rebounding, breaking by shear, breaking by traction.

The rebounding: in the breakdown mechanism due to rebounding, the collapse of the joint occurs due to the plasticization of the hole of one of the connected sheets. When the steel around the hole is completely plasticized, it is assumed that the stress distribution is constant and equal to the characteristic value at break. The following formula is used for calculating the force required to carry out refilling:

$$F_{rebounding} = \alpha\sigma_{adm\ sheet} * d_{screw} * t_{min};$$

Sheet breaking by shear: when the sheet is broken due to shear stresses there is yielding around the hole in the direction of the applied load. It is show in the *figure 14*. To calculate the force required for shear failure, the resistant area must be calculated from the hole to the edge of the sheet:

$$F_{shear} = \tau_{adm\ sheet} * A_{shear};$$

$$A_{shear} = t_{min} * (a - \frac{d_{hole}}{2});$$

Sheet breaking by traction: tensile rupture is like the previous one (by shear), except that the section of area that fails is orthogonal to the applied force. The failure area is calculated in the direction of the free edges except for the presence of holes:

$$F_{tensile} = \sigma_{adm\ sheet} * A_{tensile};$$

$$A_{tensile} = t_{min} * (l - d_{hole}k);$$

For these formulations the meaning of the nomenclature used is clarified:

- $\alpha = \frac{a}{d_{hole}}$ is the ratio that considers the distance of the hole from the edge of the sheet, the alpha value must be $\alpha \leq 2.5$.
- d_{hole} is the diameter of hole for the screw.
- t_{min} is the thickness, of the sheet with minimum thickness.
- k is the number of screws in the transverse load direction.
- a is the distance from the centre of the hole of screw and the free edge of the sheet.

To position the screws on the sheet at the correct distance from the free edges we use standard values (according to CNR 10011). these values represent limits for which maximum structural strength is obtained, however they can be modified if the project requirements impose it. The parameters to be respected for the dimensioning of the plates or perforated elements are described below.

Hole spacing (p):

- for compressed elements $15t_{min} \leq p \leq 3d_{hole}$
- for traction elements $25t_{min} \leq p \leq 3d_{hole}$

Distance from free edge (a):

- in the direction of strength $a > 2\ d_{hole}$
- for edge not stiffened $a \leq 6\ t_{min}$
- for stiffened edge $a \leq 9\ t_{hin}$

Distance from free edge (a_1):

- in a direction orthogonal to the force $a_1 > 1.5\ d_{hole}$
- for edge not stiffened $a_1 \leq 6\ t_{min}$
- for stiffened edge $a_1 \leq 9\ t_{hin}$

In the *figure 15* an illustrative image is shown which indicates the position of the parameters described above.

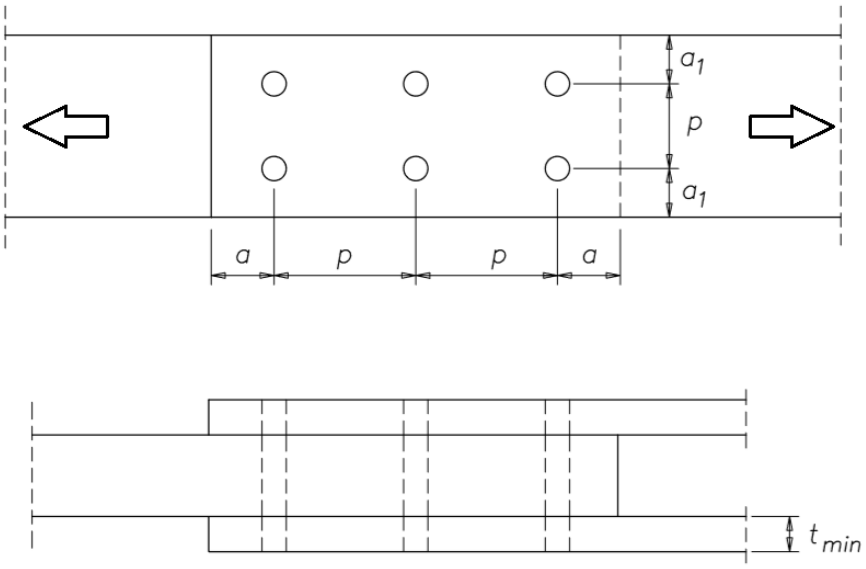

Figure 15. Rebounding Parameters

3.2 The Junctions of Sounding Rocket

3.2.1 The Loads Acting

Four junctions have been designed in the sounding rocket, their design depends on the loads they must withstand and the maximum dimensions they can support. In this chapter they are described individually showing the details and the structural characteristics that characterize them. The information on the structural theory described above is used in all junctions. Four junctions have been designed in the sounding rocket

By investigating the stresses acting on these junctions, there are two loads to which it is subjected; the first are the aerodynamic loads in flight, the second are those due to the engine running. Assuming zero angle of attack, the aerodynamic forces are produced by the fins and the nose. The fins produce more force than the nose. If we apply the resultant of the single components in their centre of pressure, we can notice that being the strength of the nose less intense, it is necessary an arm (with respect to the centre of unknown pressure) greater than that of the fins to balance the force. The centre of pressure will position itself more towards the aft of the rocket, at the point where the aerodynamic moments are zero. When the angle of attack increases, the flow also impacts the body of the rocket, increasing the pressure on the exposed surface.

This causes the pressure distribution to change, moving the centre of pressure more toward the centre of gravity.
This is show in the *figure 16.*

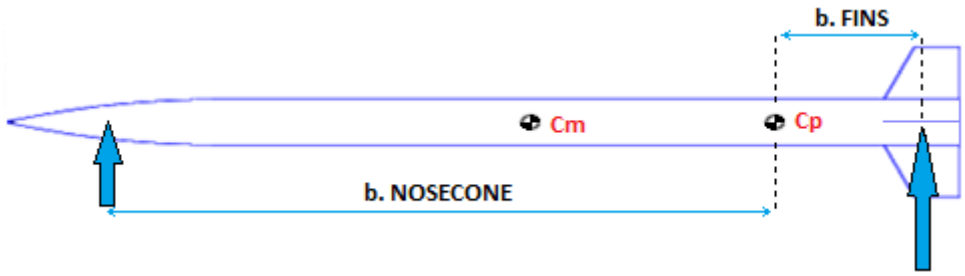

Figure 16. Areodynamic Force

The values of aerodynamic loads in the case of flight with a non-nominal trajectory can be represented by a force of 1000 N applied to the centre of pressure of the nosecone which exerts both a constant shear force over the entire rocket, both a bending moment and at the most critic develops 4000 N*m. The junction between the motor and the fluidic line is the one most subject to this type of stress. Moreover, during the flight phase the thrust of the engine generates an axial load of 5000 N. This force generates a maximum acceleration around 50 m/s^2 comparable to five times the gravity to the ground.

3.2.2 Junction n°1

This junction is located at the bottom of the rocket and acts as an interface between the catalytic dome and the structure that contains the fluid of the oxidant. The entire joint must guarantee structural functioning when subjected to loads mentioned above. In the *figure 187* can be observe a section of the junction in question. In this junction there are three components, an upper flange, a lower flange and screws for fixing both to each other. The two flanges are made in Ergal. To avoid loads in multiple directions on the screws it was decided to insert in transverse position for permit at the load to act only by shear. In this way the two plates perform a cutting action with a sliding plane in the median section of the screw. To maximize the resistance of the screw and reduce the clearance of the joint, ISO 7379 type screws have been chosen. These screws have the particularity of having the shank partially threaded with an f9 tolerance and with different diameters between the threaded part and the non-threaded

part. In this way they can be inserted by small clearance into the hole and guarantee the contact and alignment of the joints.

For the connection, M3 threading screws and M4 rectified shank with a 10.25 mm length for the ground shank have been provided. The head of the screw has an internal hexagonal to allow easy fixing of the screw and limit protrusions or holes that can affect the aerodynamics of the rocket. The accounts that justify the number of screws and their diameter are shown below.

The number one joint is also the one most stressed by the loads described above. Its position is close to the centre of pressure so that the load is of greater intensity than the others. By limiting the resulting loads there is the presence of a bending moment,

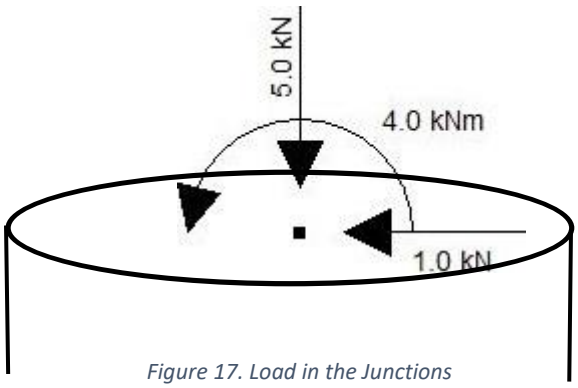

Figure 17. Load in the Junctions

a transverse cutting force and an axial load. As shown in *figure 17*, by simplifying the section of the rocket as cylindrical, we have the distribution of the forces acting on the plane of the section. The section shown corresponds to the junction to be sized. In this way it is possible to determine the direction of the loads and apply them correctly for the design and verification of correct operation. Subsequently the individual loads and their action on the joint are described.

The bending moment causes a tension state of forces in compression for half of the section, and tensile forces in the other half. The peak of the maximum acting force is where the distance of the section is maximum with respect to the neutral axis, where the moment acts. According to the theoretical formulas, the maximum tensile or compression stress generated from the moment is:

$$\sigma(y) = \frac{My}{J};$$

Where y is the distance from the neutral axis, $M = 4000\ N*m$ is the moment acting and J is the inertia of the section. The behaviour of the sigma in the section plane is linear with the distance from the neutral axis, it is possible to easily calculate the integral of the sigma in a section portion. The geometry of the (circular) section is known and therefore also its inertia. Now proceeding with a simple convergence iterative method hypothesizing a number N_{screw} of total screws for the junction, it is possible to determine the portion of section that the load on the single screw act. Placing ourselves in the most disadvantageous case, we analyze the screw on which the greatest effect of the forces acts. Note the respective section area is extrapolated the force (Q) acting on the screw:

$$Q = \frac{\sigma_{AVG}^{max} A_{tot}}{N_{screw}};$$

where,

$$\sigma_{AVG}^{max} = \frac{\sigma(y_{max}) + \sigma(y_{min})}{2};$$

with y_{max} and y_{min} respectively the sigma in the maximum and minimum distance from the section axis, for the selected portion of area (A_{tot} / N_{screw}).

Notice this strength. it is possible to add the respective axial force due to the thrust produced:

$$S = \frac{T}{N_{screw}};$$

with, $T = 5000\ N$ (thrust).

The resultant of these two forces must be applied to the screw as a shear force and the taw must be obtained on the screw. The vaue of this shear stress must be compared with the admissible one and iterate the process by increasing or decreasing the number of screws to optimize this value. To create these accounts a script was created in MATLAB, in order to optimize this value. It therefore appears that using n°28 M4 rectified shank screws are enough to withstand the imposed load with a safety factor equal to $sf = 2$.

The result of the entire joint connecting the motor to the fluidic line is shown in the *figure 18*. To return to the overall tolerances of the entire rocket, two flat surfaces are contacted between the junctions. In this way it is easy to guarantee the desired alignment and its realization.

Considering the screw with greater stress, results a local equivalent force Q=3000 N. The stress values on the screw and on the plate are obtained through the formulations in the previous chapter:

$$\tau_{max\ screw} = 297\ MPa < \tau_{adm\ screw\ class\ 12.9}\ (1080\ MPa) * \alpha_1$$

$$\sigma_{rebounding} = 187\ MPa < \sigma_{adm\ Aluminium\ 150°C}\ (248\ MPa) * \alpha_1$$

In the calculations the gamma correction factor is γ=1.25 and α_1=2

The type of screw used is a ground screw with a nominal diameter of 4 mm and a nominal diameter in the threaded area of 3 mm. For the analytical calculation the larger diameter was used as it is the one that will be in first contact with the elements of the joint.

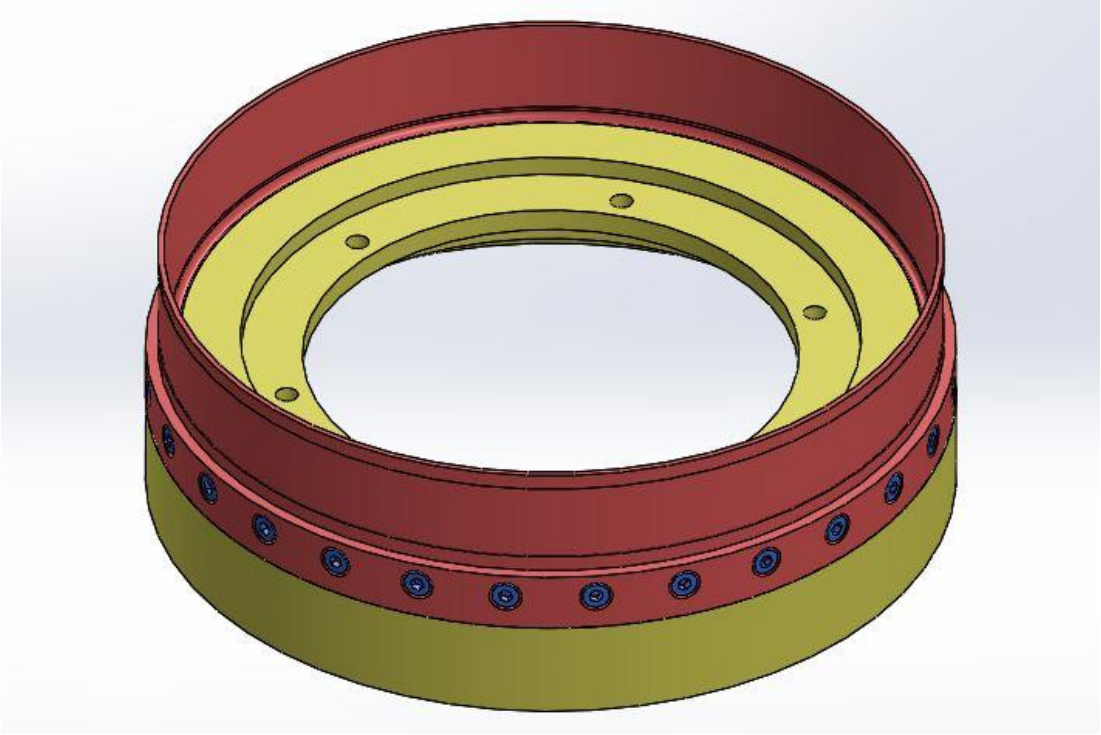

Figure 18. Junction n°1

In this first junction the type of bonding involves using a single lap joint for the upper part, while a scarf gluing for the lower part. This is because in the engine area there is a need for radial space and there is an additional load due to pressure.

3.2.3 Junction n°2

Junction number two is positioned at the end of the oxidizer tank, with the function of connecting the tank with the part of the fluidics that regulates the flow of pressurizing. This junction is positioned towards the middle of the rocket and is subject to structural loads. The design uses the same as the previously indicated joint, with the difference between the lower gluing that is the same as the upper one and the single-lap joint instead of the scarf joint. The number of screws used is 28, and it was decided to use screws with grinding shank to guarantee the least possible clearance at the joint. The thread of the screw is made to protrude because it was necessary to couple only five threads. This made it possible to reduce the weight and size of the joint. Another advantage of using orthogonal positioned screws is that they can be externally screwed and the junction height decreased. The same number of screws of junction one is maintained because it is possible to obtain a reduction in costs during construction while maintaining the same upper part. Furthermore, the agent loads are still important and this allows for greater safety.

Both parts are made by numerical control machining starting from raw material of aluminium alloy 7075-T6. The reason for this processing is due to the high tolerances required to ensure alignments during assembly.

Through an estimate of the loads act in this junction during the launch phase are highlight: a compression load due to the thrust produced by the rocket of 50 m/s^2, the bending moment acting with a value of 3000 N*m and an effort cutting of 1000 N in the orthogonal direction. The values of the loads concerning the previous junction have decreased due to the different position along the rocket and the internal pressure load is absent. The stress resultant in the most stressed screw, is about Q=2200 N, and the stress values on the screw and on the plate obtained are:

$$\tau_{max\ screw} = 175\ MPa < \tau_{adm\ screw\ class\ 12.9}\ (1080\ MPa) * \alpha_2$$

$$\sigma_{rebounding} = 110\ MPa < \sigma_{adm\ Aluminium\ 150°C}\ (248\ MPa) * \alpha_2$$

In the calculations the gamma correction factor is γ=1.25 and α_2=2

The values lower with respect to junction one because the applied loads have decreased. In the *figure 19* it is possible to observe the junction two with a section view. As you can see, there are two parts, one upper and one lower, joined by screws.

The geometry of the junction in the vicinity of the screw derives from the dimensioning to avoid breakages due to the rebounding. Furthermore, it is possible to observe a

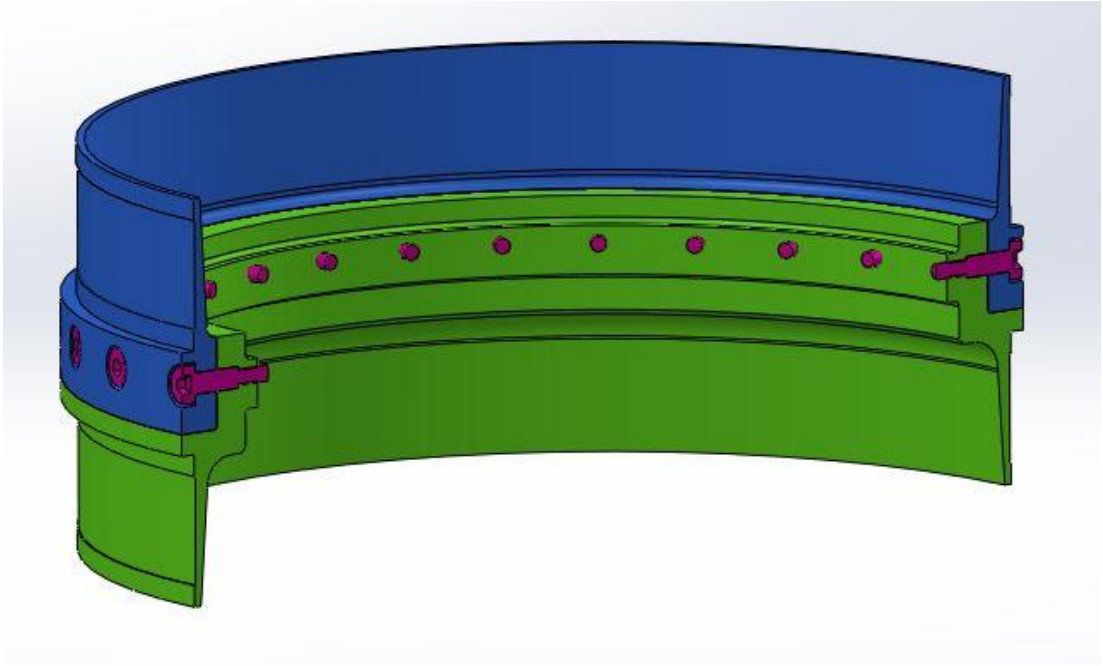

Figure 19. Junction n°2

gluing area with a geometry. In addition to the length dedicated to bonding obtained from the analysis of the agent loads, it is possible to observe two protrusions at the ends of the bonding. These are inserted to allow during assembly, to guarantee a uniform thickness of glue along the entire surface to be glued. A further reason to realize this type of geometry is because the carbon tube undergoes an ovality during the processing so that it is possible to slightly deform the tube to obtain the desired thickness of glue anywhere.

3.2.4 Junction n°3

Junction number three is present as interface between the recovery and the fluidics system. It is located at the top of the rocket and has a dual function. The first like all the other junctions is to guarantee the coupling and the alignment between the two subsystems integrated between them. The second is that of being able to guarantee the coupling of the parachute to the rocket. In fact, the upper part of this junction has been appropriately designed to withstand the opening of the parachute during landing. In the *figure 20* the junction is shown through a cross section.

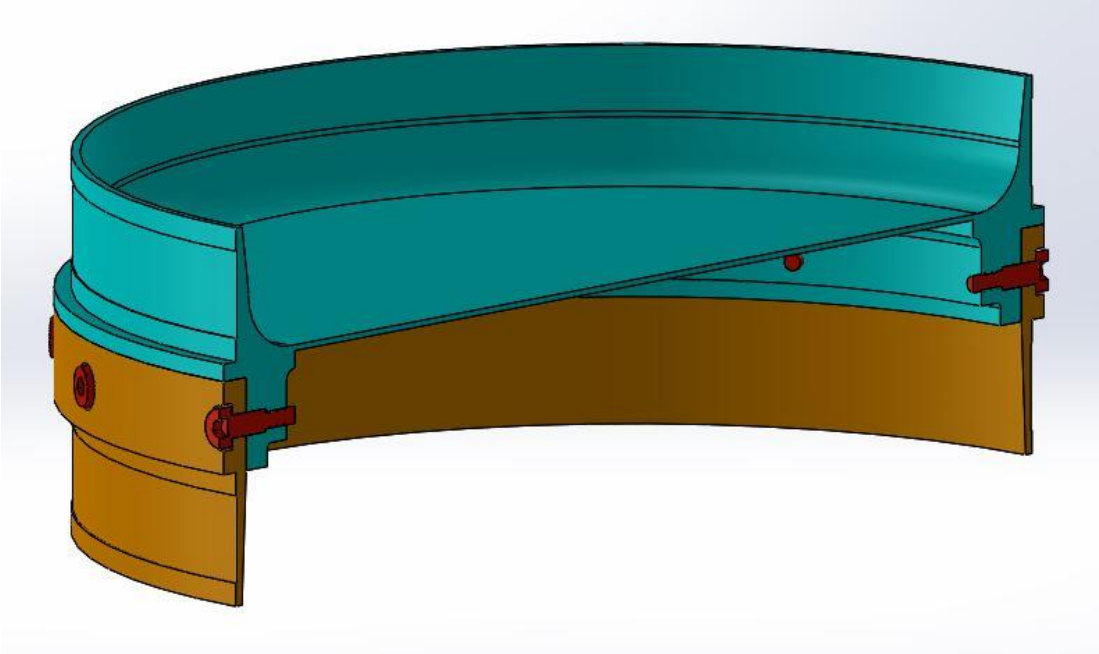

Figure 20. Junction n°3

The areas used for gluing reflect the geometry of the previous joints, guaranteeing the advantages described. Unlike the previous joints, a smaller number of screws (14 grinding screws) were used, due to the decrease in loads that the joint must bear. A requirement that this junction must is that it must allow the passage of the pressurizing tank inside it. Given the dimensions imposed by the composite carbon cylinder, the remaining space between the cylinder and the tank imposed a junction in the lower part with thicknesses lower than the previous ones. Note the external dimension of the tank defined by the manufacturer of 182 ± 3 mm, the joint has been designed so as to satisfy the assembly and to resist the imposed loads. To reduce the overall dimensions in the cross section and the size of the plates, screws with a grinding length of 8 mm are used. The overlap area for gluing has been reduced by 5 mm as the loads have been significantly reduced.

The bending moment is 2000 N*m and the axial load due to the thrust is decreased because the mass above decreases with the approach to the rocket tip. The result of the stresses acting on the joint screws and on the perforated area are:

$$\tau_{max\ screw} = 235\ MPa < \tau_{adm\ screw\ class\ 12.9}\ (1080\ MPa)$$

In this case there are two distinct cases for the rebound, as the screw does not rest with equal area on both plates, in the lower one there is a smaller thickness of support.

$$\sigma_{rebounding\ upper} = 160\ MPa < \sigma_{adm\ Aluminium\ 150°C}\ (248\ MPa) * \alpha_3$$

$$\sigma_{rebounding\ lower} = 218\ MPa < \sigma_{adm\ Aluminium\ 150°C}\ (248\ MPa) * \alpha_3$$

In the calculations the gamma correction factor is γ=1.25 and α_3=2.

After the flight phase at the opening of the parachute the distribution of the forces varies and there is a force at the opening of 2000 N in an almost axial direction at the anchor point in the upper plate. The value is lower than that used for sizing in flight, so this value was not taken into account on the screw elements. Instead it is necessary to evaluate and size the plate where the parachute is bound.

3.2.5 Junction n°4

The fourth junction is positioned between the nosecone and the recovery. Its main function is to join and hold the nosecone in place during the flight; moreover, it has special supports to fix some components of recovery and avionics. Unlike the previous junctions described, it does not interface in both parts through two buildings but is glued to the external structure of the recovery and the nosecone is joined by screws. The nosecone is fixed by screws to be easily disassembled and reassembled reducing the number of parts of the joint. The reduced intensity of the acting forces allows the nosecone to be connected directly to the metal junction through holes in the composite material.

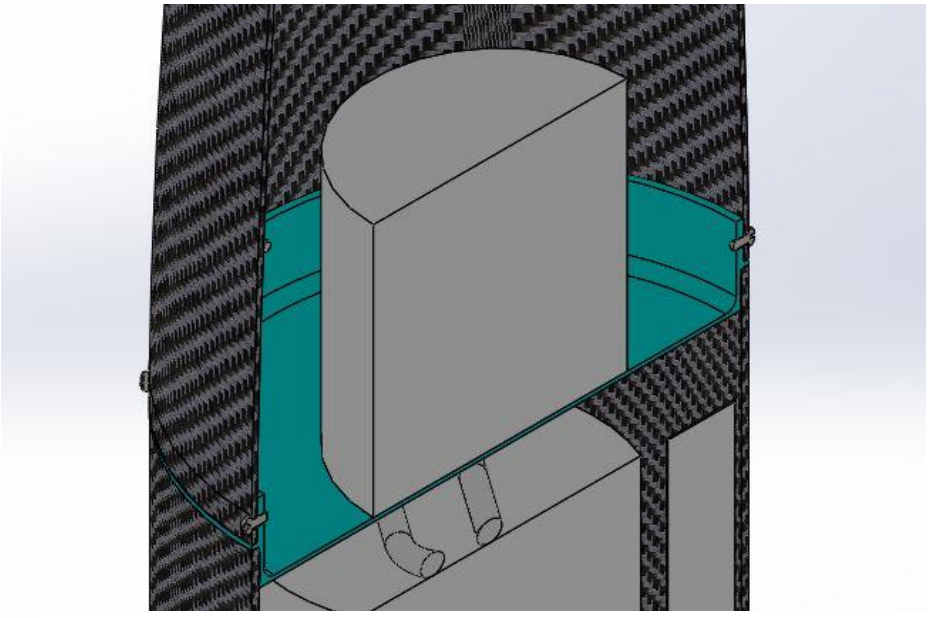

Figure 21. Junction n°4

Seven M3 screws are inserted to resist the loads acting on the carbon. The load acting on each screw is 900 N; this value is derived by making assumptions in advantage of security. Through a series of analytical calculations, it results that in each hole the pressure acting on the surface in contact with the screw is 148 MPa.

In the area inside the junction there is a plate that allows it to be drilled to fix any components necessary for avionics and recovery in position. This can be seen in the *figure 21.* The loads acting on this plate are due to the acceleration forces during launch.

Chapter 4

Bonding

In this chapter the glued structural elements are discussed, about their design, their construction and testing to validate the analytical model.

The choice to separate the rocket into joinable subsystems required the creation of joints capable of connecting the different subsystems. The junctions must maintain the structural resistance in the interface, to align the entire system and to allow the disassembly and reassembly of the rocket, these requirements are imposed for the success of the mission. For the just mentioned requirements and since the main structure of the rocket is made of composite carbon, it is chosen to make the aluminium joints, and join them to the carbon composite through bonding. Furthermore, having a detachable rocket allows access to all the components even in the pre-launch phase.

For the dimensioning of the glued elements it uses analytical methods and to test some representative samples to validate the flight configuration.

4.1. Theory of Bonding Joint

In the design of bonded composite joints, some consideration is given to each of the elements to be joined (adherents), including their geometry, size, materials of construction, actual or potential modes of failure, coefficients of thermal expansion, magnitude and nature of the loading involved [13]. Structural adhesive joints (and composites adherents) have relatively poor resistance to through-thickness (peel) stresses and, where possible, this type of loading is avoided. The two adherents have the layers that are separated by a thin layer of resin. When these materials are glued, care must be taken that the interlaminar resin does not break down before the glue layer. There are different types of configuration of bonded joints, which has different properties. The choice of the configuration of joint in the design considers both the efficiency from an analytical point of view and the possibility of realization based on the costs and limitations of the system in question. From an analytical point of view,

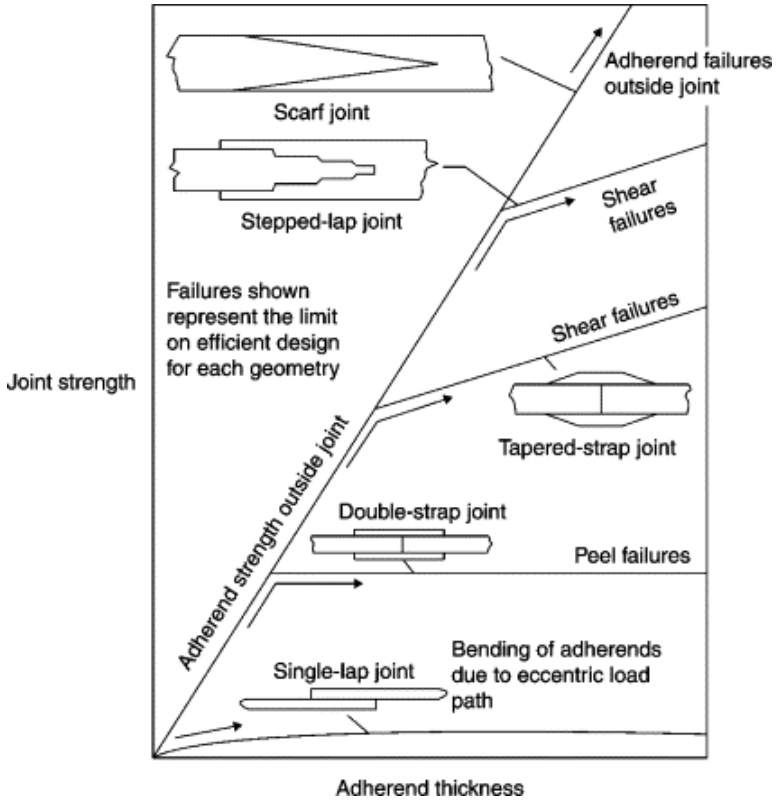

Figure 22. Bonded Joint

the *figure 22* shows the trend of junction resistance as a function of the thickness of the adherents.

The simplest configuration that can be used is the single-lap joint. However, because the loads are eccentric, a large secondary bending moment develops, that results in the adhesive being subjected to severe peel stresses. This type of joint is therefore only used for lightly loaded structure or is supported by underlying structure such as an internal frame or stiffener.

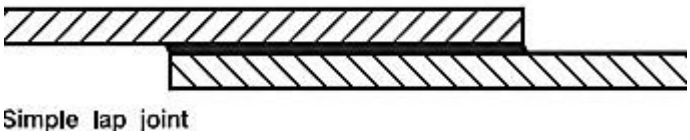

Figure 23. Single-Lap Joint

Another configuration is the scarf joint, which, when correctly designed, develops negligible stress and may be used to join composite components of any thickness. However, the scarf joint profile deviation from the ideal linear bond line caused by a machining error of the scarf end can lead to a change in the stress distribution and may compromise residual strength of the joint.

Figure 24. Scarf Joint

Moreover, from the *figure 22* emerge that, a scarf joint configuration is preferable than the single-lap joint also for adherents with thin thickness. This mainly because in the scarf joint the load is axial and does not involve bending.

4.1.1 Stress Distributions in a Single-Lap Joint

The distributions of stresses that occur most frequently on a joint, depending on the load applied, the type of adhesion and the adhesive used. The following points describe the most stresses elements and their dependence in a bonded joint:

- The stresses on the glued interface depend on the elastic stiffness of the adherents and on the elastic deformation of the adhesive layer.
- The stresses on the adhesive layer also depend on whether the adhesive has an elastic or elastic-plastic behavior. In the first case the stress peaks are greater than the elastic-plastic adhesive.
- The peel stress causes a state of stress during the loading phase which has a greater influence on the resistance of the adhesive joints.

The mechanical strength of the joints, both welded and threaded, must be provided by calculation; the same reasoning must also be done in glued joints. The most common approach for calculating the bonded joints is to refer to an average stress. This is obviously a simplified approach that does not allow us to fully exploit the potential of adhesives and that implies a certain warn in their use. For this region are use some model to describe the trends of stresses in the bonding.

Volkersen Model

Among the various theories on bonding the most simplified is that of Volkersen, which does not consider the eccentricity of the load and the effects that develop on the joint [14]. This model gives shear stress distribution on bonding length through the following formulation. The moments due to the geometric eccentricity acting on the bonding are not considered, so there are no formulations for peel stress.

Given t_t the top adherend thickness; t_b the bottom adherend thickness; t_a the adhesive thickness; b the bonded area width; l the bonded area length; E the adherend Young's modulus; G_a the adhesive shear modulus; P the applied load.

It results:

$$\tau(x) = \frac{Pw}{2b} * \frac{\cosh(wx)}{\sinh\left(\frac{wl}{2}\right)} + \left(\frac{t_t - t_b}{t_t + t_b}\right) * \left(\frac{WL}{2}\right) * \frac{\sinh(wx)}{\cosh\left(\frac{wl}{2}\right)};$$

where

$$w = \sqrt{\frac{G_a}{E t_t t_a}\left(1 + \frac{t_t}{t_b}\right)};$$

This equation shows that the maximum stress is on the extremes of the bonding, where the break is easier to occur.

Goland and Reissner Model

The model developed by Goland and Reissner, is a more advanced model than the Volkersen model because it also considers the presence of deformations from the bending moments that develop. Considering the deformation of the joint it is possible to determine the peel stress state that acts and the shear stress in the overlap length.

The shear stress distribution found by Goland and Reissner is given by:

$$\tau(x) = -\frac{P}{8c}\left(\frac{\beta c}{t}(1 + 3k)\frac{\cosh\left(\left(\frac{\beta c}{t}\right)\left(\frac{x}{c}\right)\right)}{\sinh\left(\frac{\beta c}{t}\right)} + 3(1 - k)\right);$$

where P is the applied load for unit width, c is half of the overlap length, t is the adherend thickness, υ is the Poisson's ratio and k are the bending moment factor.

$$k = \frac{\cosh(u_2 c)}{\cosh(u_2 c) + 2\sqrt{2}sinh(u_2 c)};$$

$$u_2 = \sqrt{\frac{3(1 - \upsilon^2)}{2}}\frac{1}{t}\sqrt{\frac{P}{Et}};$$

$$\beta^2 = \frac{G_a t}{8 E t_a};$$

The peel stress equation is the following:

$$\sigma(x) = \frac{1}{\Delta}\frac{Pt}{c^2}(A + B);$$

where

$$A = \left(\frac{R_2\lambda^2 k}{2} + \lambda k' \cosh(\lambda)\cos(\lambda)\right)\cosh\left(\frac{\lambda x}{c}\right)\cos\left(\frac{\lambda x}{c}\right);$$

$$B = \left(\frac{R_1\lambda^2 k}{2} + \lambda k' \sinh(\lambda)\sin(\lambda)\right)\sinh\left(\frac{\lambda x}{c}\right)\sin\left(\frac{\lambda x}{c}\right);$$

and

$$k' = \frac{kc}{t}\sqrt{3(1-\upsilon^2)\frac{P}{tE}};$$

is the transverse force factor, also

$$\lambda = \frac{\gamma c}{t}, \qquad \gamma^4 = \frac{6E_a t}{E t_a}, \qquad \Delta = 0.5(\sin(2\lambda) + \sinh(2\lambda));$$

$$R1 = \cosh(\lambda)\sin(\lambda) + \sinh(\lambda)\cos(\lambda);$$

$$R2 = -\cosh(\lambda)\sin(\lambda) + \sinh(\lambda)\cos(\lambda).$$

With these equations it is possible to determine the distribution of shear stress and peel stress in the overlap zone for GR model. Although there are many models for this determination, the Goland and Reissner model is the one that allows simplicity of calculation and good representation of stress for a single lap joint.

Both proposed models analyze the adhesive, only through elastic deformation of the glue, neglecting the plastic deformation behaviour. This allows all the adhesives to be sized, even if they do not have plastic deformation.

The strength of overlapping narrow joints is the result exclusively of the adhesion and cohesive forces of the adhesive layer. Overcoming a certain value of the overlapping layers, the stress peaks concentrate on the overlapping ends causing the resistance to decrease. For this reason, increasing the bonding length to increase strength has a limit given by the distribution of stresses. Stresses, but in particular shear stress has a negative exponential trend, limiting the bonding area only at the extremes when very long overlaps are used.

In the *figure 25* the trend of shear stress is reported for a single-lap joint with three different overlap lengths. For the three cases it is observed that, as the overlap length

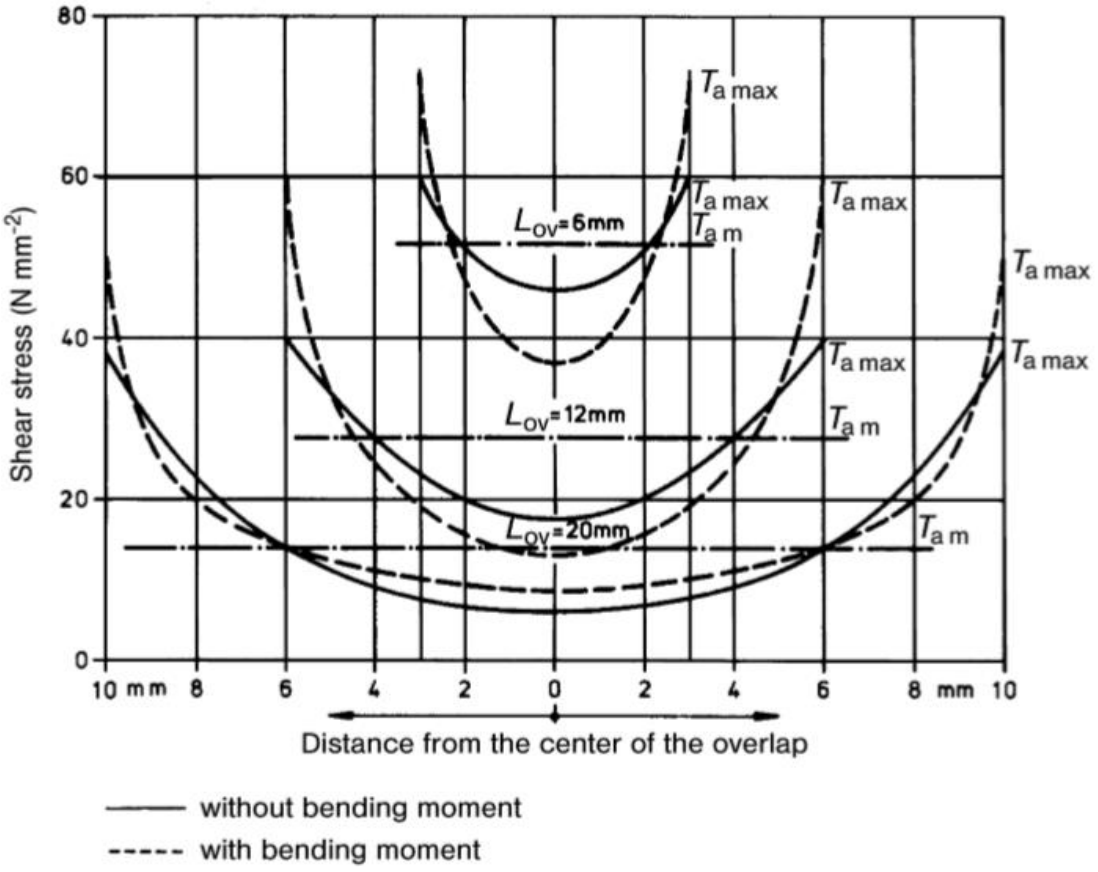

Figure 25. Shear Stress Trends in the Overlap

increases (and also the gluing area) there is a decrease in the average taw (in the figure $T_{a\,m}$ is $T_{am} = \frac{F_{load}}{A_{gluing}}$) and an increase $\frac{T_{a\,max}}{Ta\,m}$ ratio at the ends of the overlap. This leads to greater stress at the extremes when the overlap length is increased, bringing peaks much higher than the average taw value. It is important to consider this trend in the sizing phase.

In the central area of the overlap it can be observed that as the length increases the shear stress decreases making the central area less and less stressed.

As regards the presence of the bending moment, we can observe how it negatively influences the stress trend by increasing its intensity at the extremes. This causes an early failure of the junction.

When the junction deforms due to the imposed loads, a peel stress develops. Specifically, peel stress is a limiting effort at the interface that develops after the deformation of the latter. The trend described in the *figure 26* is a qualitative trend and shows how in bonding change the stresses from an area in traction to a zone in compression. This change of the sigma is due to the relationships between constrain

and deformations. The traction part causes the early structural failure in composite material, as it acts outside the plane where the fiber composites have the least resistance. This type of stress causes delamination failure, which means that the fibers of the first composite ply break, and then the real delamination occurs with interlaminar failure.

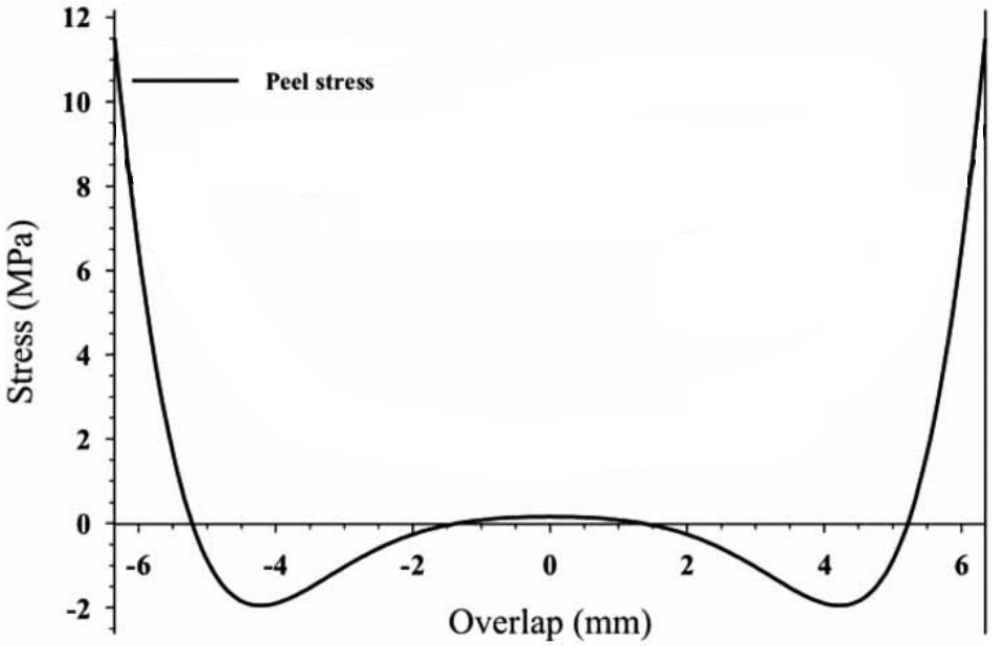

Figure 26. Peel Stress Trends

4.1.2 Stress Distributions in a Scarf Joint

The approach is an extension of the original well-recognized Volkersen's shear lag analysis for a shear loaded joint, which is frequently applied to adhesively-bonded joints. A mathematical representation consisting of linear and exponential functions is employed to model the elastic-plastic behavior commonly observed in structural adhesives. The scarf-joint develops more uniform shear stress and strain distributions with a consequent reduction in peak values than those for the conventional lap joint.
In these joints the shear stress state is constant in the overlap length. The possibility of obtaining an axial load allows the forces to transfer between the two adherents without

the presence of bending moments. The stress state is easier to determine and allows it to be defined by a simple formulation.

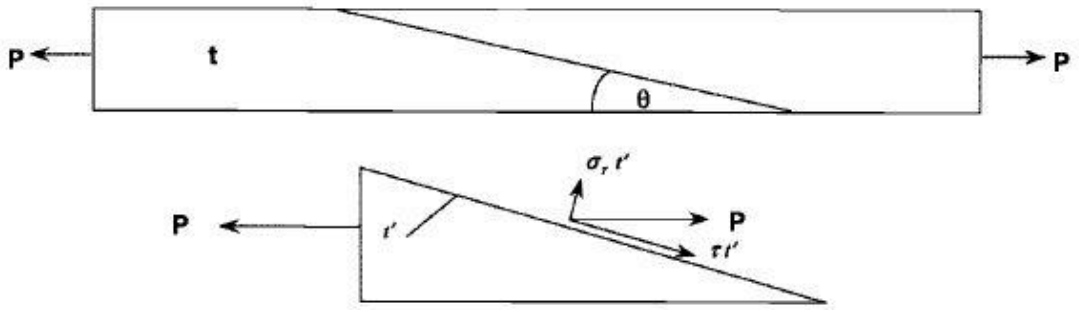

Figure 27. Scarf joint Design

In the *figure 27* a scarf joint gluing is represented, highlighting the most important parameters to obtain the results of shear stress and peel stress.

To calculate this vale the following formulas are used.

$$\tau = \frac{Pcos(\vartheta)\sin(\vartheta)}{t};$$

$$\sigma_T = \frac{Psin(\vartheta)^2}{t};$$

And the ratio σ_T/τ is:

$$\frac{\sigma_T}{\tau} = \tan(\vartheta);$$

Thus, for a taper angle of 5 °, the ratio is <0.1, showing that the normal stresses are negligible.

The uniform shear stress in a balanced scarf joint is beneficial in that the strength of the joint is not limited by local high-stress concentrations at the ends, as in a lap joint. Thus, the load-carrying capacity of the joint increases in proportion to the thickness of the adherends so that, at least in principle, the thickness of material that can be joined is unlimited. However, because there is no elastic trough to limit continuous deformation under prolonged loading, creep leading to eventual failure must be expected if the effective adhesive shear yield stress is reached. Further, joint strength will be sensitive to damage to the tapered edge.

In practice, because of the viscoplastic nature of the adhesive, there is probably no lower limit to the adhesive yield stress under prolonged loading. The reduced yield

stress and increased time-dependent behavior imposes a limitation on the allowable load in scarf joints under hot/wet conditions. Thus, design must be based on conservative estimates of elastic properties. If the adherends are dissimilar in stiffness and/or thermal expansion properties, as in a composite-to-metal joint, a much more complex analysis will be required.

The net result of the analysis for joints with adherends with different stiffnesses or thermal expansion coefficients is that the shear stress in the joint is no longer uniform. Assuming elastic behavior in the adhesive, it is found that the shear stress concentration, maximum-adhesive-stress/minimum-adhesive-stress (unity for a balanced joint), asymptotes to the lowest adherend stiffness ratio. The effect of adhesive plasticity is to extend the length over which the stress ratio is unity. The effect of thermal expansion mismatch (stiffness-balanced adherends) is more complex with the shear stress concentration rising and falling with increasing scarf length; at large lengths (very small 0) the ratio approaches unity, as for no thermal mismatch.

4.1.3 Junction Optimization to Increase Strength

Through local modifications on the junction it is possible to increase the resistance to the imposed loads [15]. An optimization of the joint geometry is important when using composite adherends, as the failure of the entire joint often occurs by delamination and not by failure between the adhesive interface and the adhering.

It is possible to change the thickness of the adhesive in order to redistribute the peel stress and vary the geometry of the adherents to reduce the stresses in the ends of the bonding.

The presence of an excess of adhesive on the ends of the bonding, allows to redistribute the stress peak on a larger area. In this way the value of the stress peak is reduced and a more homogeneous distribution of the stress trend even in an area outside the overlap. By reducing the stress peak, it is possible to postpone delamination on the composite bonding. Another improvement to optimize the bonded joint is to reduce the thickness of the bonding at the end of the overlap. Reducing the thickness of the material weakens the adherent, limiting the load transferred and thus reducing stress locally. In a case of bonding between composite material and metal, the adherence that varies its geometry to optimize bonding is the metal one.

The different possible configurations to optimize a single-lap joint are shown in the *figure 28*.

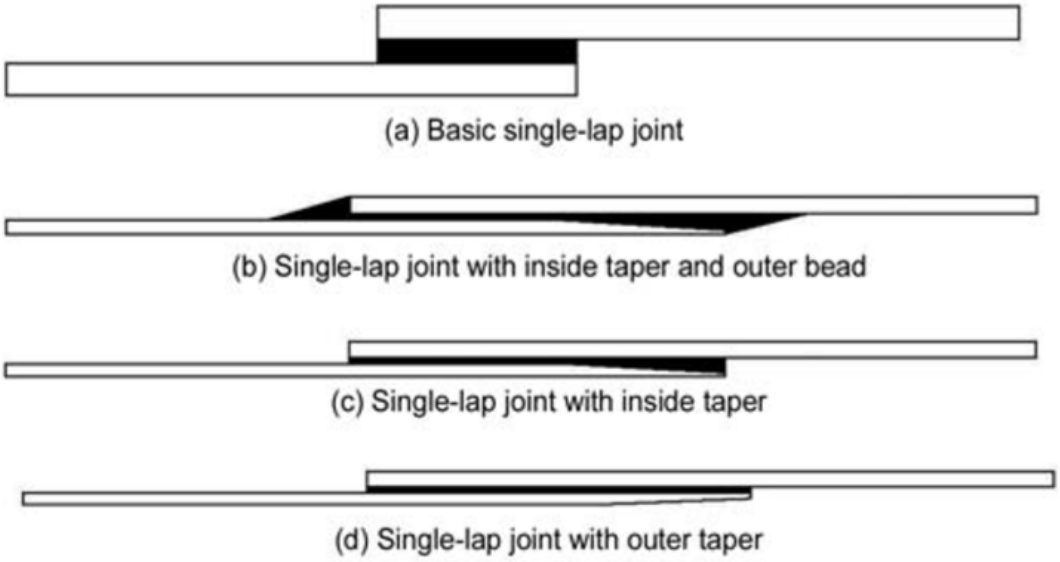

Figure 28. Different type of bonded optimization

Focusing the study on single lap joint with inside taper with and without outer bead it is possible to size the junction geometry through two parameters; one is the taper angle while the second is the tapered length, α and a respectively. A third parameter obtained by geometric construction is b, the final depth of the taper. These parameters are

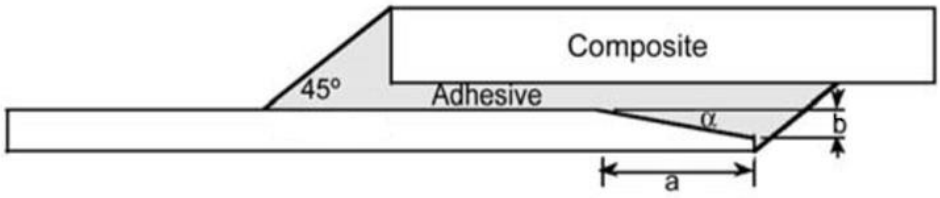

Figure 29. Better Optimization

indicating in the *figure 29.*

From experimental reported in the *figure 30* it is possible to observe the resistance of a single-lap joint (adherent carbon composite and titanium) subjected to a tension load [16]. In the case shown the values of the breaking load are to be considered qualitatively, while the trend of these with respect to the taper angle is useful for the study of optimization of the joint.

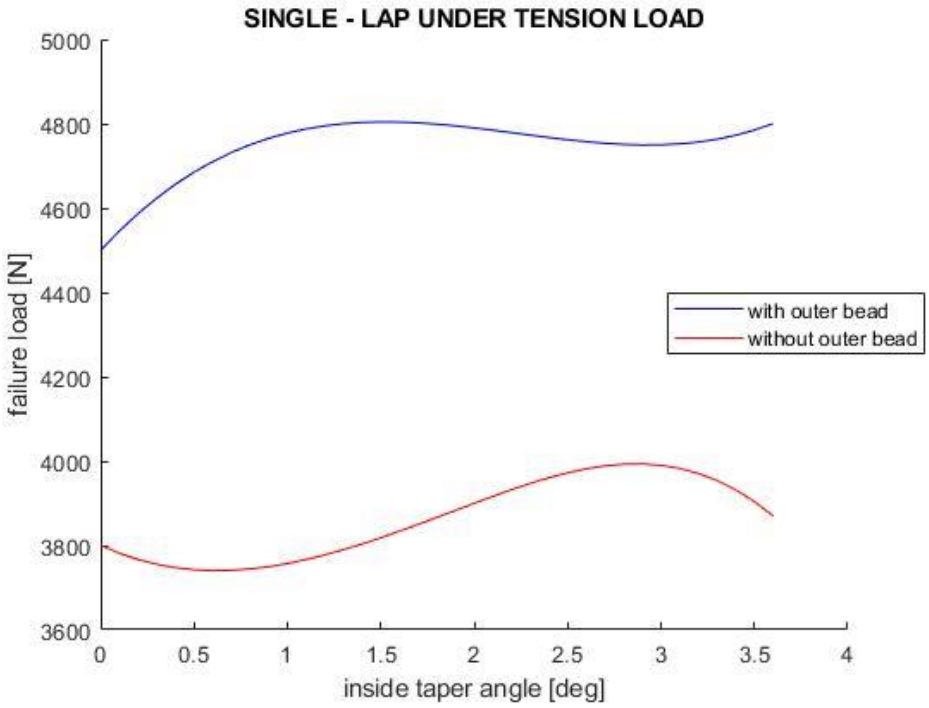

Figure 30. Trends with the Optimization

The study shows two cases, one with the presence of an adhesive layer (outer bead), and one without. As a reference value, b = 0.5 mm is used, because it leads to greater resistance results.

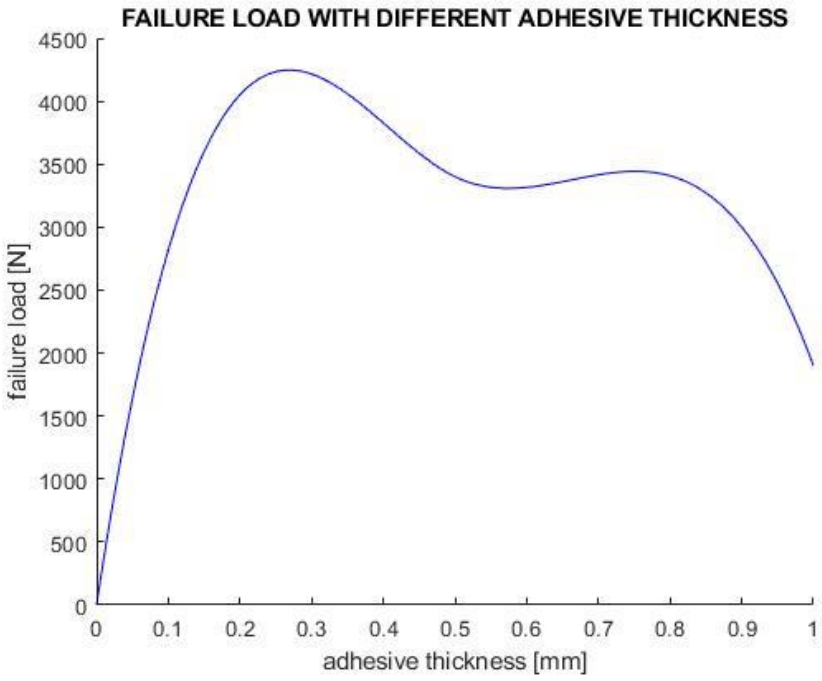

Figure 31. Influence of thickness layer of glue

It can be observed at first that the presence of an outer bead greatly increases the resistance of the joint. Moreover, it can be observed that the trends are different about the two cases. The choice of the usable configuration is with the outer bead and the value of the α parameter falls around α = 2 deg. An increase of resistance about 20% can be observed with the presence of an external layer of adhesive.

With these values of α and b, it results for reconstruction a value of a = 14 mm. A final parameter to optimize the bonded joints is the choice of the adhesive thickness between the two adherents. From numerical analysis we observe the trend shown in the *figure 31*.

If the layer of adhesive e used is large (> 0.4 mm), the resistance to the maximum bond strength is lower. This is because the glue layer deforms more easily and reaches the plastic limit with lower load values. Unlike an adhesive thickness around 0.2 mm, being thinner, it transfers loads without undergoing excessive deformation and limits the achievement of the plastic strain limit.

4.2. Single-Lap Test

Bonding is a fundamental element in the structure of the sounding rocket designed as it contributes to the union between the different subsystems. Performing representative tests of the flight model are essential to ensure effective structural strength. To do this, the tested models must be representative and without leading to excessive costs of realization.

The interface to be tested specifically is the composite carbon fiber bonding with Aluminum-7075-T6. The choice to use composite carbon fibers is due to the excellent mechanical properties compared to its density. The use of this material to realize the external structure of the rocket has forced the involvement of special junctions for the union of the various subsystems. The joints are made of Aluminium to reduce weight and have high mechanical properties. For the union between aluminium and carbon composite, it was decided to use bonding. To delimit the part of the section in operation it is necessary to study the maximum loads acting on the various bondings in the rocket. Single-lap bonding are used in the joints. Scarf-type bonding is used only in the first junction because the adherents are very thin, and this would involve lengths and thicknesses of the adherents with difficult and expensive manufacturing. The reason for inserting a scarf-type gluing in the lower part of the first junction derives from the fact that in addition to the aerodynamic throw loads, there is the presence of pressure (around 20 bar) coming from the engine.

The loads that it must support this first junction are a bending moment of 4000 N*m, the pressure of the catalytic of 20 Bar, an axial load of 5000 N and a shear force of 1000 N. Only the bending moment can lead to failure of the junction, because the axial load is unloaded all through compression on the structure. We have chosen to represent a portion of the bonding that represents the area of maximum stress. By studying the bonding area with greater stresses, it was obtained that the most distant point from the neutral axis of the rocket is the most stressed one. This is due to the strong present moment which causes two stressed zones, one in traction and one in compression.

4.2.1. Design of Bonding Area

To determine the gluing area necessary to withstand the imposed loads, it is first necessary to choose the type of glue to be used and analyze its properties. For this

project we chose to use the *3M™ Scotch-Weld™ EC-9323 B/A* [17]. This glue is supplied by the company 3M is a two-component epoxy paste adhesive which cures at room temperature or with mild to hot form, impact resistant structural bond. It has excellent adhesion to a wide variety of substrates such as metals, glass, ceramics and plastics, incl. GFRP and CFRP. Once cured it provides extremely high shear strength over a wide temperature range, with outstanding resistance to harsh environments and chemicals. From the provided datasheet it is possible to obtain some values of the mechanical properties of this glue. It is useful for the calculation to know the Young's Modulus (E_a=2870 MPa), Poisson's value (υ_a=0,37) and the shear breaking stress (τ_a). The value of the cutting stress depends on the type of adherent and the operating temperature. For this reason,
the shear stress values for Aluminum and for carbon composite are shown below, indicating when the differences at different temperatures are known.

Temperature	Adherents material	Shear strength τ_a
23 °C	Aluminium	40 MPa
80 °C	Aluminium	22 MPa
23 °C	CFRP	28 MPa

Table 9

Once the elastic modulus and the Poisson ratio are known, the shear modulus with a value of G_a=1070 MPa is obtained.
To predict the bonding strength in function of shear distribution three analytical models were chosen. The first is a calculation of constant distribution given by the formula $\tau = \frac{F}{A}$, the second is the Volkersen model which considers an axial pure shear without deformation, the third is the more accurate Goland and Reissner model which also considers generation of moments on bonding. The follow graphic show distribution of shear in the overlap and from a MATLAB script calculate in output the maximum load before breaking adhesive joint for the three different models.
To have references with shear stress values in the datasheet provided by 3M, we have chosen to use a bonding width of 25 mm (in compliance with the standard used EN

2243-1). Analyzing the maximum load on the junction for a portion of circumference with a length of 25 mm is a force F = 3500 N. This value was derived from the following calculations:

$$\sigma_{max} = \frac{My}{J};$$

where,

$$y = y_{max} = \frac{\frac{D}{2} + \frac{d}{2}}{2};$$

$$J = \frac{\pi * (D^4 - d^4)}{64};$$

$$M = 4000 * 10^3\ Nmm;$$

using as diameter *D*=195.82 mm and *d*=190.00 mm, it result a maximum normal stress of σ_{max}=47.7 MPa.

Considering 25 mm of arc in the part containing the greatest stress, the force acting on that part of the section is obtained by formulation.

$$F = \sigma_{max} * A_{25mm};$$

$$A_{25mm} = \frac{\frac{\pi(D^2 - d^2)}{4}}{24} = 73.47\ mm^2;$$

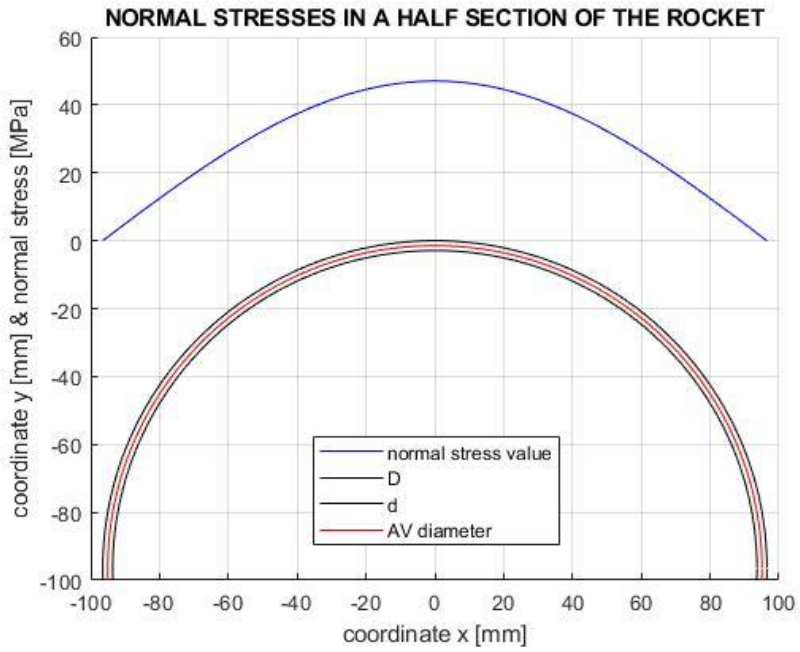

Figure 32. Half Section of the Rocket

From the *figure 32* it can be observed how to assume for a length of 25 mm the normal stress as a constant is a correct assumption if in the central zone (where the maximum stresses are found). This results in a force F=3500 N.

In this way it was possible to size the glue by using the calculation on the most stressed portion.

The stress value in the section is maximum in the central part where there is the greatest distance from the neutral axis, while it is null in the section with y = 0. The *figure 32* was created to describe the stress trend on half section of the rocket.

This simplification is possible because the circumference has a diameter such that the chosen length has an arc of a circle approximated to a straight line. From a scientific article [15], it emerged that testing the single lap joint with an axial load represents well the distribution of the $\frac{\tau}{\tau_{avg}}$ of a cylindrical joint; as the diameter of a cylindrical configuration increases, the stress distribution tends to that of a single lap joint with an axial load. For the diameters used in the rocket this simplification is worth as the diameter is such that the study of a portion of it is fine to represent the complete geometry.

What remains to be determined is the length of overlap needed to be able to withstand the load. To determine it, it was decided to consider the shear shear value lower between the two adherents employed. The one chosen is given by the bonding on the polymeric matrix carbon composite with a value at 23 °C equal to $\tau_{a\,23^\circ}$=28 MPa while at 80 °C $\tau_{a\,80^\circ}$=14 MPa.

Through the formulation $\tau = \frac{F}{A}$ we get that the length of overlap in first approximation is $l_{ov\,23^\circ}$=5 mm and $l_{ov\,80^\circ}$=10 mm.

The *figure 33* have been inserted to obtain a representation of the shear stress trend. In the first, reference is made to the room-temperature case with an overlap length of 5 mm.

As announced by the theory, it can be observed that in the extremes of the bonding a shear stress value higher than the average value is obtained. This is due to the fact that the transfer of forces between the two adherents is not constant but focuses more on the extremes. Furthermore, in the GR model, whose trend is shown in blue, there is a further increase in shear stress due to the fact that the deformations in the gluing are

considered. In the second graph, on the other hand, the shear stress trends are shown for an overlap length of 10 mm and an average thawing stress of 14 MPa.

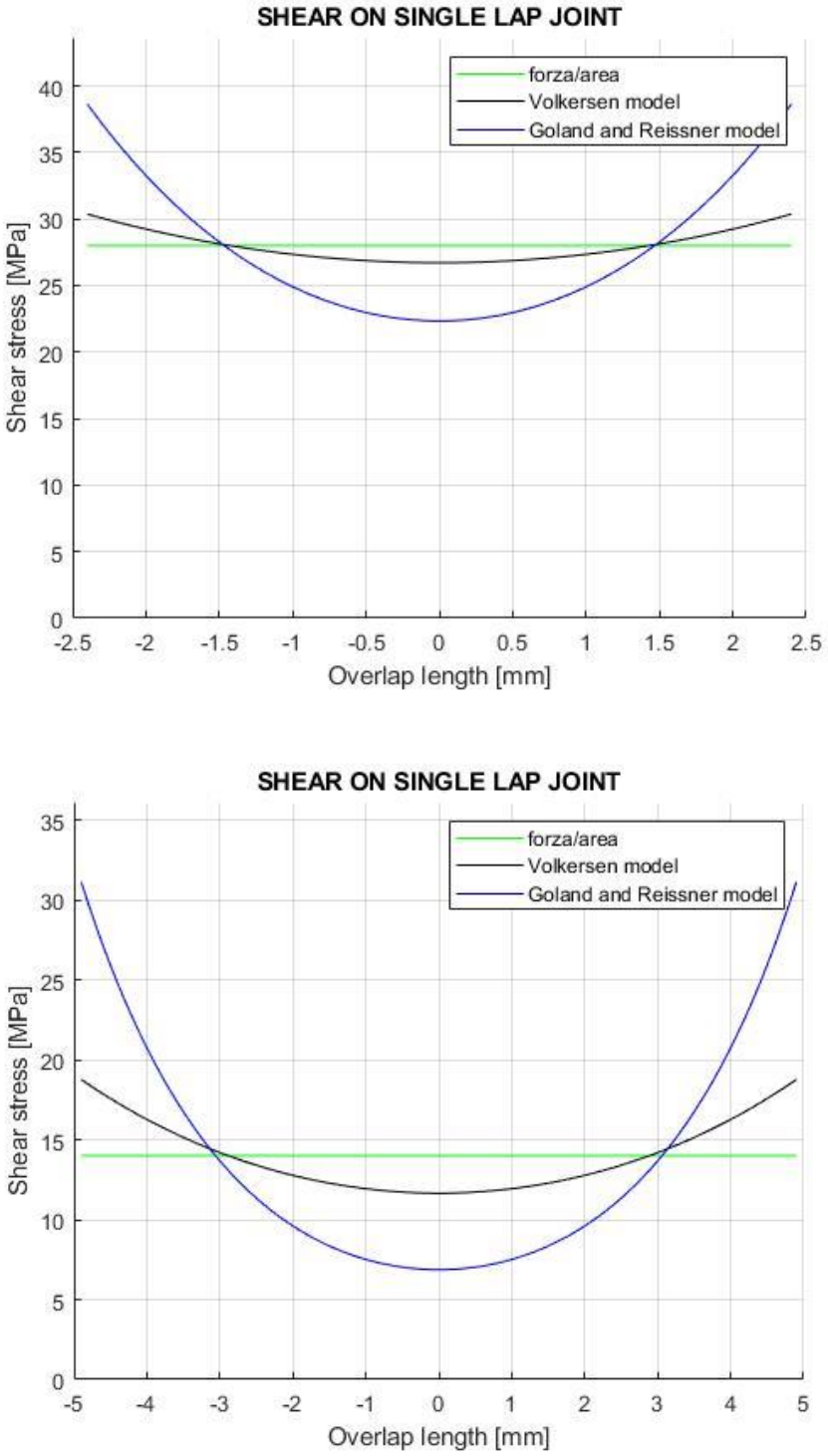

Figure 33. Shear Stress Analytic Trends

It can be seen that by increasing the bonding length there is an increase τ/τ_{AV} at the ends and a decrease in the central zone. This trend is accentuated the more the bonding

length is increased. And as if the load were more distributed at the ends of the gluing, making the central area with less resistance at shear.

It is possible to choose the type of care to obtain the polymerization of the glue and confer the properties to the gluing.

The test carried out by the 3M company to find the value of shear stress in bonding uses standardized bonding dimensions (25.4 mm wide and 12.5 mm overlap).

For this type of glue, the one that requires 24 hours at 23 ± 2 °C under a pressure of 100 KPa was followed by a 120 min post cure at 65 ± 3 °C. The first part treats us at room temperature is necessary to provide a first polymerization phase for subsequent completion in the oven. The choice is to use a solidification in the oven both for greater shear stress values and for shorter process times. However, as shown in the datasheet, the failure of the bonding did not occur due to failure of the adhesive or of the interface but due to delamination of the composite.

n conclusion it can be stated that the need to withstand the load imposed in the rocket during the flight phase leads to having a gluing height of 10 mm as the temperatures reached in this area, although for a few seconds they are around 80 °C. Through this analysis of the load distribution and the necessary gluing values some glued joint samples were made to verify and validate the theoretical models.

4.2.2. The Bonded Samples

4.2.2.1 Theory of the Bonded Samples

To verify what has been analyzed so far, it has been chosen to test the bonding through representative samples and to obtain significant results it was decided to represent two bonding areas. The first is an area with an overlap size of 12.5 mm and a width of 25 mm; these dimensions were chosen to represent the EN 2243-1 standard with which 3M performed the tests for the value entered in the data sheet. In this way it is possible to have a reference value on which to observe a possible discordance and deviation of the results obtained between the test done and the value in the datasheet. The second area chosen has an overlap of 28 mm and a width of 25 mm, this length was chosen by imposing a safety coefficient to the value previously obtained, to withstand the operating condition of 80 °C.

In this way, by testing both samples it is possible to have both an area that provides values attributable to the data sheet, and an area that can be validated and inserted in the flight model. The designed samples will be pulled through a traction machine that positions the sample through two clamps and applies the imposed load. In order to make the sample easily adaptable, it was decided to use two metal inserts as an interface to the traction machine. In this way two specular and symmetrical gluing areas have been inserted.

Since this configuration is slightly different from a single lap joint, in fact it takes the

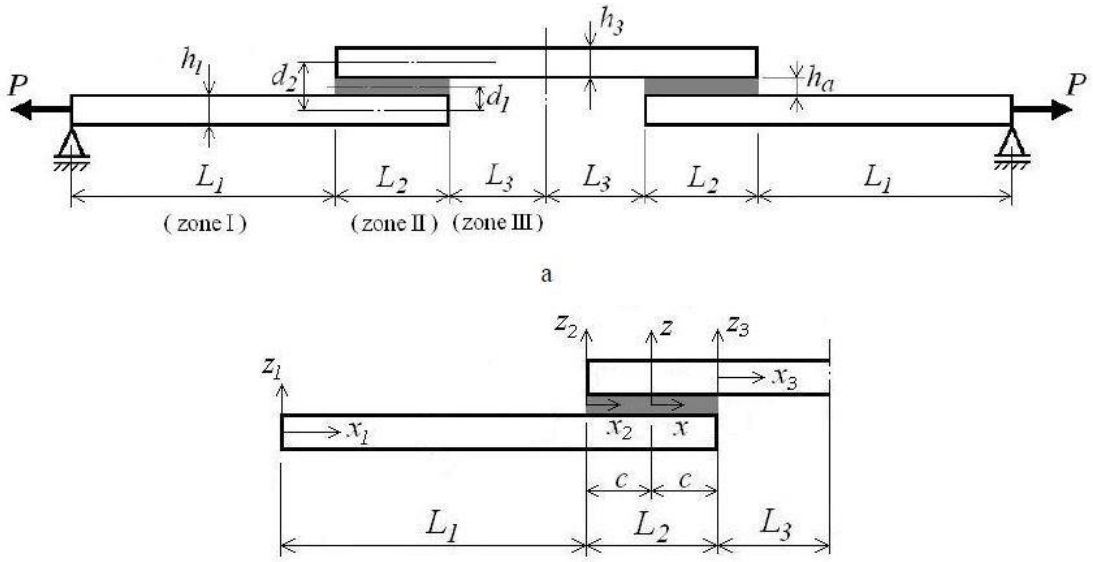

Figure 34. Strap Joint Design

name of single strapped-joint, a new formulation is used to define the forces with which the samples are broken [18].

In the *figure 34* the geometry used and the respective dimensions to be inserted in the following formulation are represented in a schematic way. There are also three reference systems, the system on which we focus is the one within the bonding. It should be pointed out that the tensile force P is expressed per unit of length as the results are two-dimensional and easily traceable to the three-dimensional case.

The model start defining the stiffness of the three zones:

$$D_1 = D_3 = \frac{Eh^3}{12(1-\upsilon^2)} = D;\ D_2 \approx \frac{E(2h)^3}{12(1-\upsilon^2)} = 8D;$$

E is the minimun value from E_1 and E_2 that are respectively the Young modulus of the two adherents; h and υ are also the minimun thikness and the maximum Poisson

ratio of the two adherents. A thin adhesive layer with thickness *ha* (*ha* << *h*) was considered.

First, the equations describing the flexions to which the adherents are subjected in the three zones, under the action of the force *P*.

$$w_1(x_1) = A_1 \cosh(\beta_1 x_1) + A_2 \sinh(\beta_1 x_1) \qquad (0 \le x_1 \le L_1),$$

$$w_2(x_2) = A_3 \cosh(\beta_2 x_2) + A_4 \sinh(\beta_2 x_2) + d_1 \qquad (0 \le x_2 \le L_2),$$

$$w_3(x_3) = A_5 \cosh(\beta_3 x_3) + A_6 \sinh(\beta_3 x_3) + d_2 \qquad (0 \le x_3 \le L_3);$$

where

$$Q_k = \sqrt{\frac{P}{D_k}} \qquad (k=1,2,3);$$

By imposing proper boundary and continuity conditions, were obtained the following expressions of the six integration constants:

$$A_1 = 0;$$

$$A_2 = \frac{1}{B_3 \cosh(\beta_1 L_1)}\left[B_1 + d_1\left(\frac{\beta_2}{\beta_1}\tanh(\beta_2 L_2) + \frac{\beta_3}{\beta_1}\tanh(\beta_3 L_3)\right)\right];$$

$$A_3 = \frac{1}{B_3}\left[B_1 \tanh(\beta_1 L_1) - d_1\left(1 + \frac{\beta_3}{\beta_2}\tanh(\beta_2 L_2)\tanh(\beta_3 L_3)\right)\right];$$

$$A_4 = \frac{1}{B_3}\left[\frac{\beta_1}{\beta_2}B_1 + d_1\left(\tanh(\beta_2 L_2) + \frac{\beta_3}{\beta_2}\tanh(\beta_3 L_3)\right)\right];$$

$$A_5 = -\frac{1}{B_3}\left[(d_2 - d_1)\, B_2 + \frac{d_1}{\cosh(\beta_2 L_2)}\right];$$

$$A_6 = -A_5 \tanh(\beta_3 L_3);$$

where

$$B_1 = \frac{\beta_3}{\beta_1}\frac{\tanh(\beta_3 L_3)}{\cosh(\beta_2 L_2)}(d_2 - d_1);$$

$$B_2 = 1 + \frac{\beta_2}{\beta_1}\tanh(\beta_1 L_1)\tanh(\beta_2 L_2);$$

$$B_3 = B_2 + \beta_3 \tanh(\beta_3 L_3)\left(\tanh\frac{(\beta_1 L_1)}{\beta_1} + \tanh\frac{(\beta_2 L_2)}{\beta_2}\right);$$

to consider bending moments and forces at the inner and outer ends of the overlap the following expression are used:

$$M_i = PA_5;\ \ V_i = PA_6\,\beta_3;$$
$$M_o = PA_2\sinh(\beta_1 L_1);\ \ V_o = PA_2\,\beta_1\cosh(\beta_1 L_1);$$

Knowing the overlap length, it is possible to determine the stress taw and sigma in the bonding. By imposing at the variable *x,* the value between $-c \le x \le c$ and $c = L2/2$ were obtain:

$$\tau(x) = C_0 + C_1\,cosh\,(\lambda x) + C_2\,sinh\,(\lambda x);$$

$$\sigma(x) = C_3 cosh(\xi x)cos(\xi x) + C_4 cosh(\xi x)sin(\xi x) \ldots$$
$$+C_5 sinh(\xi x)cos(\xi x) + C_6 sinh(\xi x)sin(\xi x);$$

where

$$\lambda = \sqrt{\frac{G_a}{h_a}\left(\frac{2}{Eh} + \frac{h(h+h_a)}{2D}\right)};\quad \xi = \sqrt[4]{\frac{E_a}{2h_a D}};$$

E_a and G_a are the tensile and the shear modules of the adhesive.

The values of constants C_i (i = 0, 1, … , 6) will be calculated by using formulas:

$$C_0 = \frac{P}{2c} - \frac{G_a}{2c\lambda^2 h_a}\left[\frac{2P}{Eh} + \frac{h}{2D}(M_o - M_i)\right];$$

$$C_1 = \frac{G_a}{\lambda h_a \sinh(\lambda c)}\left[\frac{P}{Eh} + \frac{h}{4D}(M_o - M_i)\right];$$

$$C_2 = \frac{G_a}{\lambda h_a \cosh(\lambda c)}\frac{h}{4D}(M_o + M_i);$$

$$C_3 = \frac{E_a}{4Dh_a B_4}[\xi(H_{SC} - H_{CS})(M_o - M_i) + H_{CC}(V_o + V_i)];$$

$$C_4 = \frac{E_a}{4Dh_a B_5}[\xi(H_{CC} + H_{SS})(M_o + M_i) + H_{CS}(V_o - V_i)];$$

$$C_5 = \frac{E_a}{4Dh_a B_5}[\xi(H_{CC} - H_{SS})(M_o + M_i) + H_{SC}(V_o - V_i)];$$

$$C_6 = \frac{E_a}{4Dh_a B_4}[\xi(H_{SC} + H_{CS})(M_o - M_i) + H_{SS}(V_o + V_i)];$$

where

$$B_4 = \xi^3(\cos(\xi c)\sin(\xi c) + \cosh(\xi c)\sinh(\xi c));$$
$$B_5 = \xi^3(\cos(\xi c)\sin(\xi c) - \cosh(\xi c)\sinh(\xi c));$$
$$H_{CC} = \cosh(\xi c)\cos(\xi c);\ \ H_{SS} = \sinh(\xi c)\sin(\xi c);$$
$$H_{CS} = \cosh(\xi c)\sin(\xi c);\ \ H_{SC} = \sinh(\xi c)\cos(\xi c).$$

Through these formulas it is possible to create a script in MATLAB Software in which by inserting the dimensional parameters of the samples it is possible to obtain in output the values of shear stress and peel stress in the glue length.

In the realized script the dimensions of the gluing area and the geometric parameters of the sample that will be made are set. The mechanical properties of the glue and of the material with which the adherents are made are also included. The thickness of the layer of glue is also defined, which is an important parameter for the result obtained, in this case the value is h_a=0.25 mm. Since a stress dependency is also the distance between the two bonded areas, a value of 30 mm is used since the stress trend decreases with increasing distance. The variation is asymptotic and beyond this value there is no longer a large variation for large increments.

The results obtained from the distribution of shear stress and peel stress are represented by the *figure 35.*

The most important dimensional values to obtain this trend are: the length of overlap l_{ov}*=12.5 mm*, the distance between the glues of 30 mm, applied force F_{load}*=8400 N*. The force that has been imposed is that which results using the more simplified formula F / A, using a shear strength of 28 MPa.

The graph shows that the stress distribution is not perfectly symmetrical. This is due to the fact that the geometry used is not simply flat but has dimensions that represent the junction in the rocket. A geometry similar to a flat slab is not used in both directions, but only in the direction of the composite. This can be observed in the paragraph on the realization of the samples for the bonding tests.

The value of shear stress has a maximum at the beginning of bonding with a value around 120 MPa while in the opposite part it has a value of 23 MPa. Calculating the average value of the taws in bonding, the average taw value is 27.0 MPa. This last value is very close to the value calculated using the F/A formula of 28 MPa.

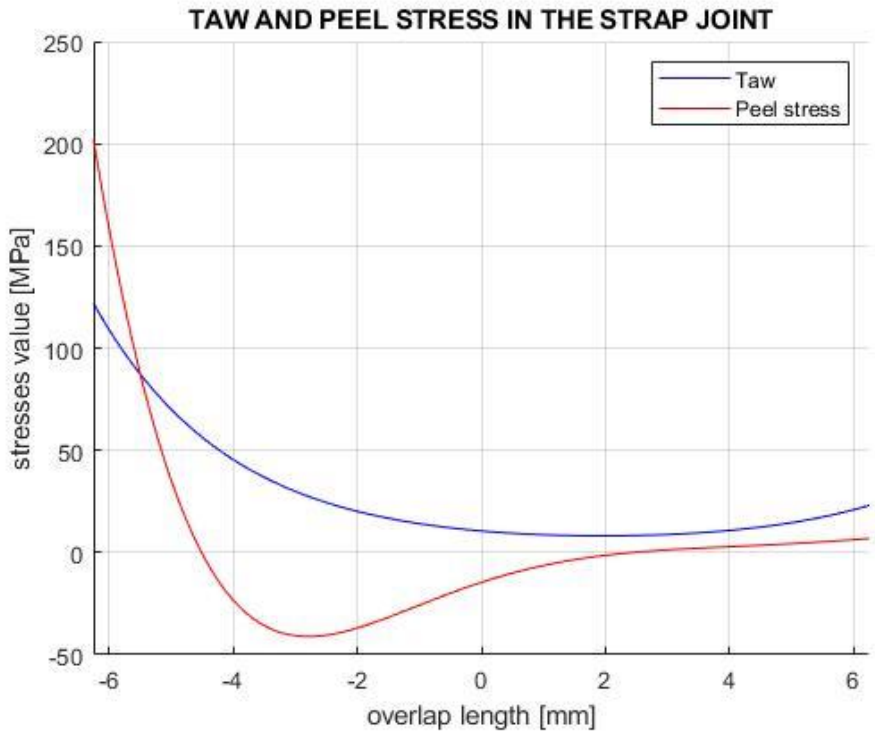

Figure 35. Stresses in Strap Joint

The peel stress has maximum values at the extremes of the overlap of 200 MPa and 6 MPa, while it reaches a minimum value which corresponds to a zone in compression of -41 MPa. The result obtained shows how by using a more specific formulation it is possible to know the stress distribution along the entire length. The average value of the stresses is thus redistributed according to the geometry. The value provided by the data sheet refers to an average taw. The test for this type of geometry uses an EN 2243-1 standard which provides a single-lap joint for gluing. By entering the geometric dimensions of this standard, the shear and peel stress patterns are plotted using the GR model. It can be seen from the *figures 36,37,38* that the maximum value of the taw is around 80 MPa while the peel stress is 100 MPa. These peak values are smaller than those obtained in the configuration scarf, although it is used for both a force F_{load}=8400 N. If the local taw deviates from the average one, it results that, for example, to obtain a maximum difference, as in the configuration used by the data sheets, the maximum force applicable with the geometry chosen to carry out the junction tests must be reduced by 2700 N. In this case two breaking forces are hypothesized, the first is through the average taw having a maximum force of 8400 N. The second hypothesis

is observing the values of $\frac{\tau}{\tau_{AV}}$ and $\frac{\sigma}{\sigma_{AV}}$, the maximum force in this second case is 5700 N.

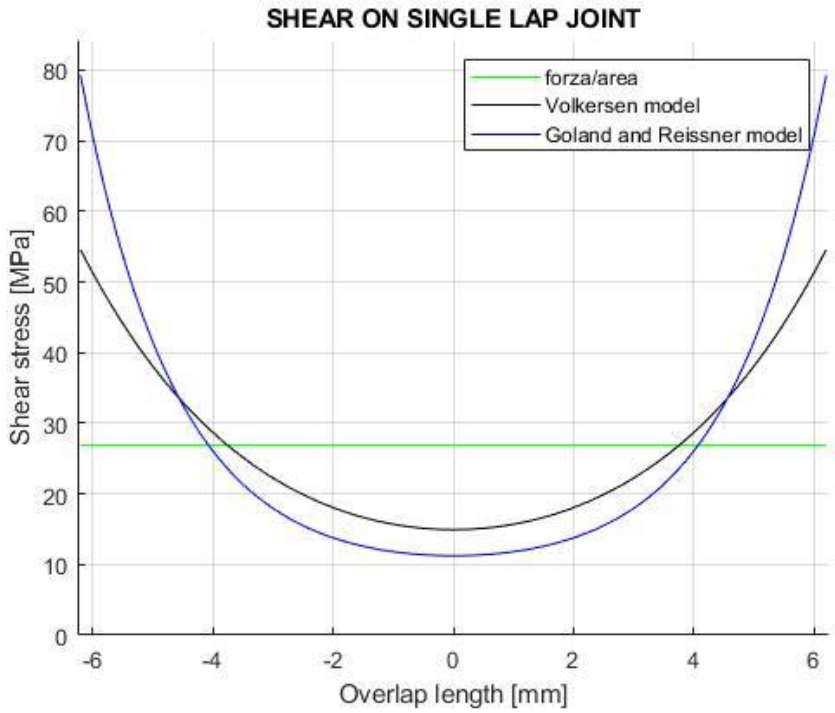

Figure 36.

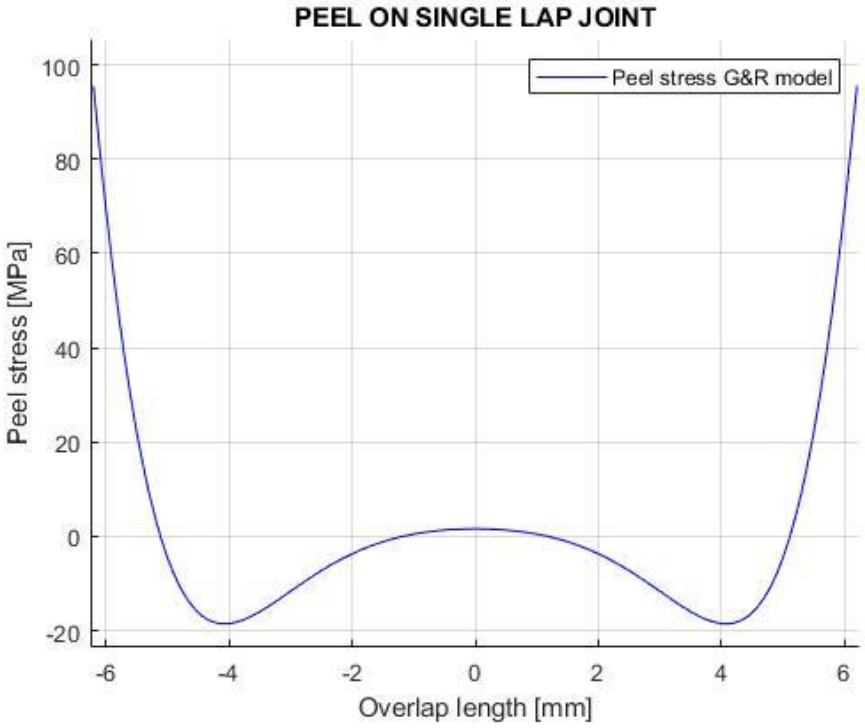

Figure 37.

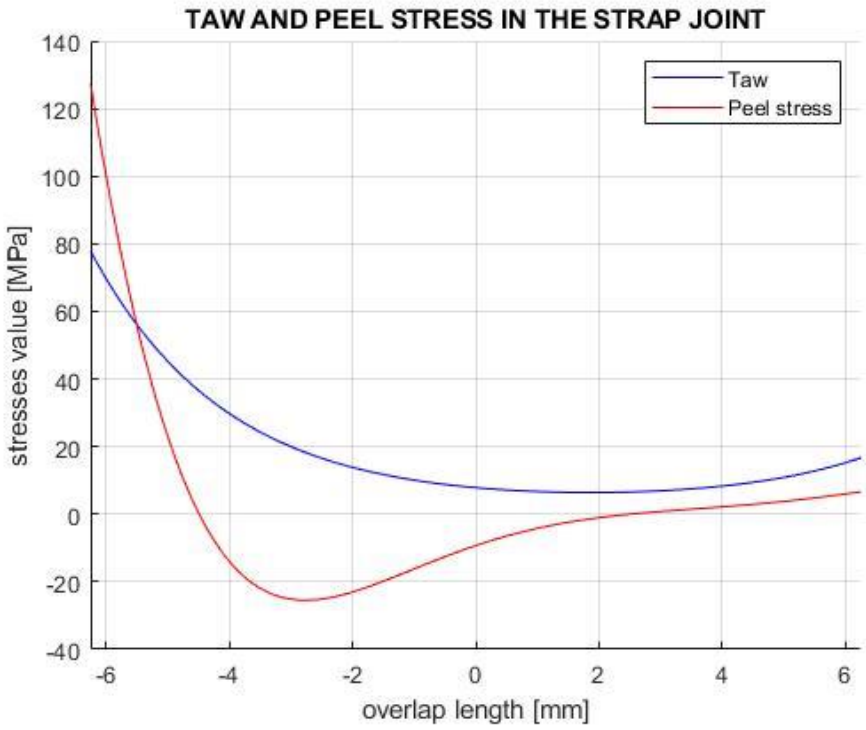

Figure 38.

In conclusion, from this theoretical analysis we can foresee the two cases of bonding failure. In the tests that have been designed, samples are used with reference geometries and some that can validate the bonding strength during flight. To obtain an answer on which of the two breaking values is expected, it is observed from the results that the tests will give.

4.2.2.2 Design of the Bonded Samples Realized

To have an axial load and limit the formation of a local moment, a symmetrical structure was created with two identical gluing area for each test. The components of the assembly are a composite plate with lamination defined by the one used in the external structure and two aluminium inserts on which the composite is glued. These inserts have two M10 threaded hole to join them a threaded bar for connect the samples at the traction machine. Standard sizing formulas are used for the design of the metal elements. The maximum load acting between the various samples is due to the maximum gluing area and the value is around 20 kN if the test is carried out at room temperature. Through this value it was verified whether the hole provided for the

threaded bar was enough to support the load without yielding. The verification is done on the thread of the Ergal component, as it is the least resistant material.
This value of force was obtained by applying a safety factor (sf = 2) and considering a correction for the presence of a bending moment (γ = 1.25 is usually used).

$$F_{traction\,\max M10} = \frac{\tau_{adm\ Ergal} * A_{res}}{\gamma * 0.33} \approx 30\ kN$$

where,

$$A_{res} = \pi d_{res} p_{screw}, \qquad \tau_{adm\ Ergal} = \frac{\sigma_{adm\ Ergal}}{\sqrt{3}};$$

After checking the resistance on the hole, it is important to size the gluing area and its geometry. As already announced, there are two gluing lengths that are tested. For both it was chosen to use a geometry that improves the resistance of the glue by tapering

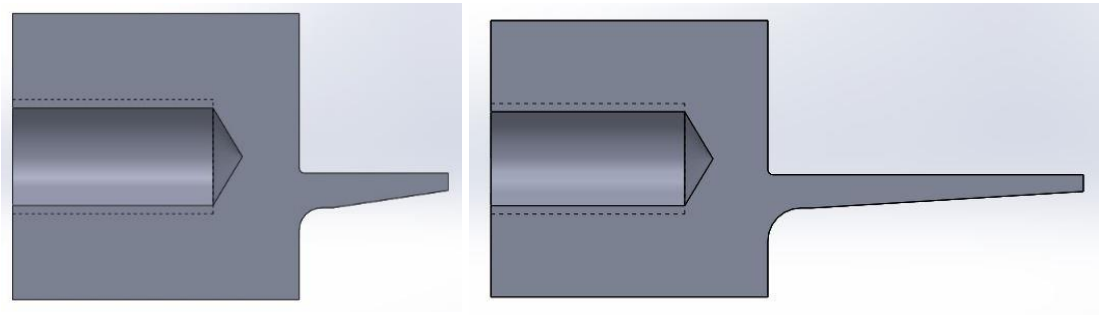

Figure 39. Strap Joints Designed

the plate externally. In the *figure 39* the geometry designed is shown. The hole for the bar is positioned so that the resulting tensile forces are in axis with each other and can reduce the formation of moments.
The two samples represented in the image differ in the length of bonding and the inclination of the tapered part.
A composite plate is glued between the two aluminium inserts (Ergal). The plate is laminated according to the rolling used in the rocket, in this way the interface that will be present in the flight configuration is represented. In addition to the type of lamination, the same 3 mm thickness is used, which is of great importance for the distribution of stress.

4.2.2.3 Realization of the Bonded Samples

Three main phases were performed to make the samples. The first consists in the realization of the components to be assembled, the second is the phase in which templates have been made to position the parts during the gluing phase and finally the last one is the gluing procedure.

Realization of the part: To make the ergal components, a numerically controlled (CNC) machine are used, they have been machined from full of Ergal bars to extract the designed piece.

To obtain the composite plate, it was decided to laminate a series of pre-impregnated carbon sheets to obtain a single piece. The laminated slab has larger dimensions than those required for the samples, so by the numerical control, the samples are made. In this lamination there are three types of ply in carbon fiber composite. The first type is the woven, that is a weave of fibers between them divided in weft and warp at 0 and 90 degrees. A second type of ply is the unidirectional where the fibers are placed in the same direction. Finally, the biaxial ply where the fibers are arranged at ±45 degrees without intertwining but only superimposed and held together by the matrix. The lamination being symmetrical and balanced allows obtaining good results in the autoclave phase, without surface tensions and without deforming the foil. In this way, although the lamina has a thin thickness, a curved geometry is not obtained but remains flat. The symmetry of the lamination allows this because the different ply of material have different expansions for the different directions in the plane, having a symmetrical composite two expansions are compensated by those of the opposite ply, allowing what has been described. The ply in the laminate phase are pre-preg (pre-impregnated) with an epoxy matrix. The choice of matrix depends on the design choices and above all on the operating temperature near the material. For the main structure of the rocket, a resin was chosen for ambient operating temperature. In the rocket cylinder there are no significant stagnation points that can reach critical temperatures for the composite.

Making the templates for gluing: In bonding it is important to be able to check the thickness of glue over the entire area and to be able to guarantee the desired alignments

during the polymerization phase of the glue. To do this it is necessary to fix the parts to be glued using external supports, in which case templates have been made to do this. To obtain excellent tolerances with reduced costs, they were made by 3D resin printing. The tolerance obtained from this process is around the tenth of a millimeter and this has allowed both to guarantee the desired glue thickness and the alignment of the components. The template has a slot for the axial alignment of the two inserts, and a second slot for the axial alignment of the composite plate. The glue thickness is around 0.25 mm with a tolerance due to the processing of ±0.1 mm. This thickness is given by the template that allows to space the two parts of the desired thickness. Furthermore, to avoid difficulties in the gluing phase, the template is designed so as not to come into contact with the bonding edges so as not to stick to the sample.

Sample bonding: Before describing how the components must be glued to make the samples to perform the tests it is necessary to increase the roughness of the surfaces where the glue must adhere. An abrasive paper is used for the composite surface, in order to increase the roughness on the surface resin layer. Instead, the metal inserts are subjected to a sandblasting process in order to create spaces in which the glue can adhere.

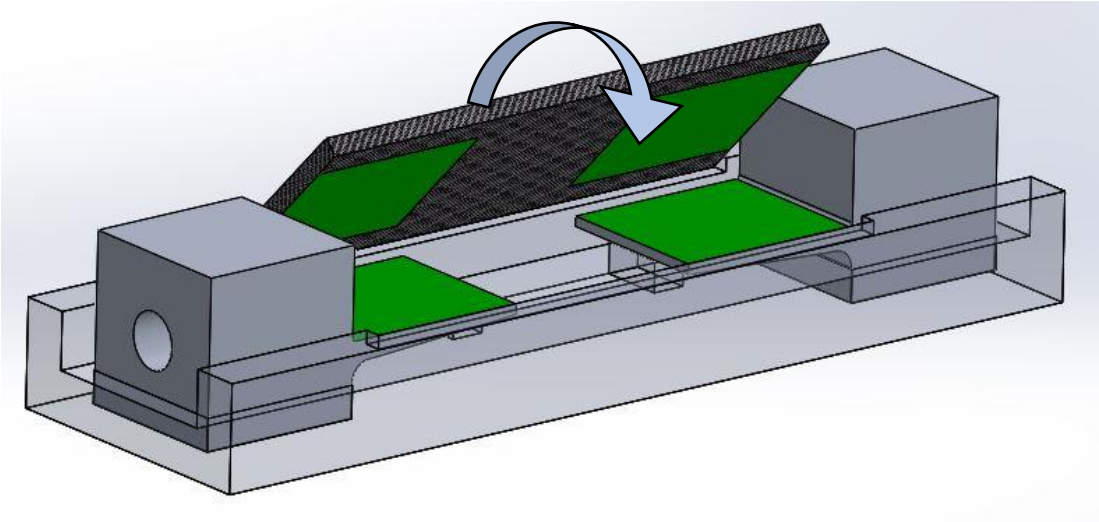

Figure 40. Strap Joint Assembly

In the *figure 40* it is shown how the system must be assembled to obtain the desired result. The areas in which the glue is to be deposited are shown in green. When the

glue has been spread the two surfaces must overlap and the composite sheet must come into contact with the template and position itself inside the two metal inserts (as shown in the figure).

Once the assembly has been assembled, it is necessary to wait 24 hours at room temperature to allow the glue to start curing. After waiting for this first phase, the template is removed, and the sample is placed in a controlled temperature oven at 65 ° C for 120 minutes. In this way the glue polymerizes completely as it can confer the structural properties to the joint.

Figure 41. Strap Joint Assembly Result

The result of this process is shown in the *figure 41*, the lower part of the glued assembly is shown. You can observe the excess glue that is spilled. This effect does not significantly affect the test result, the glue thickness was measured and is 0.3 mm which is within the desired tolerances. The sample is aligned as desired and does not present distortions for the cure in the oven for the polymerization of the glue.

4.2.3 Carrying out the Bonding Test

To proceed with the tests, the boundary conditions are first established to perform the tensile tests. It is planned to produce 4 samples of which two have a gluing area with a length of 12.5 mm while the other two have a length of 28 mm. The reason why there are two samples on each configuration is to obtain the minimum availability on the results obtained. To perform the tests, a test procedure table was created with all the types of specimens studied, with the different bonding areas and the respective breaking loads.

	SAMPLE	OVERLAP GEOMETRY	TEST TEMPERATURE [°C]	EXPECTED BREAKING LOAD [kN]	STOP TEST
Test n°1	n°1	12.5 mm x 25 mm	23	5.7÷8.4	FAILURE
Test n°2	n°2	12.5 mm x 25 mm	23	5.7÷8.4	FAILURE
Test n°3	n°3	28 mm x 25 mm	80	6.0÷9.8	FAILURE
Test n°4	n°4	28 mm x 25 mm	80	6.0÷9.8	FAILURE

Table 10

To heat the sample is used a thermal resistance that allows to spread heat. The wire on which the current is circulated is wrapped in a thermal sheath to achieve the desired temperature externally and not to burn the sample. The entire system is thermally shielded and once it reaches a temperature of 80 °C measured using a thermometer, the heat supply system is switched off and the traction test is started.

The samples are numbered to be identified even after the test has been performed. The preparation for the test is simple, the connecting bars are screwed, then the samples are fixed on the clamps of the traction machine. Before fixing both ends, in each of the tests, the position of the machine is reset. When the machine is zeroed, it is also possible to fix the second clamp and start the tensile test. It is important to program the sampling frequency of the position sensor, and the speed with which the force is increased during traction. Thus, it is possible to increase the resolution of the test and have results with a good sensitivity.

4.2.4 Test Result

The tested samples are those indicated in *table 10*, the first two were tested at room temperature, while the other two were tested at 80 °C.

They are tested by a traction machine, in which they are fixed by the two clamps. In output the machine supplies the acting force and the respective displacement of the

sample. In this way it is possible to observe the tensile strength of the bonding. The trends of the curves for the samples n° 1 and n° 2 are reported.

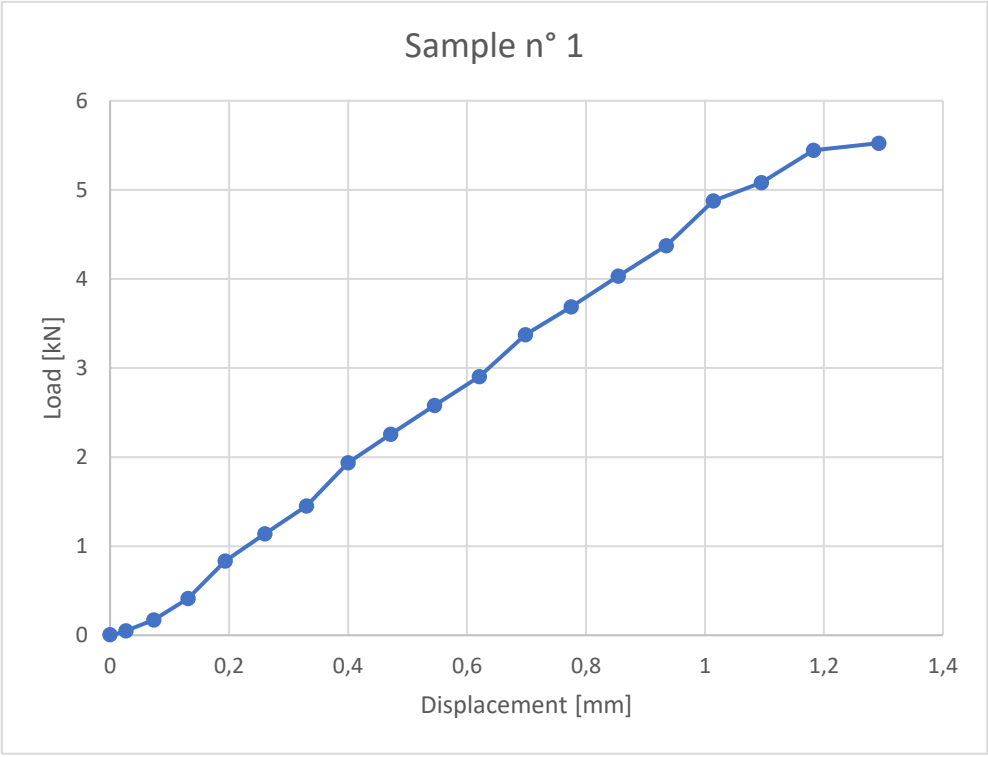

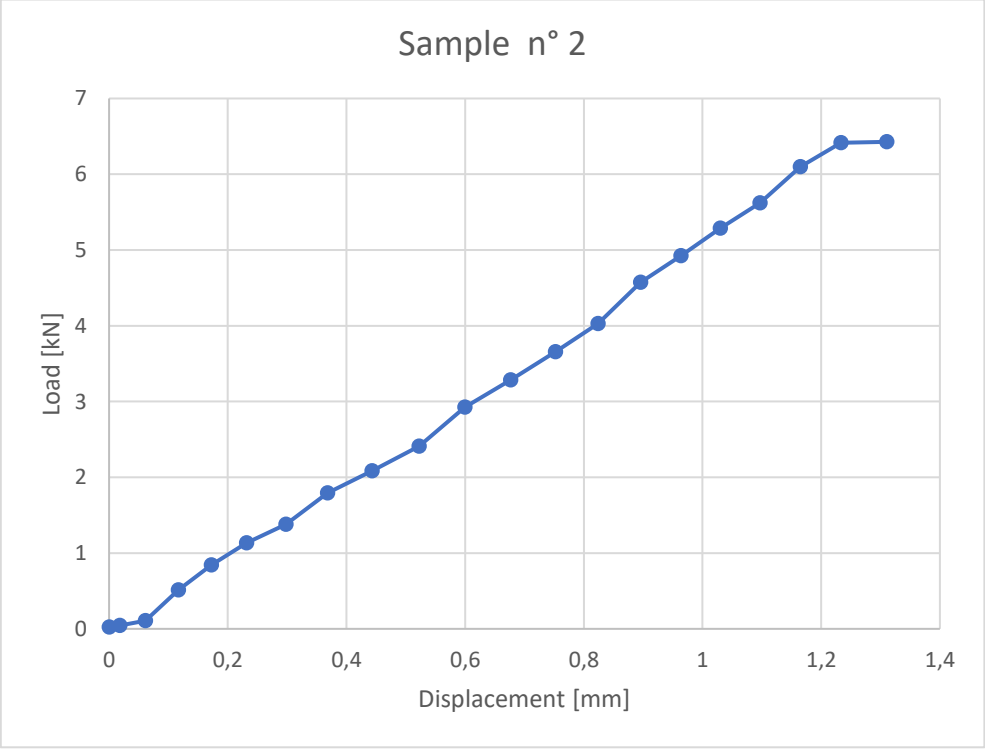

Figure 42. Samples 12.5mm x 25 mm Test Trends

It can be observed that the strength to which the bonding has been broken in the first case is 5.7 kN in the second case it is 6.4 kN. The expected value was 8.4 kN if an average shear stress distribution was considered. The value obtained is lower as there were mechanical misalignments in the machine which significantly affected the results. This has caused tensional states different from a pure cutting condition.
In the *figure 43* the samples are shown after the break.

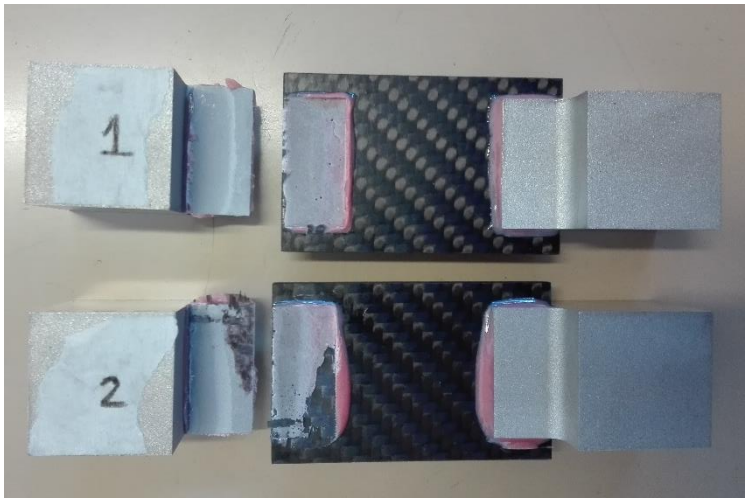

Figure 43. Failure Result Samples 1 & 2

In the sample 1 it is observed how the failure occurred on the interface between the aluminium and the layer of glue. In the sample 2, it can be observed how in the most part of the bonding area the failure occurred in the glue-aluminium interface, while there is also a small part in which the composite material has suffered a delamination of the interfacing fabric layer with glue.
After having tested the first two samples, we proceed with the installation of samples 3 and 4 in the machine. The configuration foresees being able to heat the bonding up to 80 °C and to monitor the temperature supplied through a thermocouple. In order to maintain a uniform temperature, the resistance and the sample in the area of interest are covered with aluminium foil. In the *figure 44* the system installed before the test is shown.

Figure 44. Test Configuration for Samples 28 mm x 25 mm

When the thermocouple indicates the desired temperature, wait about a minute to even out the area and then proceed with the test.

The following graphs showing the force-displacement curves were obtained from the machine output.

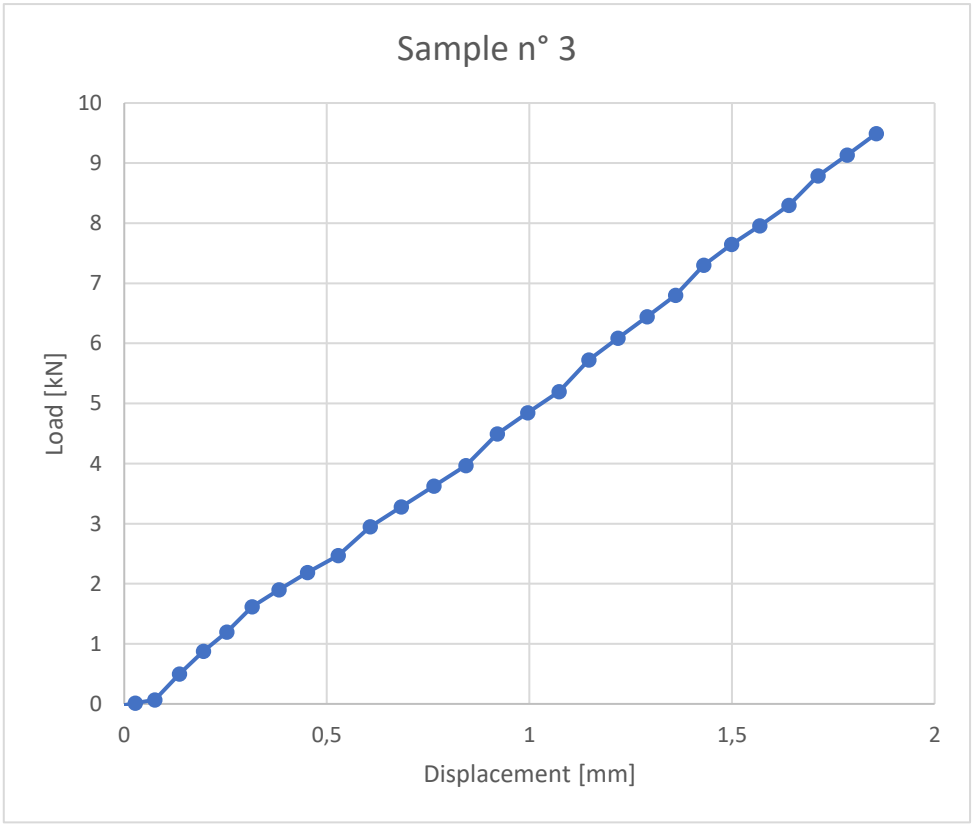

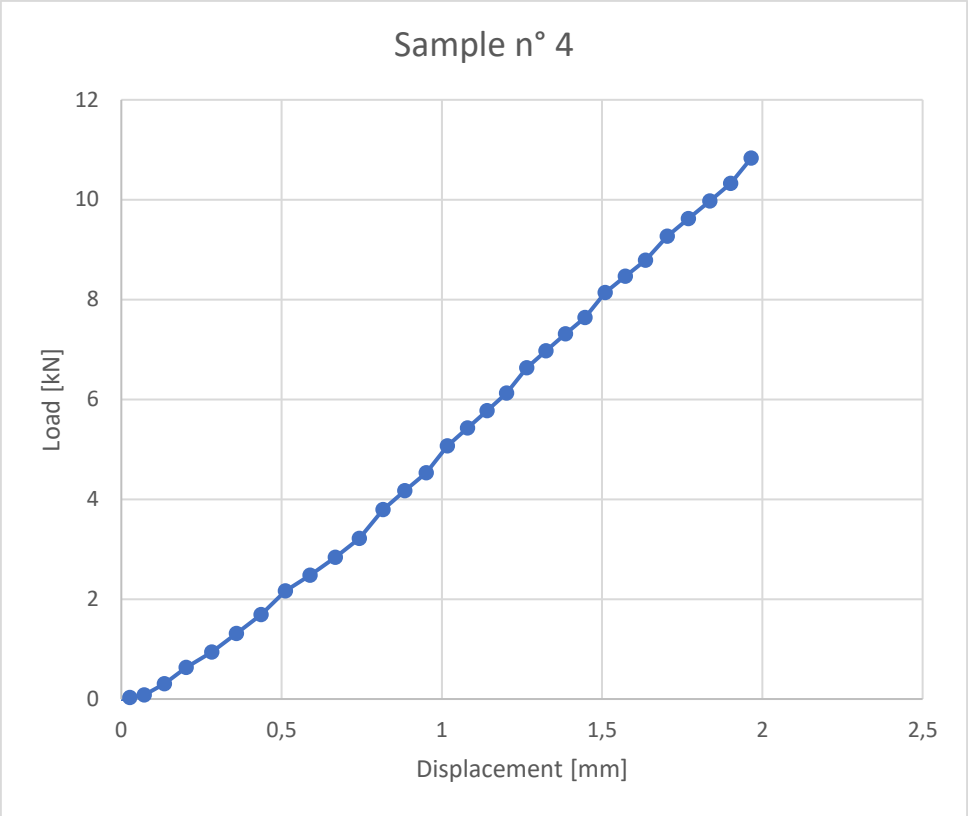

Figure 46. Samples 28mm x 25 mm 80° C Test Trends

In sample 3 the break occurred at 9.5 kN but not in the heated area. In sample 4 the breaking point occurred at 10.8 kN in the area where the bonding was heated. During the test before the rupture, at about 7 kN for both samples crunching noises were heard although the gluing had not completely yielded. The expected rupture result from the distribution of the average stress shear was for a force of 9.8 kN.

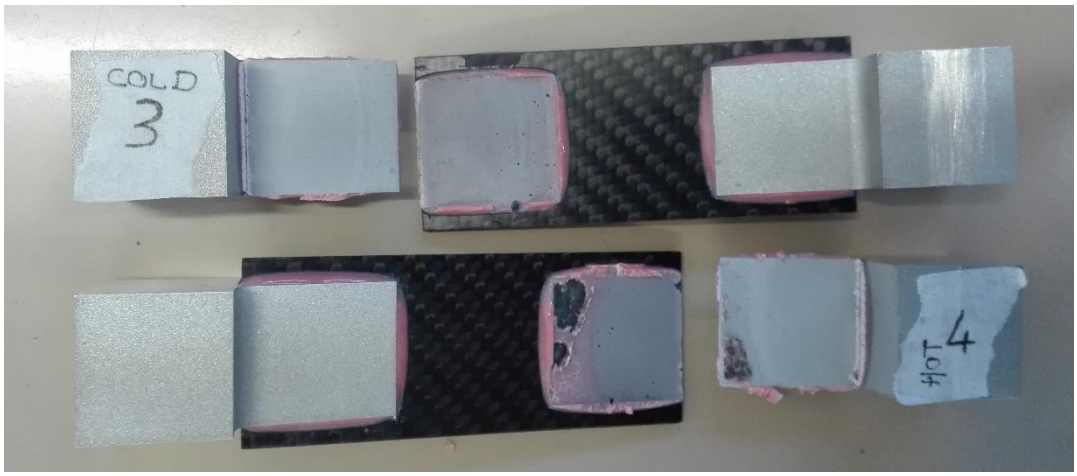

Figure 45. Failure Result Samples 3 & 4

The samples are shown in the *figure 45* after being tested.
As with the previous samples, the composite was delaminated in one case while the glue-aluminium interface was transferred in the other.
During the casting phase, the gluing area with a length of 28 mm overlap and 25 mm in width must withstand a load of 3 kN. This value is less than a factor of 2 of the value at which the first cracks were heard during the test, and a factor of 3 with respect to complete rupture. This allows you to use bonding in the flight configuration.
Furthermore, comparing the test with the "short" bonding from 12.5 mm to the "long" one from 28 mm it is possible to observe how the tapered geometry used in the Ergal allowed to obtain the expected result even if there were any misalignments present.
Furthermore, after the tests carried out, the temperature increases to 80 ° C does not affect the result appreciably if the exposure takes place for a few minutes as in the case of the flight of the rocket.

4.3 Scarf joint test

It was decided to carry out some tests regarding the scarf-type bonding that was carried out in the engine area. The pressure in the catalytic at around 25 bar acts normal to the walls stressing the external structure. The weak element in this area is given by the bonding on which traction forces act.

To ensure the correct operation of the engine and the structural resistance of the rocket during the launch, a test model was created to represent the distribution of loads acting on the bonding. To realize the test, two Ergal plates and a carbon tube are interfaced. These three parts are glued together to form the assembly to test.

The composite material cylinder interfaces symmetrically with the aluminium plates with two bonding. A high precision lathe was used to accurately realize the coupling between the conical surfaces. The processing of the composite was done starting from the hollow cylinder, while for the aluminium components the starting blank was a solid cylinder.

The taper has an angular inclination of 3 °, this value was chosen both as a function of the desired bonding area and to approach the optimal inclination value deriving from the theory.

Figure 47. Scarf Joint Test Design

To allow the glue to adhere to the surface of the adherents, these are worked superficially increasing their roughness. For the parts in Ergal it is necessary to make a sandblasting, while for the composite cylinder it is enough to work on the lathe to

Figure 48. Scarf Joint Gluing Area

have a good surface roughness. Before proceeding with the deposition of the layer of glue the surface was cleaned of dust residues. After depositing the glue layer, the components are assembled. The polymerization adhesive must be subjected to the cure cycle in the oven.

To pressurize the sample, there are two threaded holes of type G1 / 2 (gas 1/2) through which it is possible to apply two lines of fluidics and pressure sensors. This type of threading ensures that the pressure acting inside the system is maintained.

To guarantee a safety situation, the tank is filled with water to limit the number of pieces in case of breakage or explosion. Water, unlike gas, being not compressible does not accumulate energy when it is put under pressure. In this way, if there is a structural break in the tank, there is no explosion but a leak of pressurized water, limiting the danger. The pressure inside the tank are monitored by a pressure sensor, which is inserted into the hole of one of the two ends. The water is loaded from the other end where the pressure is applied.

Before describing the geometry of the bonding area, the forces that act and how much bonding is subjected to the stresses are analyze. The operating pressure is around 25 bar (2.5 MPa) that act in a surface area of $A_{N\ TOT}$= 28352 mm^2. The resulting axial force is:

$$F_{N\,TOT} = A_{N\,TOT} * Press = 2.5 * 31682 \cong 71\ kN$$

where, $F_{N\,TOT}$ is the force acting normal the surface of ending plate in aluminium.
The bonding must guarantee with a good safety factor that the agent load does not cause the structural breakdown of the system. In this case it was chosen that the truncated cone on which the two surfaces are superimposed by gluing together the components, present a height of 42 mm. Through the theoretical formulas the designed gluing area is obtained.

$$A_{bonding} = \pi(r_1 + r_2)a = \pi(98.80 + 94.95)42.18 \cong 25674\ mm^2$$

To obtain the maximum axial force that can be loaded is necessarily know the type of glue used and the working temperature. In this bonding there is the catalytic element which has an important thermal source, but the configuration is thermally shielded from phenolic material. In this way the thermal source present comes from the external aerodynamic effects that lead to the achievement of a temperature of 80 °C. The *3M™ Scotch-Weld™ EC-9323 B/A* is used which guarantees good impermeability to pressurized gases and has an excellent bonding strength at these temperatures. The characteristic of being an epoxy resin allows to isolate and seal the inside of the motor with the external environment. The shear strength value for this type of glue at the given temperature is about 14 MPa. From the calculations result that the axial force with which the designed bonding resists is:

$$F_{strength\ max} = \tau * A_{bonding} \approx 359\ kN$$

For the test phase, the bonding strength will be tested until the joint fails. However, in the design phase it is also necessary to locally insert the load due to the bending moment acting on the structure. Leading to lower the safety factor from four to two.
Specifically, analyzing the geometry in the gluing area, it can be observed that to guarantee a uniform glue thickness and to align the components axially, a relief is inserted at the end of the joint. This thickness allows the insertion of the two pieces and the concentricity during assembly, except for some imperfections in the realization of the parts.

The operations carried out during the test are performed to validate the bonding strength. The following table shows the different phases of the test that are carried out:

	Pressure [bar]	Temperature [°C]	Pressurizing Fluid
Test n° 1	20	Room temperature (23°C)	Water
Test n° 2	20	Room temperature (23°C)	Gas
Test n° 3	40	Room temperature (23°C)	Water
Test n° 4	40	Room temperature (23°C)	Gas
Test n° 5	up to break	Room temperature (23°C)	Water

Table 11

Following the order of the tests to be performed on the sample it is possible to obtain valid results as bonding is increasingly stressed. If there is no failure due to the first four stages of the test, it will break down further increasing the pressure up to that which leads to the failure of the bond.

Before starting the test, all necessary elements must be positioned and integrated. In the the system is shown before the test starts. The carbon cylinder with the two bonded flanges is fixed by a support ring to an external structure. This structure is closed by a

Figure 49. Scarf Joint Test Configuration

metal mesh to protect the operators and any surrounding objects during the test. The pressurizing pump is connected to the bottom of the sample. In this configuration the pressure sensor is placed in parallel with the pump in order to monitor the pressure.

4.3.1 Test result

Once the test configuration has been mounted, proceed with the different planned steps. Initially water is brought under pressure up to 20 bar, after a waiting time of 5 minutes in which the stationary pressure is maintained, it was observed if there were actually visual pressure losses. This operation was done both for the water and gas test. Finally, the

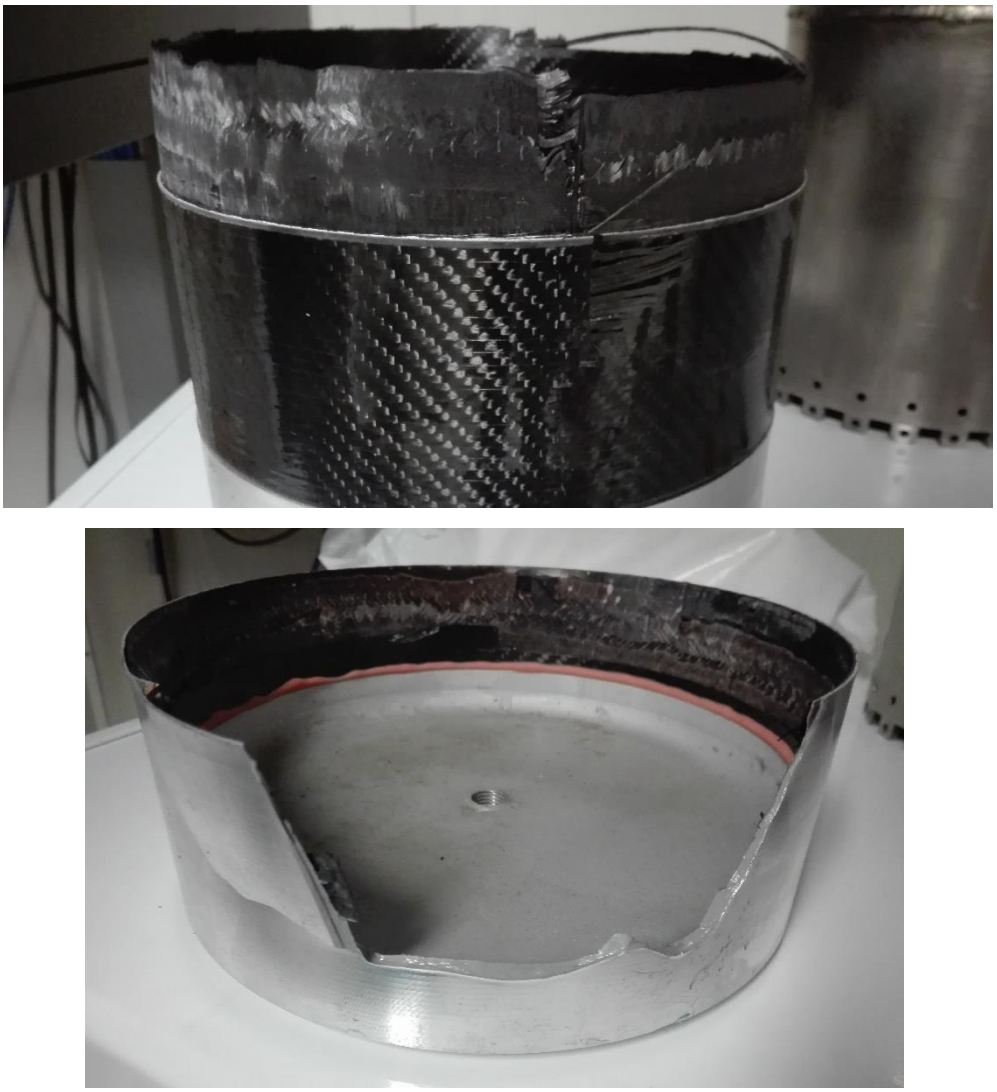

Figure 50. Scarf Joint Test Resut

configuration containing water was used and the sample was broken. The measured breaking pressure is 148 bar. The images show the sample after the test.

It can be seen that by proceeding with different pressurization cycles, the bonding did not have yielding or internal cracks. This allows for a safety margin in the configuration used during the flight phase. The tested bonding made it possible to validate the pressure resistance and also the pressure gas impermeability.

The failure occurred due to failure of the bonding as the entire aluminium plate was detached. In particular, the delamination of the carbon in the glued area occurred.

Chapter 5
Additional Tests of some Components of the Sounding Rocket

Inside the rocket there are two other structural elements that need specific tests to validate their use in the final configuration of the rocket. These elements are the holes for the screws in the carbon, and the class 12.9 screws used in the joints. In this chapter some test procedures will be described to represent the resistance with the appropriate loads of these two elements.

In particular, tests will be carried out on the rebound due to the presence of screws in the composite material when stressed by shear stress, and tests on the resistance of class 12.9 screws when an impulsive load act.

5.1 Test in the Composite Material Holes

Perforated connections were used in the junction that connects the nosecone to the entire rocket. Given the complexity of establishing the theoretical behaviour of how the composite behaves in the hole area, it was decided to carry out representative tests. Since the overall properties of the composite material derive from a combination of several ply, this complicates the calculation of the structural strength. However, the presence of holes complicates the behaviour of the latter because the fibers lose continuity. In this way the perforated area weakens structurally. The forces are transferred between the fibers through the matrix but locally having made a hole there is a non-homogeneous transfer. Moreover, the matrix has a lower resistance than the fibers for which there is less structural resistance.

To verify the stresses, test specimens were made. The failure mode of a bolted joint is due to three factors, the rupture, the break in the area between the hole and the outer edge or the breaking of the screw. The main failure of composite materials is by

delamination. That is the breaking of some laminae that separate from the others, producing fibrous material and causing the failure of the structure. Each lamination has its own delamination characteristic and also the ultimate breaking load

5.1.1 Test Description

This section describes the configuration used to perform this type of test. To get good results and to get accurate tests, a traction test machine is used. This allows you to obtain real-time data on the progress of the test and then be able to analyze the graphs obtained and make conclusions.

To study the behaviour of the composite material in a bolted connection that acts through shear loads it is necessary that the realized samples have a geometry such as to reproduce this type of configuration. For this reason, three test components were used. First, it was decided to use a sample of carbon fiber composite material with a lamination corresponding to that used in the main structure of the rocket. This allows us to obtain useful results to validate and bring new knowledge in the field of composites.

Using a plate specially made according to the required specifications, it is possible to cut samples with dimensions suitable for the test to be performed using a numerically controlled machine. Since the rocket is expected to use bolted connections even in composite components, a diameter of 4 mm holes and a plate thickness of 3 mm is used in the tests. In the *figure 51* the dimensions of the sample used to do the test are represented. The lack of knowledge of the behaviour of composite materials as bolted junctions has led to the use of the rebounding rules used in isotropic materials. This at least as a first approximation.

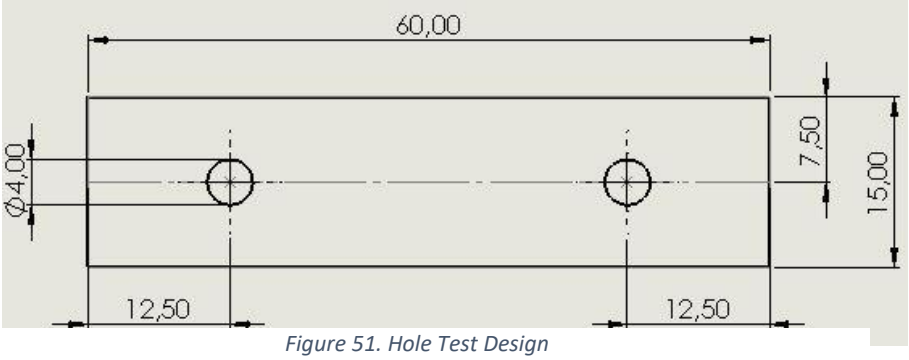

Figure 51. Hole Test Design

The geometry used has two holes aligned and of equal diameter. Furthermore, a symmetry is used in the sample to get more precision from the test.
The second component used is M4 screws with partially threaded shank. The screw hole union is possible through interference which allows the screw to be inserted and the stem part positioned without threading on the hole. This allows the pressure exerted by the screw to be free of elements that generate voltage peaks and that allows to evaluate a correct rebound.
Finally (as can be seen in *figure 52*) two steel inserts were used to connect the sample to the machine. Which allow to transfer the load imposed by the machine to the screws, which stress in composite carbon.

Figure 52. Hole Test Configuration

The following table shows the test procedures to be performed for the three samples.

Sample	Load imposed [kN]
n°1	FAILURE
n°2	FAILURE
n°3	FAILURE

Table 12

5.1.2 Test Results

The results obtained from the tensile tests are shown through the following graphs where the displacements are represented as a function of the imposed load. Before each test the machine is reset to have the real movements of what is happening on the sample. The graph represents the deformation (in mm) as a function of the load (in kN) that is imposed by the machine on the sample.

The trend of the three graphs is similar. In the first part there is a displacement due to

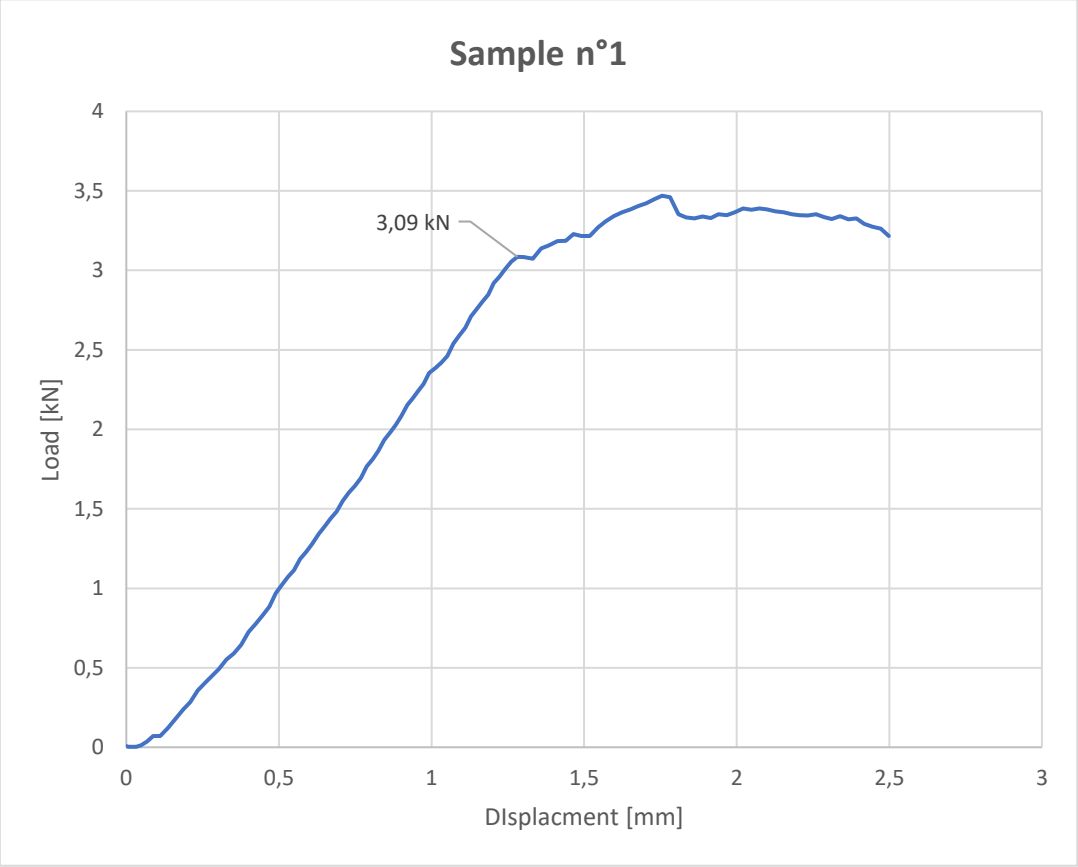

the tolerances that are inside the sample so that with small forces involved there are displacements. This because there are small clearance and therefore they are cancelled with the first imposed forces. Subsequently there is a constant deformation pattern depending on the imposed force increment. For all three samples there is an elastic pattern in the first part, while in the second part, although the load resistance strength increases, the delamination phase begins.

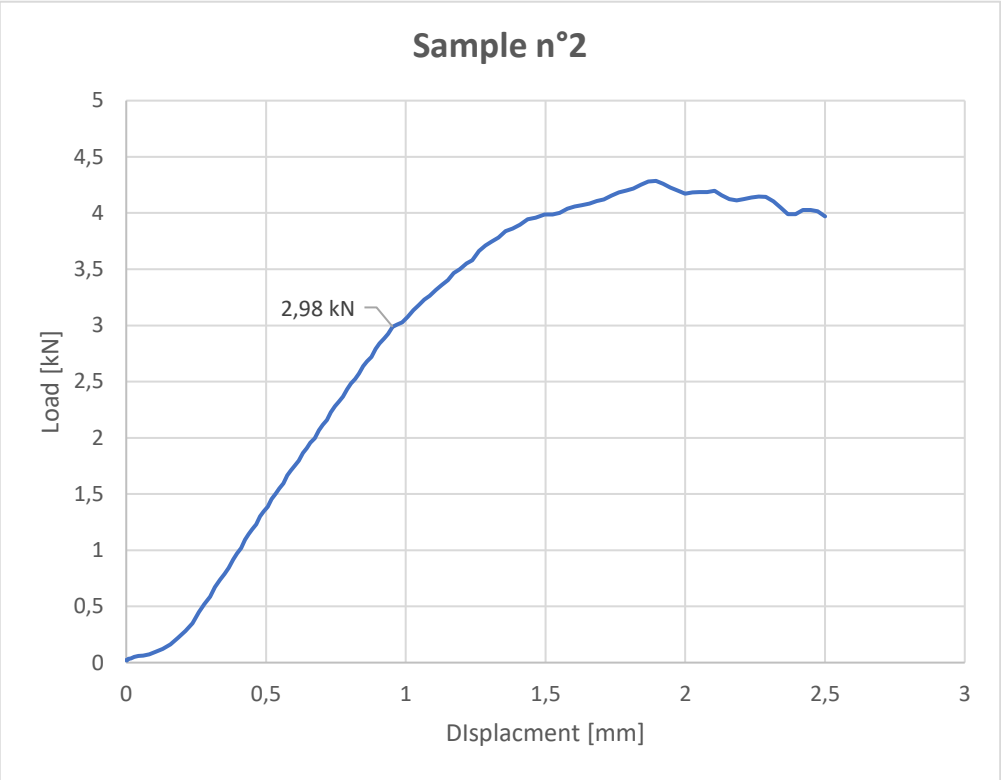

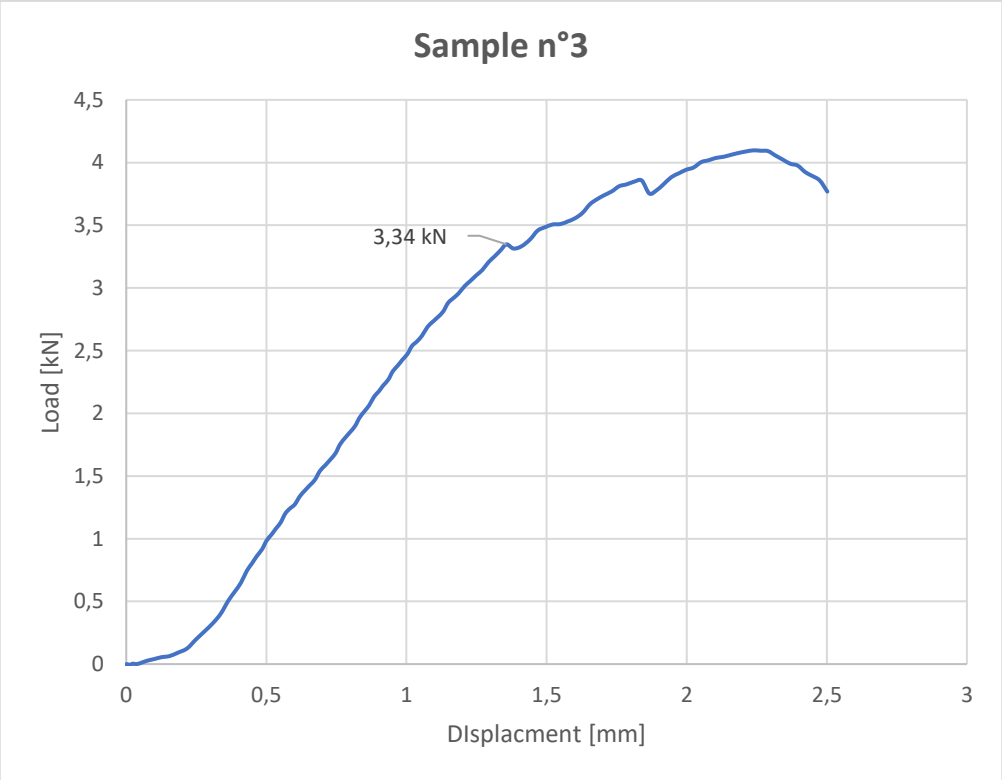

Figure 53. Hole Test Results

In the delamination zone, however, there is an increase in resistance, when the sample is already failed. This happens because the orientation of the fibers is multidirectional. After intralaminar failure, the fibers oriented in the orthogonal direction continue to resist of the load. For structural reasons it is necessary to avoid the rebounding of the hole for which the first failure is taken as the limit value.

The results of the three tests are also represented through the linear regression line. The values shown have the initial displacement cleared when the part of the graph with elastic deformation begins. Three different slopes can be identified for the three samples, and three different values where the cracks begin to propagate. The value of interest for the application of perforated elements in the rocket is that of the value to which the cracks begin to propagate. The elastic limit value for this test configuration is around 3 kN. Beyond which the sample fails.

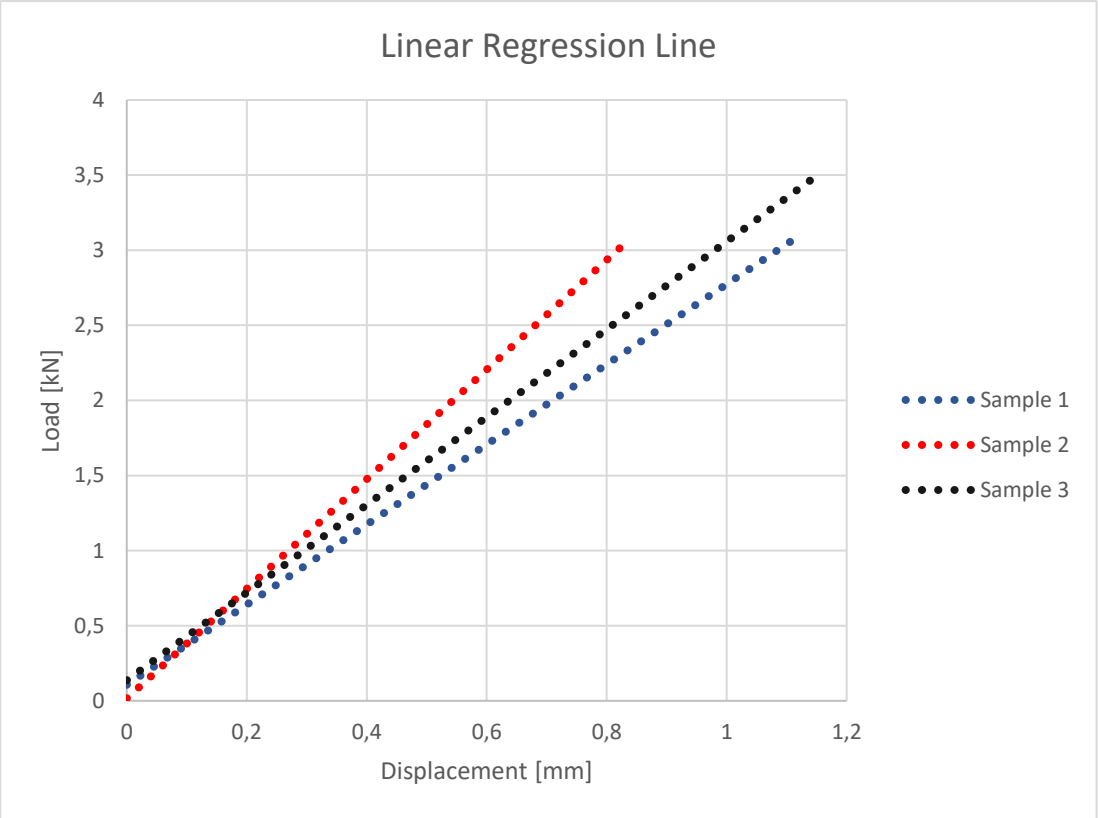

Figure 54. Hole Tests Regression Lines

The tested samples present an important delamination. An example is shown in the *figure 55,* where it is possible to observe how the composite material appears at the end of the test.

Before the complete delamination and intralaminar rupture the rebounding took place. This is observed since even the pieces that have come off have even the slightest

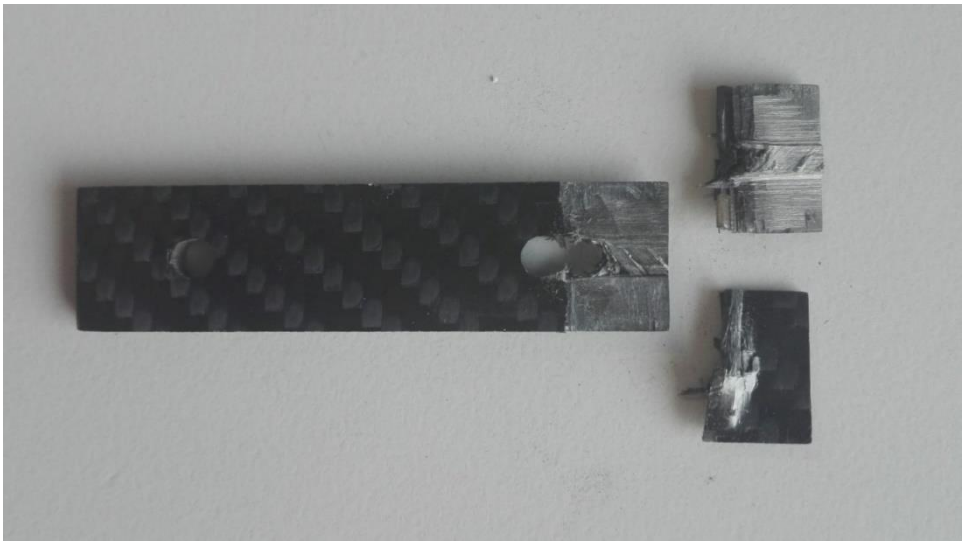

Figure 55. Hole Test Sample Result

possible ovalization of the hole. The delamination takes place to achieve the intralaminar resistance value ILSS (intralaminar shear strength). From the results obtained and known the dimensions of the hole it is possible to obtain the maximum pressure stress that this configuration of laminate can assume before reaching failure. From follow formula are possible have the maximum sigma in the hole before the delamination:

$$\sigma_{reboundig} = \frac{F}{d_{hole}\, t_{hole}} \approx \frac{3000}{4 * 3} = 250\ MPa$$

This value can be used to design bolted joints of composite material for the rocket structure.

5.2 Shear test on High Resistance Screw

In the sounding rocket project, high strength screws were used to join the joints. It was decided to use screws with a partially threaded shank, having f9 tolerance. Commercially this type of screws are manufactured with resistance class 12.9. Their

high resistance to static load is due to the material with which they are made. However, although the material allows excellent resistance properties, the fragility to impulsive

Figure 56. ISO 7379

stresses also increases. During the ignition of the rocket there are acceleration loads that are not static but have an impulsive behavior. For this reason, tests are carried out to stress the screws through the stresses that represent the load during this phase.
The described screws have a shank diameter of 4 mm with a length around 12 mm, while the threaded part has an M3 diameter. Their application serves to maintain an excellent alignment between the two elements to be joined. In fact, thanks to the shank in tolerance it is possible to insert the screws in the plate with a minimum clearance and align the two plates.

5.2.1 Test Description

Before proceeding with the test and with the design of the samples and the respective inserts it is important to study what is the load to which the screws must withstand. To do this it is necessary to observe inside the rocket which junction is most stressed and how.
During the launch of the rocket the impulsive loads are those due to the thrust given by the engine. The acceleration initially produced is around four times the gravitational acceleration, while towards the end of the ignition it is around five. This acceleration imposed on the mass of the rocket is translated into force by Newton's law. The resulting load is around 5 kN. It is not applied slowly but behaves like a step input. It is very important to be able to represent this load on the screws that will have to withstand during the flight. This type of load is axial, so it is divided between the number of screws in the joint. The impulsive load acting on the screws is the total one divided by the number of screws (n° 28) obtaining as final value 180 N. Analyzing the

system and its dynamics of impulsive loads there are no others during the flight of the rocket. For completeness in the tests to be carried out, tensile tests of the screw are also carried out until failure. To have a reference value the screw must withstand a semi-static load of at least 3 kN. By means of the following calculations, on the other hand, the breaking value for this type of screw is provided.

Given the $\sigma_{ult.\ screw}=1200\ MPa$ are obtained:

$$\tau_{ult.screw} = \frac{\sigma_{ult.screw}}{\sqrt{3}} \approx 700\ MPa$$

and for a diameter of 4 mm are obtain a maximum breaking load F of

$$F = \tau_{ult.screw} * \frac{\pi\ d_{screw}^2}{4} \approx 700 * \frac{\pi\ 4^2}{4} = 8800\ N$$

The action of the load must be representative of the one acting on the junction and of pure cut. To maintain the analogy and to correctly represent the state of stress acting on the screw, specimens are made with specific inserts to guarantee this aspect. The realized inserts are shown through an assembly (*figure 57*) which shows the chosen configuration.

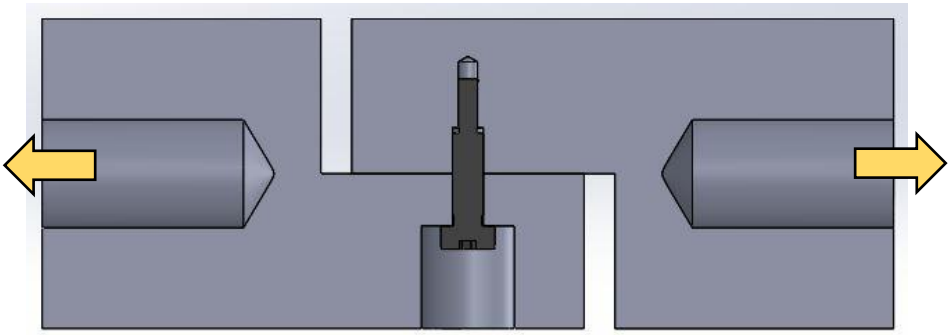

Figure 57. Screw Test Design

The two inserts are made of C45 steel as they must withstand the imposed load. Furthermore, their geometry is such that a shear load can be transferred to the screw in the intermediate section of the unthreaded stem. Each insert has a M10 threaded hole to insert a bar with which the connection to the traction machine is made.

Another important element is the hole for the screw that must be made with a diameter and tolerance such as to insert the screw providing the minimum clearance to the joint. To allow this, the reference standards for a shaft-hole coupling have been used.
The screw has a 4 mm diameter shank with a f9 tolerance, in view of the possibilities of working, it was decided that the hole had a H7 tolerance with a base diameter of 4 mm.
As shown in the figure, the mechanical backlash is between 0.010 mm to 0.052 mm this because the coupling f9-H7 allows this interval.

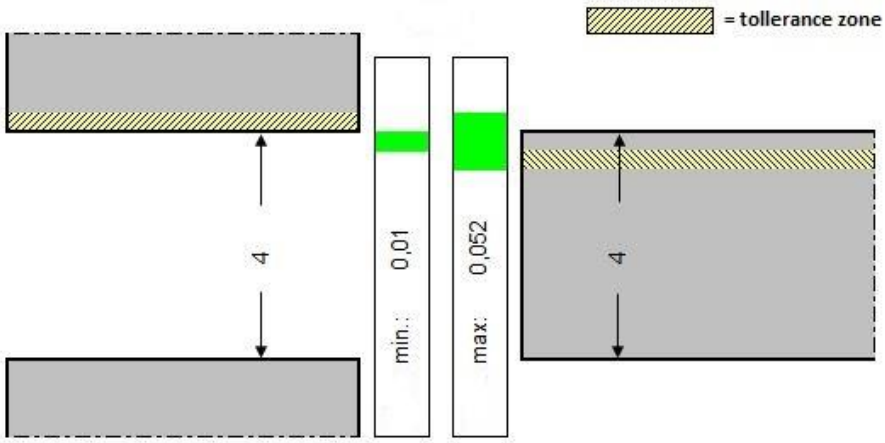

Figure 58. Mechanical Backlash

To carry out the impulsive load a weight between 18 and 20 kg is used, which is fixed by means of an eyebolt (DIN 580 M10) to the sample, which is constrained in the other end to a structure that acts as a base. The system must be able to be away from the ground so that the load can drop off. In this way the 180 N that will be applied to the structure will have a step input, since they can impulsively stress the screw. As for the breaking test, it is performed in the laboratory using a traction machine with a capacity exceeding 10 kN. The samples thus loaded can be broken.
It is important that the results show the force-strain behaviour of the screw. To obtain the maximum deformation before breaking the screw.

5.2.2 Test Result

The screw to be tested is an ISO 7379 class 12.9. The parts are assembled and the screw fixes the two elements to be inserted in the traction machine. Once the sample

Figure 59. Screw Test Configuraiton

is constrained, you can see in the *figure 59* how the system looks before running the test.

The traction machine is operated with the extensometer of the machinery which reports force information and sample displacements. Re-elaborating the results file it is possible to obtain the shear stress trend depending on the displacement. The results obtained are shown in the *figure 60.* From these results positive results are obtained

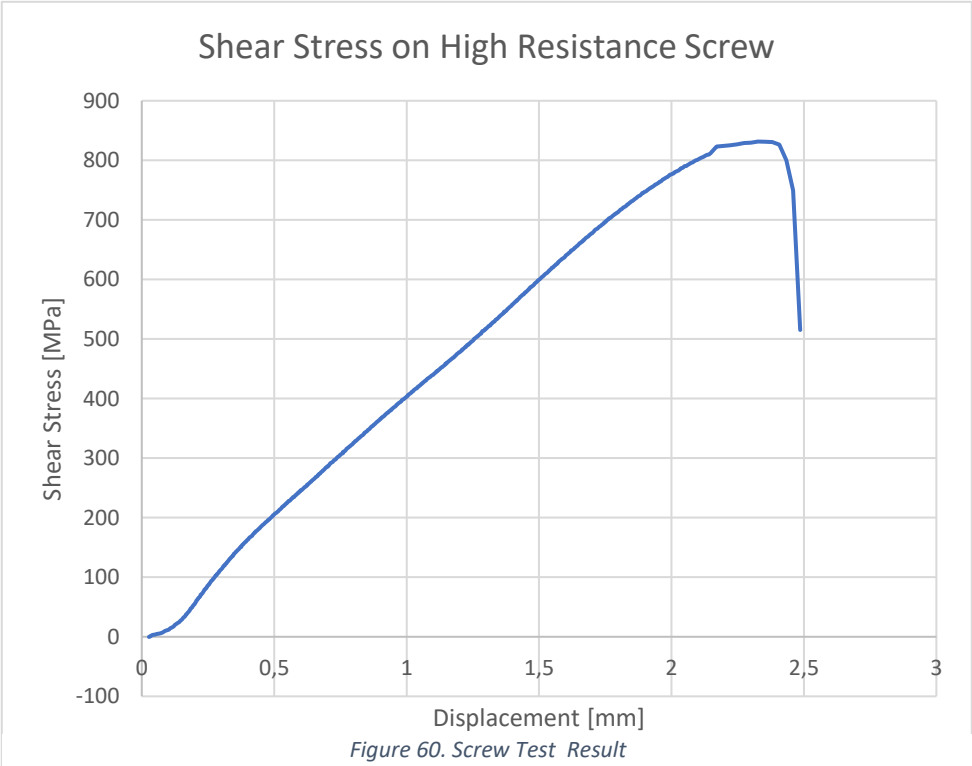

Figure 60. Screw Test Result

with the theory presented, furthermore it is possible to validate the insertion of the screw in the flight model.

The graph shows four different trends; a first part where displacements occur due to small increases in strength. This is due to the couplings of the assembly in which there is no actual deformation of the parts but the coupling tolerances are delete.

The second part is given by the elastic deformation that occurs in the screw. This trend has a very linear voltage-deformation curve with a constant slope. In this phase the screw elastically deforms without having plasticization. In fact, the plastic deformation phase is the third, which is very short due to the high fragility of the material used to make class 12.9 screws. In the graph it can be seen that the third zone goes from 700 MPa to 800 MPa where the screw breaks. The last zone is an area of non-analytical interest but derives from the machine's stopping time.

It can be stated that the screw can be inserted in the flight configuration because during the flight on the single screw a 3 kN load is expected, and from the test it emerged that the break occurred at 10 kN while the yield occurred around 9 kN. Getting a security factor of around three.

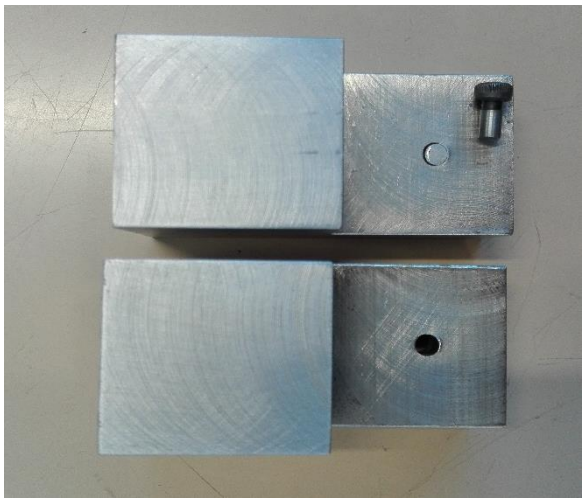

Figure 61. Screw Test Sample Result

Finally, it is shown in the *figure 61* how the sample looks after breaking. It is possible to observe the screw that has broken to shear and that the hole has undergone refill in the part near the cutting area.

Summary and Conclusion

The design and study of some structural parts of the sounding rocket allows to insert them in the flight configuration. After a brief introduction to sounding rockets, the joints were designed. These are very important structural components that perform a dual function. They have the purpose of separating the different subsystems allowing the transport of the disassembled rocket. Furthermore, they are intended to combine the various elements that cannot be designed if the rocket were made with a single structure.

Structurally they have the purpose of keeping the rocket aligned and resisting when the forces acting during the launch.

For this reason, they are carefully designed both from the point of view of the material with which they are made and their geometry.

Four connection points are chosen in which the four junctions have been inserted. In relation to the position of the single junction in the rocket, the stress state of the forces acting at that point is studied.

Specifically, two types of forces always act, the first being axial and in compression due to the thrust produced by the rocket; the second is a force on the section, resulting from the bending moment that is caused by the aerodynamic forces. This last value is strongly dependent on the trajectory, in fact, to have greater safety in the design the moment caused by the non-nominal flight is used to design.

Subsequently the optimal configuration was chosen to be carried out both to satisfy the imposed requirements and to obtain contained production costs. For this reason, it was decided to attach a metal junction made of two connectable parts to the external composite carbon fiber structure. The upper part is glued to the upper structure, while the lower part is glued to the lower structure. The two parts are fixed together by screws in the circular section of the rocket.

The three components described (the metal junction, the connecting screws and the bonding) have been designed and sized according to the requirements and have also been tested individually to approve their resistance to in-flight loads.

Before proceeding with the testing, the stress trend within the glue layer for gluing was studied; optimizing the geometry to have greater resistance for the same glued area.

The screws and consequently the junctions have been sized to avoid rebounding and yielding of screws and holes, leading to choosing screws with rectified shank and tolerance f9. In this way there are no displacements due to the coupling tolerances. This allows the junction to be aligned with the rocket axis once it has been set.

The results obtained from the tests carried out were positive and allowed to approve the planned configuration. Both the screws and the single-lap type bonding have been broken beyond the limits of forces obtained from the analytical calculations. The value of the breaking force exceeds by a factor 2 the forces acting locally. The test can be considered reliable as the thermal conditions in flight have been reproduced.

The gluing in the motor joint (scarf joint) has been broken and the measured pressure is 148 bar, much higher than that present when the motor is running. Moreover, the bonding is also impermeable to gaseous fluids.

Finally, the holes on the composite material were tested, which show a resistance to rebound around 250 MPa, allowing their insertion into the n ° 1 junction that connects the nosecone with the rocket.

After the tests carried out it is necessary to interact with future developments such as the realization of complete joints for the individual subsystems, verify the alignment during assembly, perform motor tests complete with the entire subsystem and finally go to launch the rocket and obtain the most important feedback. The success of the launch.

BIBLIOGRAPHY

[1] William R. Corliss. “NASA Sounding Rocket 1958-1968” *Scientific and Technical In/ormation Office 1971 NATIONAL AERONAUTICS AND SPACE ADMINISTRATION WaJhington, D.C. NASA SP-4401*

[2] Martin J. Chiaverini, Kenneth K. Kuo. “Foundamentals of Hyibrid Rocket Combustion and Propultion” Ed. by Martin J. Chiaverini, Kenneth K. Kuo.

[3] E. Paccagnella. “Scaling of Hybrid Rocket Motors with Swirling Oxidizer Injection” PhD thesis. Università degli Studi di Padova, a.a.2014-2015.

[4] Alan Baker, Stuart Dutton, Donald Kelli. “Composite Materials for Aircraft Structures” Ed. by Joseph A. Schetz.

[5] Database of material. *http://www.matweb.com/index.aspx*

[6] Alcoa Research Laboratories, 29 April 1958. As published in “Aerospace Structural Metals Handbook”, Vol 3, Code 3203, CINDAS/Purdue University,1995, p.24.

[7] Gruit company, in data sheet name “Gurit general data sheet”

[8] Torayca Industries, INC, data sheet “T700S data sheet”

[9] M. Stella. “Progettazione di un serbatoio in composito per un sounding rocket ibrido” PhD thesis. Università degli Studi di Padova, a.a.2018-2019.

[10] Statement UNI EN ISO 898-1.

[11] Statement UNI EN 1993-1-8.

[12] R.Giovannozzi. “Costruzione di Macchine” Vol.1. Ed. by Patron 1980.

[13] Alan Baker, Stuart Dutton, Donald Kelli. “Composite Materials for Aircraft Structures” Ed. by Joseph A. Schetz.

[14] Rene´ Quispe Rodrìguez, WilliamPortilhodePaiva, PauloSollero, Marcelo RicardoBertoniRodrigues, E´der LimadeAlbuquerque. “Failure Criteria for Adhesively Bonded Joints”

[15][16] Mahmood M. Shokrieh1 Larry B. Lessard, and Adnan Golubovic. “Adhesively Bonded Carbon/Titanium Joints Under In-plane and Bending Loads”

[17] Technical Data Sheet “3M™ Scotch-Weld™ EC-9323 B/A”

[18] Marin SANDU, Adriana SANDU, Dan Mihai CONSTANTINESCU “Strength of Adhesively Bonded Single-Strapped Joints Loaded In Tension” University “Politehnica” of Bucharest